CATO – CO$_2$ capture, transport and storage
towards a clean use of fossil fuels in the energy economy

CATO Workpackage WP 4.1

Deliverable WP 4.1-2

Subsurface mineralisation:
Rate of CO$_2$ mineralisation and geomechanical effects
on host and seal formations

A review of relevant reactions
and reaction rate data

S. Hangx
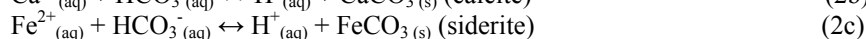HPT Laboratory, Department of Earth Sciences
Utrecht University

Table of contents

1 Introduction

1.1 CATO and the present PhD project

There is general agreement that CO_2 emissions need to be reduced in order to limit climate change and global warming effects. One way of disposing of carbon dioxide is by subsurface mineralisation (Bachu et al., 1996; Holloway, 1996; Wawersik et al., 2001), which entails the injection of CO_2 into the subsurface where it will be converted into carbonates, and hence rendered immobile. Research on subsurface mineralisation is the main focus of Work Package 4.1 of the Dutch international research programme CATO (CO_2 capture, transport and storage). CATO aims to build up a strong and coherent knowledge network, combined with adequate dissemination of knowledge, in the area of CO_2 capture, transport and storage. This network will gather and validate knowledge, develop novel technologies for CO_2 capture and storage, built up capacity to implement these technologies, and explore to which extent specific Clean Fossil Fuel options are acceptable to society.

The principle behind CO_2 sequestration by subsurface mineralisation is based on a number of sequential chemical reactions: (1) CO_2 dissolves in the reservoir water to form carbonic acid, and subsequently bicarbonate; (2) the bicarbonate reacts with cations present in the reservoir water in order to form stable carbonates. This whole process can be represented schematically as

$$CO_{2\,(g)} + H_2O_{(l)} \leftrightarrow H_2CO_{3\,(aq)} \leftrightarrow H^+_{(aq)} + HCO_3^-{}_{(aq)} \tag{1}$$
$$Mg^{2+}{}_{(aq)} + HCO_3^-{}_{(aq)} \leftrightarrow H^+_{(aq)} + MgCO_{3\,(s)} \text{ (magnesite)} \tag{2a}$$
$$Ca^{2+}{}_{(aq)} + HCO_3^-{}_{(aq)} \leftrightarrow H^+_{(aq)} + CaCO_{3\,(s)} \text{ (calcite)} \tag{2b}$$
$$Fe^{2+}{}_{(aq)} + HCO_3^-{}_{(aq)} \leftrightarrow H^+_{(aq)} + FeCO_{3\,(s)} \text{ (siderite)} \tag{2c}$$
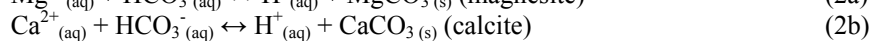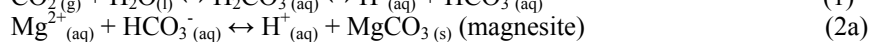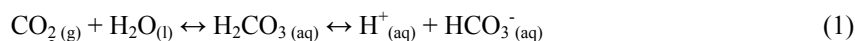
If sufficient cations are present, these reactions can lead to the long term, safe, storage of carbon dioxide as stable carbonates. When CO_2 is injected into an impure sandstone reservoir, feldspars and clays present in the rock will act as the cation source, and protons present in the reservoir water, as a result of carbon dioxide dissolution, will leach out the necessary cations from the silicate structure. In order to model the progress, efficiency and geochemical/geomechanical effects of any such mineralisation process, data are needed on the response of appropriate reservoir rocks to CO_2 injections.

The present PhD project, Study on rate of CO_2 mineralisation and geomechanical effects on host and seal formations, forms part of CATO Workpackage WP 4.1. It aims to

(1) determine the reaction rates of any relevant reactions taking place
(2) characterise the bulk uptake rate of CO_2
(3) determine the petrophysical factors that affect reaction
(4) determine the effect of reaction on the porosity, permeability and geomechanical response of the host and seal rock
(5) give implications for the choice of suitable sites or downhole additives.

Data produced will be incorporated into the Shell numerical modelling work on subsurface mineralisation within CATO WP 4.1.

1.2 Scope of this report

The first experiments planned in the present PhD project aim to determine the reaction rate of several basic reactions occurring during CO_2 injection in a sandstone reservoir. One of those reactions is that of Ca-rich feldspar, e.g. anorthite, reacting with CO_2 to form both calcite and kaolinite

$$CaAl_2Si_2O_{8\,(s)} + CO_{2\,(g)} + 2H_2O_{(l)} \leftrightarrow CaCO_{3\,(s)} + Al_2Si_2O_5(OH)_{4\,(s)} \tag{3}$$

Systematically performed experiments at various $P(CO_2)$, temperature, and grain size will provide reaction rate equations, which are most likely rate-limited by the dissolution of the feldspar and phyllosilicate phases, and not by the dissolution of carbon dioxide or the precipitation of calcite.

In order to get an impression of the order of magnitude beforehand, a careful study of the already available data on the various minerals and their reactions is necessary. This report constitutes such a literature research. It focuses the one hand, on the available kinetic data, e.g. dissolution reactions, solubility of various minerals and reaction rates, and, on the other, on the thermodynamic data

available, e.g. standard Gibbs free energies, enthalpies and entropies, as well as heat capacities and molar volumes. For completeness the inventory contains data on not only on the principle clastic rock-forming minerals, i.e. *all* plagioclase feldspars, from albite to anorthite, quartz, and various clays, but also on the formed products, i.e. carbonates and kaolinite, CO_2, H_2O, and common aqueous species.

All data obtained is tabled and depicted in the appendices in order to give a clear overview of the quantitative data. Discussions of the data on the rock-forming minerals are given in two separate sections: the first describes the kinetic data, the second the thermodynamic. A third section shortly describes the phase relations and equations of state of carbon dioxide and water. This is followed by some recommendations on the use of the data, as well as the derivation, from the available data, of a simple equation to calculate the amount of carbonate produced per cubic meter of impure sandstone rock. All symbols used are shown in Table 1. Finally the data are used to define the design of our future experiments.

Table 2 Symbols list			
symbol, definition [units]		*symbol, definition [units]*	
a_i	activity of species i	M_i	maximum amount of carbonate precipitated as a function of i [kg]
A_s	total surface area [m^2]	N_{grains}	number of grains
A_{grain}	surface area of a grain [m^2]	N	coordination number
d	grain size [μm]	P	pressure [bar]
φ	porosity	R	reaction rate [mol/m^2 s]
ϕ	fugacity coefficient	ρ_i	density of species i [g/cm^3]
k	reaction rate constant [s^{-1}]	T	absolute temperature [K]
m_i	mass of species i [kg]	W	vol.-% of water
m_i	molar mass of species i [g/mol]	X	vol.-% of anorthite
$\dot{M}$	amount of carbonate precipitated/unit volume/s [kg/m^3 s]	N_i^{moles}	number of moles of species i

2 Equilibrium constants and kinetic data

The main CO_2 fixing reactions expected when CO_2 is injected into impure wet sandstones can be summarised by a number of serial and parallel reactions, as shown in Fig. 1. The rate-limiting step in such serial-parallel reaction sequences will in general be the slowest step of the fastest parallel branch. Amongst the above reactions, it is well established in the literature that the silicate dissolution reactions are likely to be the slowest and hence most important in controlling reaction progress (Sorai et al., 2003). In the following, attention is therefore focused on dissolution kinetics as well as solubility of quartz, feldspar, and clays. Though it does not participate in the main carbonation reaction sequence we start with quartz for simplicity.

2.1 The dissolution of quartz

2.1.1 Dissolution reactions and equilibrium constants

Quartz dissolution is a congruent process, which occurs via hydrolysis of the silica framework to form silicic acid. In turn, the silicic acid dissociates (Dove & Crerar, 1990; Volosov et al., 1972), though only in highly alkaline solutions (pH > 10) (Fig.2)

$$SiO_{2\,(s)} + 2H_2O_{(l)} \leftrightarrow H_4SiO_{4\,(aq)} \qquad (4)$$
$$H_4SiO_{4\,(aq)} \leftrightarrow H_3SiO_4^-{}_{(aq)} + H^+{}_{(aq)} \qquad (5)$$
$$H_3SiO_4^-{}_{(aq)} \leftrightarrow H_2SiO_4^{2-}{}_{(aq)} + H^+{}_{(aq)} \qquad (6)$$

For various forms of silica, hydrolysis and dissociation reactions, and their appropriate solubility and dissociation constants, are summarized in Appendix 1a.

Solubility of minerals can be determined by three different methods: (1) weight loss of quartz in a known amount of water; (2) chemical analysis of dissolved silica remaining in solution, after quick cooling and opening the reaction vessel; and, (3) chemical analysis of dissolved silica in small amounts of solution extracted from the reaction vessel while the vessel is maintained at high temperature and

a. CO_2 mineralisation via anorthite dissolution

$$CO_{2\,(g)} + H_2O_{(l)} \leftrightarrow H_2CO_3*_{(aq)}$$

$$CaAl_2Si_2O_{8\,(s)} + 2\,H^+_{(aq)} + H_2O_{(l)} \leftrightarrow \mathbf{Ca^{2+}_{(aq)}} + Al_2Si_2O_5(OH)_{4\,(s)}$$

$$CaAl_2Si_2O_{8\,(s)} + 8\,H_2O_{(l)} \leftrightarrow \mathbf{Ca^{2+}_{(aq)}} + 2\,Al(OH)_4^-{}_{(aq)} + 2\,H_4SiO_{4\,(aq)}$$

$$H_2CO_3*_{(aq)} \leftrightarrow \mathbf{H^+_{(aq)}} + \mathbf{HCO_3^-{}_{(aq)}}$$

$$HCO_3^-{}_{(aq)} \leftrightarrow \mathbf{H^+_{(aq)}} + \mathbf{CO_3^{2-}{}_{(aq)}}$$

$$Ca^{2+}_{(aq)} + CO_3^{2-}{}_{(aq)} \leftrightarrow CaCO_{3\,(s)}$$
$$Ca^{2+}_{(aq)} + HCO_3^-{}_{(aq)} \leftrightarrow CaCO_{3\,(aq)} + H^+_{(aq)}$$
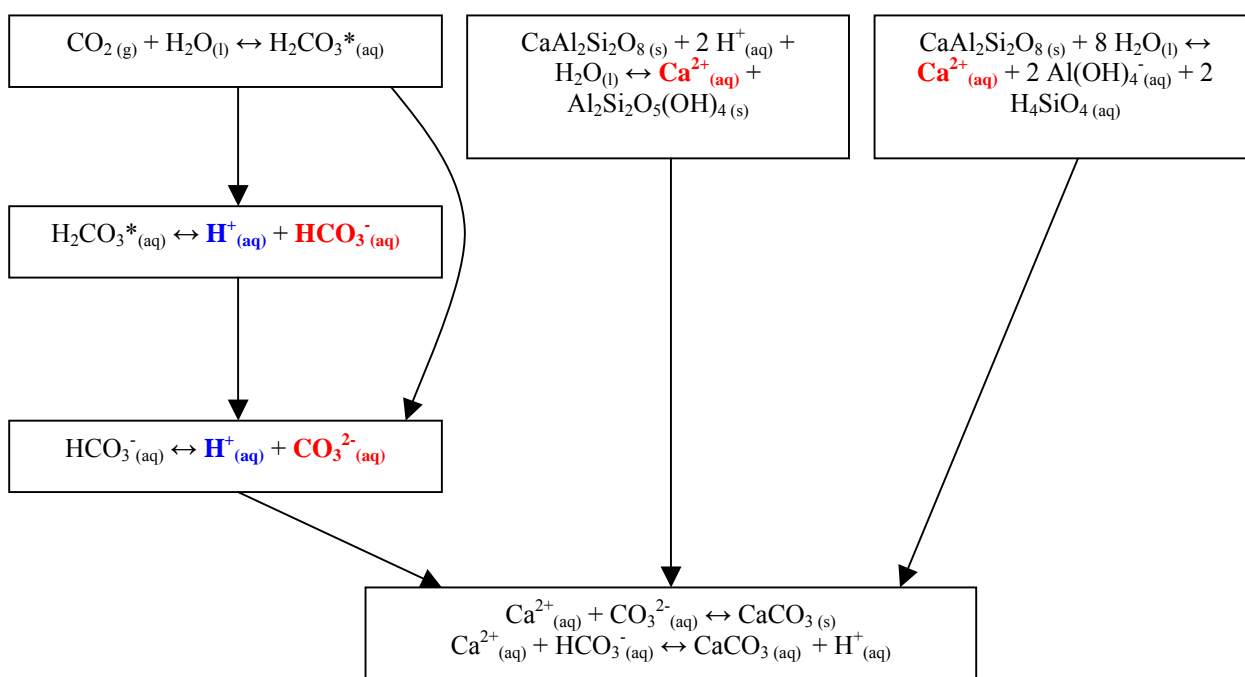
b. CO_2 mineralisation via Ca-rich clay dissolution

$$CO_{2\,(g)} + H_2O_{(l)} \leftrightarrow H_2CO_3*_{(aq)}$$

$$3\,\text{Ca-montmorillonite} + 2\,H^+_{(aq)} + 23\,H_2O_{(l)} \leftrightarrow 7\,Al_2Si_2O_5(OH)_{4\,(s)} + 8\,H_4SiO_{4\,(aq)} + \mathbf{Ca^{2+}_{(aq)}}$$

$$H_2CO_3*_{(aq)} \leftrightarrow \mathbf{H^+_{(aq)}} + \mathbf{HCO_3^-{}_{(aq)}}$$

$$HCO_3^-{}_{(aq)} \leftrightarrow \mathbf{H^+_{(aq)}} + \mathbf{CO_3^{2-}{}_{(aq)}}$$

$$Ca^{2+}_{(aq)} + CO_3^{2-}{}_{(aq)} \leftrightarrow CaCO_{3\,(s)}$$
$$Ca^{2+}_{(aq)} + HCO_3^-{}_{(aq)} \leftrightarrow CaCO_{3\,(aq)} + H^+_{(aq)}$$
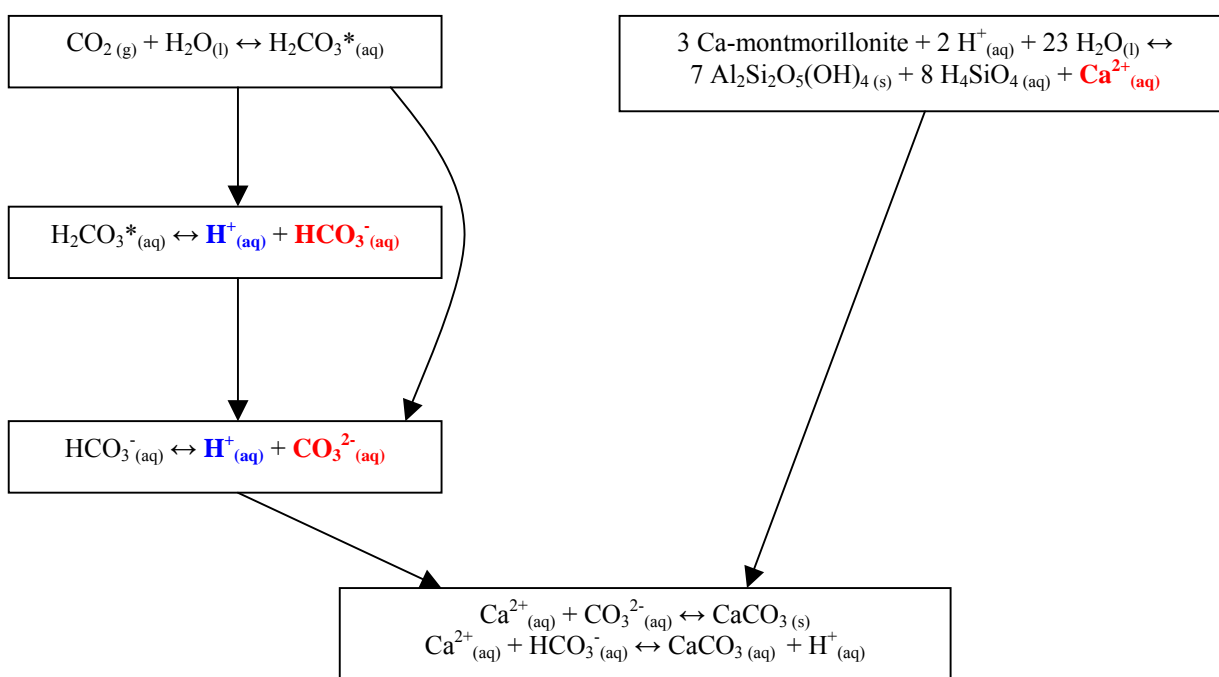
Fig. 1 Reaction schemes showing (a) the serial and parallel reactions occurring during the dissolution of anorthite; and, (b) the serial and parallel reactions occurring during the dissolution of Ca-rich clay. In both cases, the protons formed by the CO_2-dissolution-branch (blue) will attack the anorthite and clay, resulting in the release of Ca^{2+}-ions. The calcium and bicarbonate or carbonate ions from the parallel branches (red) will together result in the precipitation of calcite.

pressure. The first method works best when enough quartz dissolves into solution to give measurable weight loss values, so at conditions where solubilities are moderate to high. The second method, the chemical analysis of quickly cooled solutions, works best when either the run temperatures are below 300°C to 350°C, or when the reaction vessel can be cooled to room temperature and opened within one or two minutes. The last method has the same advantages as method 2, but in addition allows sampling of the fluid in the reaction vessel at various temperatures and pressures without cooling and opening the vessel.

Most solubility equations were derived using available experimental data from various authors, using various analytical methods (Fleming & Crerar, 1982; Fournier & Potter, 1982; Volosov et al., 1972). New solubility experiments (Gunnarsson & Arnórsson, 2000; Rimstidt, 1997; Rimstidt & Barnes, 1980) determined the silica concentrations by chemically analysing quickly cooled solutions. Solubility constants for reaction (1) were derived by linear regression of log K vs. 1/T graphs of the available data (Fleming & Crerar, 1982; Gunnarsson & Arnórsson, 2000; Rimstidt & Barnes, 1980; Volosov et al., 1972). Volosov et al. (1972) used a general equation, instead of linear regression, and data from various authors to derive equations for the first and second dissociation reaction. In a way similar to that for the derivation of the solubility constant of reaction (1), log m_{H4SiO4} was plotted against log V (Fournier & Potter, 1982), 1/T (Rimstidt, 1997; Volosov et al., 1972), or the differential heat of reaction, ΔH^θ (van Lier et al., 1960) to obtain solubility equations.

The solubility of quartz in pure water strongly depends on temperature (Fournier & Potter, 1982; Rimstidt, 1997; van Lier et al., 1960; Volosov et al., 1972), as seen in Appendix 2. There appears to be little variation in the solubility concentrations among various article, except for Fournier and Potter (1982). At a

Fig. 2 Distribution of dissolved forms of silica. Lines connect equal molar concentrations of dissolved forms of silica *(Volosov et al., 1972).*

temperature of 25°C and a pressure of 1 bar quartz solubility varies between 10.8 ppm (van Lier et al., 1960) and 12.5 ppm (Volosov et al., 1972), in contrast to the solubility concentration of Fournier and Potter (1982), which is ~ 6ppm (App. 2a). The former solubility concentrations are believed to be more accurate, as they are in better agreement with values measured in ancient groundwaters (Rimstidt, 1997). As can be seen in Appendix 1a, the solubility constant for the dissolution of silica decreases when going from quartz to amorphous silica. In addition the solubility concentration of SiO_2 increases (App. 2a and b). This effect is most likely the result of an increase in crystal structure disorder when going from quartz to amorphous silica.

Recommendations have been made on the use of the equations stated in Appendix 1a and 2a. The solubility constants for silica dissolution are best represented by equation 1, for quartz, and 7 for amorphous silica. Cristobalite is not considered to be of importance for our problem, but was stated for completeness. Little data is known on the dissociation constants of silica, Appendix 1 only states the constants calculated by Volosov et al. (1972). The solubility of silica is calculated best using equation 4 in Appendix 2a.

2.1.2 Dissolution rates

In order to determine the dissolution rate of silica as a function of pH, dissolution experiments have been performed at various pH and temperature, by various methods. The dissolution of silica is assumed to occur via a transition state (Rimstidt & Barnes, 1980)

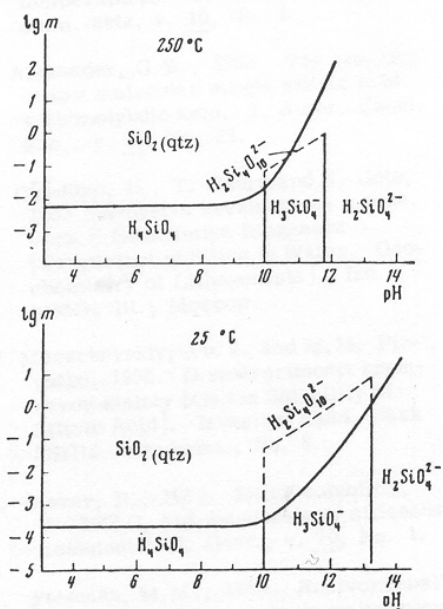$$SiO_2 + 2H_2O \leftrightarrow (SiO_2 \cdot 2H_2O)^* \qquad (7)$$
$$(SiO_2 \cdot 2H_2O)^* \rightarrow H_4SiO_4 \qquad (8)$$
and
$$H_4SiO_4 \leftrightarrow (SiO_2 \cdot 2H_2O)^* \qquad (9)$$
$$(SiO_2 \cdot 2H_2O)^* \rightarrow SiO_2 + 2H_2O \qquad (10)$$

For various forms of silica the transition state is assumed to be the same (Fig. 3) (Rimstidt & Barnes, 1980). As all forms of silica have different Gibbs free energies of formation the forward reaction rate constant will therefore be different for all species. However, since the product of dissolution of these species is the same for all, namely H_4SiO_4, the backward reaction rate constant is the same for all species.
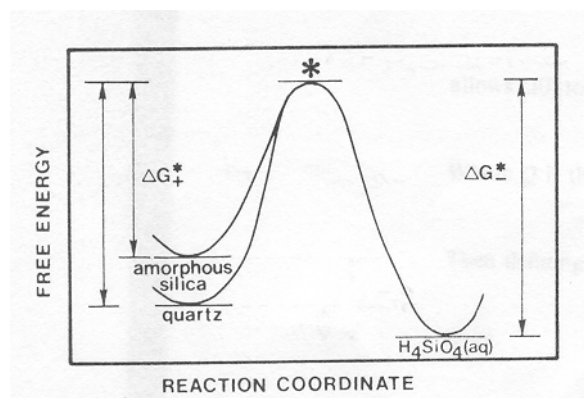

Fig. 3 A schematic illustration of the free energy maximum through which reactants must pass to become products *(Rimstidt and Barnes, 1980).*

Experiments were performed as either batch (Blake & Walter, 1999; Brady & Walther, 1990; Tester et al., 1994; van Lier et al., 1960), or as flow-through experiments (Dove, 1994; Dove & Crerar, 1990; Dove & Nix, 1997; Gíslason et al., 1997; Knauss & Wolery, 1988). In addition to their own measurements, some authors used previous obtained data to back up their own experiments (Dove, 1994; Dove & Elston, 1992; Knauss & Wolery, 1988; Tester et al., 1994). Dove and Elston (1992) only evaluated data obtained by other authors. In general, batch experiments are performed by placing a reacting fluid plus a known amount of silica in a batch reactor vessel and heating the system to the appropriate experimental temperature. At regular intervals fluid samples are drawn from the system to monitor the dissolved silica concentration with time. During flow-through experiments a fluid of known composition continuously flushes the reaction vessel, containing the silica sample and reacting fluid. The approach to steady state of the system is monitored and effluents are analysed for their silica concentration. From these data silica dissolution rates are calculated using various methods. Unless stated otherwise, the obtained reaction rates and reaction rate constants are net reaction rates and net reaction rate constants. All reaction rate equations and their activation energies, as well as a visual representation of the variation of dissolution rate with pH and the forward reaction rate constant with temperature, are shown in Appendix 3a and 4aI/II.

Dissolution experiments have shown that the dissolution rate of quartz is strongly pH dependent at higher pH (pH > 7), increasing with increasing pH (Brady & Walther, 1990; Dove & Elston, 1992; Knauss & Wolery, 1988) (Appendix 4aI). At lower pH the effect of acidity on dissolution is negligible, and the dissolution rate can be considered to be independent of pH. However, Knauss and Wolery (1988), as well as Brady and Walther (1990), noted that at extremely low pH (pH < 2) the dissolution rate of quartz appeared to be slightly pH dependent again, and increased with increasing pH. The dependence of dissolution rate on pH can very well be explained by a surface charge controlled mechanism. The point of zero charge, pH_{PZC} is ~ 2.2 for quartz (Brady & Walther, 1990), so at low pH the surface charge is electrically neutral, indicating an equal number of $\equiv Si-OH_2^+$ and $\equiv Si-O^-$ surface complexes. As the

Fig. 4 25° and 60°C rates plotted as a function of ionic strength. The data are fit to straight lines with slopes of 0.2 with the exception of the line through the 60°C, pH 11.5 data and those at pH < 6 *(Brady and Walther, 1990).*

solution becomes more alkaline, the quartz surface becomes more and more electrically negatively charged, increasing the number of $\equiv Si-O^-$ complexes. These surface complexes are thought to weaken the Si-O-Si structure, due to increased reactivity, and hence increase dissolution. As the number of negatively charged surface complexes increases with increasing pH, so does the dissolution rate. A similar explanation can be used to describe the dissolution rate behaviour at very low pH (pH < 2). At this pH the quartz surface is positively charged, and it is very likely that this positive charge also weakens the Si-O-Si network structure.

The dissolution rate of quartz is significantly influenced by ionic strength (Fig. 4) and temperature (Appendix 4aII), as both tend to increase the reaction rate constant, and hence the dissolution rate. The

dissolution rate appears to be of first-order with respect to negatively charged surface species concentrations at high pH. However, in near-neutral pH solutions the effect of ionic strength is only small, as shown by Brady and Walther (1990). Most likely, increasing temperature results in an increase in dissolution rate, due to increasing reactivity and/or activity with increasing temperature.
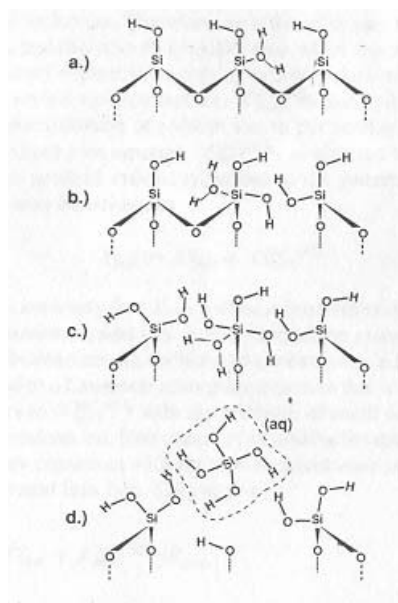

Fig. 5 Schematic illustration of the dissolution process in deionized water *(Dove and Crerar, 1990).*

Addition of ions to the reacting solution also significantly increases the dissolution rate of quartz, as demonstrated by Dove and Nix (1997). In general, it was concluded that the dissolution rate of quartz is cation-specific, meaning that the dissolution rate is more enhanced by monovalent ions than by divalent ions. The effect of cations in solution on dissolution rate at near-neutral pH showed a first-order dependence of dissolution rate on cation concentration. Dissolution rates were slowest in pure water and increased with cation addition, $Mg^{2+} < Ca^{2+} \approx Li^+ \approx Na^+ \approx K^+ < Ba^{2+}$. Dove and Crerar (1990) observed the same effect of electrolytes on reaction kinetics and they even derived a reaction rate equation incorporating the effect of electrolytes. In general, it is believed that the dissolution rate is increased due to an increase in reactivity of siloxane groups by the disruption of the structure of the mineral-solution interface as a result of coordination of alkali cations with the surface (Dove & Crerar, 1990; Dove & Nix, 1997). A more extensive description of the dissolution mechanism of quartz is given in the section below.

The dissolution rate for quartz and amorphous silica dissolution is calculated best using equation 6 and 10, respectively, as they apply to a large temperature range. However, they do not apply in the acid pH range, but since there are no complete reaction rate equations available at lower pH we are forced to use the next best thing. The best reaction rate equation for ligand promoted dissolution is considered to be equation 13, as it can be used for various ligands.

2.1.3 Dissolution mechanism

The dissolution of quartz is considered to be a surface reaction controlled mechanism. Dove (1994) suggested that in solutions with a pH varying from pH_{PZC} (point of zero charge, pH 2.2 for quartz (Brady & Walther, 1990)) to 7.5 the dissolution rate of quartz is relatively slow. At low pH values the surface of quartz is electrically neutral due to the equal number of positive and negative charged complexes (Brady & Walther, 1990; Dove, 1994). Since the surface potential and charge are small they have little influence on the structure of water near the surface compared to the bulk water. Therefore, at these pH conditions the dissolution rate of quartz is limited by the slow reaction of the surface with weakly nucleophilic molecular water. At more neutral pH values increasing ionisation of the surface affects the hydrogen-bonded structure and gives a small polarization to the interfacial water, giving rise to more Si-O bond rupture (Dove, 1994). A simplified dissolution mechanism is illustrated in Fig. 5, which shows the interaction of a water molecule with a Si-O-Si bond by orientating the negatively electrically charged oxygen atom towards the silicon ion. This process of pushing electrons onto the siloxane group lengthens the Si-O bond, and eventually leads to its rupture. The reaction describing this process can be written as (Dove & Crerar, 1990)

$$\equiv Si\text{-}O\text{-}Si\equiv + H_2O \leftrightarrow Si\text{-}O\text{-}Si\cdot OH_2^\dagger \rightarrow 2 \equiv Si\text{-}O\text{-}H \qquad (11)$$
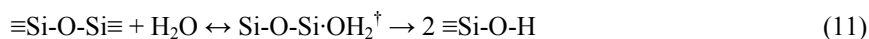
The breaking of the first Si-O-Si bond is probably the most energetic step, and hence the progress of this intermediate reaction limits the dissolution process at a reaction rate constant of $4.86\cdot10^{-9}$ mol/m^2 s at 200°C. The following steps of water approach and water weakening of the remaining bonds attached to the structure probably require substantially less energy and the reaction proceeds until the final result is the release of aqueous H_4SiO_4. The addition of alkali cations to the solution will increase the dissolution rate by interaction between the alkali cations and the quartz surface, as will be explained in more detail below (Dove & Crerar, 1990).

In more hydroxide-rich solutions the quartz surface is associated with higher reactivity, either by (1) attack of the quartz surface by the OH⁻ ions (Brady & Walther, 1990; Dove, 1994); or by (2) the formation of surface complexes as a result of the interaction between the quartz surface and cations present in solution (Dove & Crerar, 1990).

Firstly, in a high pH environment (pH > 10) the quartz surface has a net negative surface charge due to the formation of Si-O⁻ surface complexes, which results in an electric field gradient. In turn, this gradient causes the structure of water near the surface to change and protons of the hydroxide ions exchange with the surface.
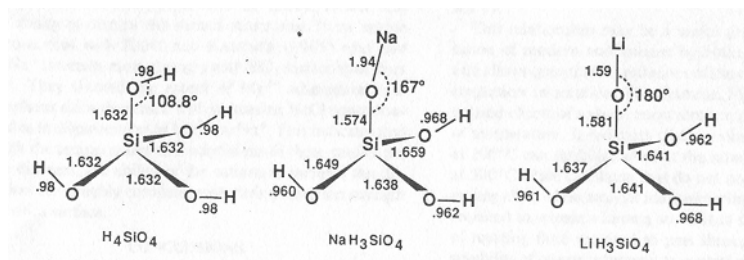

Fig. 6 Optimized bond lengths and angles for the static molecular models of H_4SiO_4, NaH_3SiO_4, and LiH_3SiO_4 *(Dove and Crerar, 1990)*.
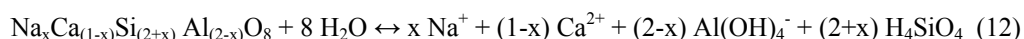
Secondly, alkali cations in solution can also cause an increase in dissolution rate, due to the formation of surface complexes, Si-O-M⁺, where M is a monovalent or divalent alkali cation (Brady & Walther, 1990; Dove & Crerar, 1990). The formation of these alkali cation surface complexes results in the lengthening of the Si-O bonds. As can be seen in Fig. 6, the Si-O bond length for an optimised H_4SiO_4 molecule is 1.632 Å, whereas the weakest Si-O bridging bond for the NaH_3SiO_4 and LiH_3SiO_3 molecules are as large as 1.659 Å and 1.641 Å, respectively. Therefore, the alkali cations exert an influence on the electron distribution to lengthen, and hence weaken, the Si-O bonds. Its is also clear that the three remaining Si-O bonds become longer and the Si-O-M angle opens, which makes it possible for the water molecules, or hydroxide ions, to approach the Si-O lattice bonds more rapidly (Dove & Crerar, 1990).

2.2 The dissolution of feldspar

After discussing quartz as a simple silicate, we will continue with the various plagioclase feldspars. These feldspars are, besides quartz, the principle clastic rock-forming minerals in impure sandstone rocks. Much of the principles and mechanisms discussed above do also apply for feldspars. For carbon dioxide sequestration mainly the Ca-rich feldspars are of interest.

2.2.1 Dissolution reactions and equilibrium constants

The general reaction for the dissolution of plagioclase feldspar in water can be described as (Arnórsson & Stefánsson, 1999)

$$Na_xCa_{(1-x)}Si_{(2+x)}Al_{(2-x)}O_8 + 8\ H_2O \leftrightarrow x\ Na^+ + (1-x)\ Ca^{2+} + (2-x)\ Al(OH)_4^- + (2+x)\ H_4SiO_4 \quad (12)$$

In general, feldspars dissolve congruently at acid and alkaline pH, and incongruent at neutral pH. For various plagioclase feldspar compositions the dissolution reactions in neutral, acid and CO_2-charged water, together with their solubility constants, are summarized in Appendix 1b.

Studies of mineral saturation in aqueous solutions involve two steps: (1) derivation of equilibrium constants (K) for mineral hydrolysis from thermodynamic data taking into account the effects of variable composition of the minerals and ordering, as appropriate; and, (2) calculation of individual aqueous species activities from analytical data on the waters to retrieve values for the respective activity product (Q). Comparison between the two allows evaluation of saturation states of waters with respect to feldspars as a function of their composition and Al-Si ordering (Arnórsson & Stefánsson, 1999). Dissolution reactions for primary minerals in aqueous solution have been expressed in terms of those aqueous species that were generally found to be dominant in natural waters. This way errors in calculated Q were minimized (Arnórsson & Stefánsson, 1999; Stefánsson, 2001).

Arnórsson and Stefánsson (1999) recalculated the solubility constants of various feldspars as a function of temperature. In order to do so they recalculated the Gibbs free energy of formation of the chosen feldspar minerals by using heat capacity data from other authors. Stefánsson (1999) used part of the thermodynamic data calculated by Arnórsson and Stefánsson (1999), in addition to thermodynamic data for aqueous species, to calculate his solubility constants as a function of temperature. For

comparison, a visual representation of the temperature dependence of the solubility constants for various plagioclase feldspars is shown in Fig. 7.

The equilibrium constants for the dissolution in acid or CO_2-rich fluids (Stumm & Morgan, 1981) are uncertain in their origin, though recalculation by using Gibbs free energies of formation have proven them to be accurate.

The solubility data of feldspar is limited, and does not vary much among different authors. Equations 14 to 19, 21 and 22 (Appendix 1b) are thought to give the best representation of the available data, and Arnórsson and Stefánsson (1999) data is chosen over Stefánsson (1999) data, as the latter is derived from the former.
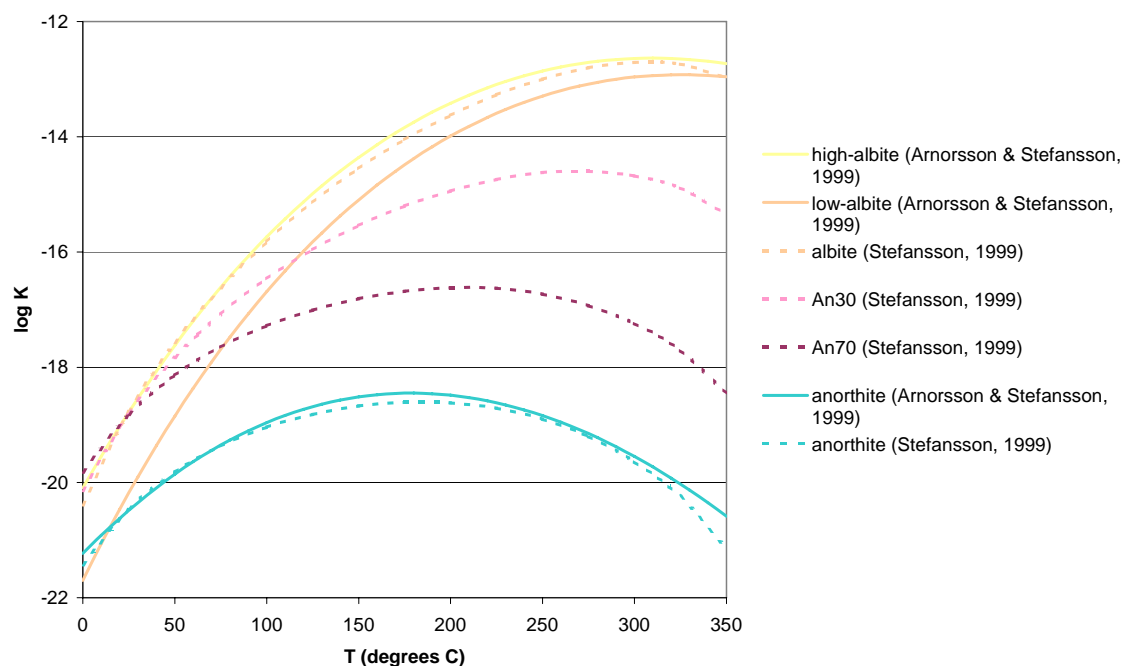

Fig. 7 The solubility of end-member plagioclase feldspars and solid solutions of fixed composition. There is a good agreement between the data of Arnórsson and Stefánsson (1999) and Stefánsson (1999).

2.2.2 Dissolution rates

Dissolution rate experiments on feldspars were conducted in ways similar to those on quartz: (1) batch experiments (Amrhein & Suarez, 1992; Casey et al., 1991; Hamilton et al., 2001); (2) flow-through experiments (Berg & Banwart, 2000; Hellmann, 1994; Knauss & Wolery, 1986; Oxburgh et al., 1994); or, (3) surface titration experiments (Blum & Lasaga, 1988; Oxburgh et al., 1994). The latter was mainly used to derive reaction rate equations as a function of surface charge. Fluid samples and effluents of the former two experimental methods were analysed for various elements, e.g. Al, Si, Na and Ca and, using this data, dissolution rates were calculated by various methods. All derived reaction rate equations, the reaction rate constants, and the required activation energy, are shown in Appendix 3b. A visual representation of the dissolution rates as a function of pH, and temperature, is shown in Appendix 4b. It is clear that, as temperature increases, the dissolution rates become more pH dependent in the acid and alkaline pH regions. The activation energy required for dissolution is also higher (~ 80 kJ/mol) in more acid and alkaline environments, than in the near-neutral pH region (~ 65 kJ/mol).

In general it can be seen that feldspar dissolution rates can be divided into three different pH regions (Blum & Lasaga, 1988; Hamilton et al., 2001; Knauss & Wolery, 1986; Oxburgh et al., 1994)

1) low pH region (pH < 4): the dissolution rate decreases with increasing pH
2) near-neutral pH region (pH 4-8): the dissolution rate shows no dependence on pH
3) high pH region (pH > 8): the dissolution rate increases with increasing pH, though this pH dependence is less pronounced than for the "low pH" region.

10

It is generally agreed that this behaviour of dissolution rate, under varying pH conditions, can be expressed by the following equation

$$R = k_{H+} \, (a_{H+})^{-n} + k_{OH-} \, (a_{OH-})^{m} \tag{13}$$

The values of n and m can vary between zero and one, as can be seen in App. 3b. Not only vary the values of the exponents among feldspars of different composition, there is also a large variation in values among different authors for similar feldspar compositions. In general, it is suggested that the dissolution rate of feldspars increases with anorthite content, so more calcic feldspars dissolve faster (Casey et al., 1991; Oxburgh et al., 1994). In addition to the effect of anorthite content, Hamilton et al. (2001) and Oxburgh et al. (1994) showed that the Al/Si ratio also affects the dissolution rate. For feldspars with varying Al content, but similar Na content, it is seen that the dissolution rate increases with increasing Al/Si ratio (Hamilton et al., 2001).

Other factors affecting the dissolution rate of feldspars are: (1) the reactive site density (Amrhein & Suarez, 1992; Holdren Jr. & Speyer, 1987), which in turn is related to the "reactive surface area", though not in a proportional manner; (2) cations in solution, e.g. aqueous Al (Amrhein & Suarez, 1992; Muir & Nesbitt, 1991); (3) ligand absorption, e.g. oxalate (Berg & Banwart, 2000; Blake & Walter, 1999), citrate (Blake & Walter, 1999), or carbonate (Berg & Banwart, 2000); (4) mineral heterogeneities, e.g. more rapid dissolution of Ca-rich phases than Na- or K-rich phases (Casey et al., 1991; Inskeep et al., 1991); and, (5) the formation of a leached layer (Amrhein & Suarez, 1992; Hellmann et al., 2003; Muir et al., 1990; Muir & Nesbitt, 1991; Nesbitt & Muir, 1988) or precipitated phase (Amrhein & Suarez, 1992; Berner & Holdren Jr., 1977; Nugent et al., 1998) on the surface of the feldspar.

The first factor states that the dissolution rate of feldspar, or any other mineral, is related to its reactive surface area, the part of the surface that actually participates in the dissolution reaction, i.e. reactive sites like dislocations, crystal defects or twin boundaries. However, Amrhein and Suarez (1992) have shown that the relation between dissolution rate and specific surface area is not a simple one, and though the density of reactive surface sites per unit area varies systematically with grain size, it does not so in a linear way (Holdren Jr. & Speyer, 1985).

Secondly, the addition of cations to solution could affect the dissolution rate of feldspars, though not all cations have this effect (Amrhein & Suarez, 1992; Muir & Nesbitt, 1991). Addition of "feldspar building" ions, e.g. Ca, Mg, Si, and Al, to solution resulted in different effects on the dissolution rate. In general, Ca, Mg, and Si ions appeared to have no effect on the dissolution rates of labradorite (Muir & Nesbitt, 1991), and anorthite (Amrhein & Suarez, 1992) in acid solutions. This in contrast to Al, which significantly inhibited dissolution at pH 3.6 to 6.0 (Amrhein & Suarez, 1992; Muir & Nesbitt, 1991), though not at pH 3.0 (Amrhein & Suarez, 1992). Inhibition of dissolution by Al was assumed to be the result of the blocking or retardation of H^{+} supply from the bulk solution to the surface by aqueous aluminium. As the release of Al from the silicate surface to solution depends on the concentration gradient between the solid and solution, addition of aluminium to solution decreases this gradient and therefore slows down the release of Al from the solid, and hence the dissolution rate (Muir & Nesbitt, 1991).

Thirdly, the addition of ligands to solution also affects the dissolution rate, as they tend to form surface complexes. Carbonate is believed to form $\equiv Al\text{-}CO_3^{-}$ surface complexes with positively charged Al-surface groups (Berg & Banwart, 2000). A similar process is applicable to organic acids (OAs), though since the structure of these acids is rather extensive, the exact stereochemical configuration and geometry of the formed ligand-surface complexes is not clear (Blake & Walter, 1999). Blake and Walther (1999) have studied the effect of citric and oxalic acid on the dissolution rate of albite, labradorite, and orthoclase. They concluded that there is a similarity in dissolution behaviour of alkali feldspars with similar Al content, i.e. albite and orthoclase, and a greater solubility of the more Al-rich feldspar, labradorite, in the presence of OAs. They observed a trend of greater Si and Al release as a function of higher OA concentration, and a greater effect of citrate, a tricarboxylic ligand, relative to oxalate, a dicarboxylic, at the same concentrations. The latter observation was explained by the larger size and additional carboxyl group of citrate, in comparison to oxalate. This may allow citrate to bridge Si surface sites and interact with more than one Al site, and thus have a larger on feldspar dissolution than oxalate at the same concentration. Though, even if citrate only forms one surface complex, the third carboxyl group may still interact with a second metal site on the feldspar surface or in solution.

The fourth factor applies the observation of Casey et al. (1991) and Oxburgh et al. (1994), the higher solubility of more Ca-rich feldspar compared to Na-rich feldspar, to the mm, or even nm, scale. TEM imaging of a zoned labradorite by Inskeep et al. (1991) has shown that the more Ca-rich lamellae

were dissolved preferentially over the more Na-rich ones. These mineralogical heterogeneities influence the measures dissolution rate significantly.

The last factor states that the dissolution of feldspar is influenced by the formation of leached layers or precipitates. Coating of the feldspar grains by these layers is assumed to change the dissolution mechanism from transport-controlled to diffusion-controlled, as released ions must now first diffuse through the coating before being released to solution. The existence of these layers will be discussed in more detail below.

Most reaction rate equations presented in Appendix 3b are incomplete, and the only equations of interest, for our range of in-situ conditions, would be equations 18a, 19a, and 20a for albite, and 24 for anorthite. For the calculation of the dissolution rate of feldspar with other compositions, e.g. labradorite or bytownite, equations 28 and 29 are suitable, though they only apply at room temperature. No suitable equations for ligand promoted dissolution are available.

2.2.3 Dissolution mechanism

The mechanism of dissolution of feldspars has been a point of debate among various authors. Essentially, silicate mineral dissolution can be categorised into three hypotheses:

1) dissolution via a surface-controlled reaction
2) formation of a leached or altered layer at the mineral-solution interface
3) formation of protective coatings at the crystal surface

This section will only deal with the first hypothesis, the other two will be discussed later on. In the first hypothesis, it is suggested that silicate mineral dissolution proceeds via a surface-controlled reaction. Knauss and Wolery (1986), as well as Hamilton et al. (2001) and Berner and Holdren (1977), suggest that dissolution was controlled by the non-uniform attack at the surface, preferentially at crystal defects, along twin boundaries or at dislocations, which intersect the surface.

As for quartz, the dissolution of feldspar is related

Fig. 8 Optimized geometries of the a) albite, b) jadeite, and c) nepheline structure. The bond lengths in brackets are average values *(Hamilton et al., 2001)*.

to the formation of surface complexes; however, due to the presence of Al in the feldspar framework dissolution is no longer limited to the formation of Si-surface complexes. The type of surface complex formed at a given solution pH is related to the pH_{PZC} of the metal cation site; the pH_{PZC} values of SiO_2, $Al_2^{IV}O_3$, and $Al_2^{VI}O_3$ are 2.2, 5-7, and 8, respectively (Brady & Walther, 1989; Oxburgh et al., 1994). This implies that at low pH values the feldspar surface is positively charged due to the formation of $\equiv Al-OH_2^+$ surface complexes, and at high pH values $\equiv Si-O^-$ surface complexes are dominant, resulting in a negative surface charge. As a result of the formation of these surface complexes, at acid pH dissolution will be mainly concentrated at the Al-surface site, while, at alkaline pH, dissolution focuses on the Si-surface sites (Brady & Walther, 1989; Hellmann, 1999; Oxburgh et al., 1994). At near-neutral pH, however, the dissolution rate is independent of surface charge, as it is mainly occupied by neutral $\equiv Si-OH$ and $\equiv Al-OH$ surface complexes. Oxburgh et al. (1994) suggested that, at near-neutral pH,
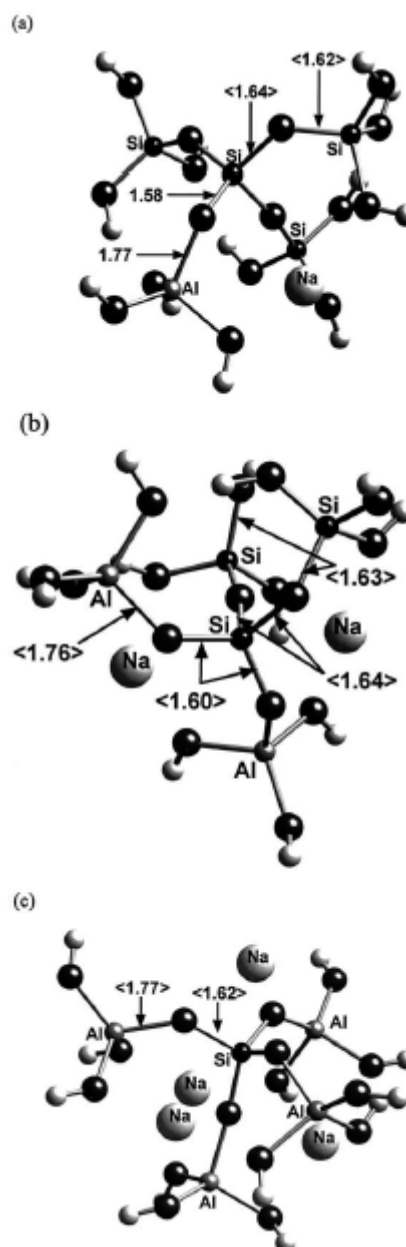
reaction occurs at neutral Al-surface sites, due to the fact that an Al-O-Si bond is weaker than a Si-O-Si bond (Hamilton et al., 2001).

In addition, Hamilton et al. (2001) and Oxburgh et al. (1994) both concluded that variations in Al content among feldspars could explain the observed increase in dissolution rate going from albite to anorthite. Hamilton et al. (2001) studied the effect of the Al/Si ratio on the dissolution rate of feldspar glasses: albite ($NaAlSi_3O_8$; Al/Si = ⅓), jadeite ($NaAlSi_2O_8$; Al/Si = ½), and nepheline ($NaAlSiO_4$; Al/Si = 1). As can be seen in Appendix 4b, nepheline dissolution rates were significantly higher than those of albite, up to three orders of magnitude. This difference is explained by the difference in feldspar structure, which is related to the interconnection between AlO_4 and SiO_4 tetrahedra (Hellmann, 1999). Increasing the Al/Si ratio means replacement of Si atoms by Al atoms, which results in an increase in Si-O-Al bond length, as can be seen for the transition from albite, through jadeite, to nepheline in Fig. 8 (Hamilton et al., 2001). As a result of this bond length increase AlO_4 tetrahedra are preferentially removed from the feldspar framework. Albite contains SiO_4 tetrahedra that are interconnected, and therefore the loss of AlO_4 tetrahedra will not affect the kinetics of surface SiO_4 tetrahedra detachment, i.e. ≡Si-OH complexes, in albite. This in contrast to anorthite, which contains completely isolated SiO_4 tetrahedra, and therefore anorthite dissolution requires only the breaking of, weaker, Al-O-Si bonds, instead of both Al-O-Si and Si-O-Si bonds, as is the case for albite dissolution (Hellmann, 1999).

2.2.4 Leached layer theory

The second hypothesis, stated in the previous section, postulates that an altered layer, usually depleted in alkali or alkaline earth cations, is formed at the silicate-solution interface, which controls dissolution. Leached layers are the result of non-stoichiometric dissolution and near-surface alteration at acid to neutral pH, they are generally not observed at basic pH (Casey et al., 1988; Casey et al., 1991; Hellmann et al., 2003). Depth profiles of these altered zones typically show a depletion in interstitial cations, i.e. Na, K, Ca, and framework elements, i.e. Al, retention of Si and O (Hellmann et al., 2003; Muir et al., 1990), and enrichment in aqueous species, i.e. H (Casey et al., 1988).

However, there is a significant difference between naturally formed leached layers and laboratory produced layers: naturally formed leached layers are aluminium-rich (Nesbitt & Muir, 1988), while laboratory produced layers are Si-rich (Hellmann et al., 2003; Inskeep et al., 1991; Muir et al., 1990). In addition, these laboratory-produced layers are usually also depleted in Ca and Na. These altered layers usually have a thickness of several hundreds of angstroms, and this thickness may also vary with feldspar composition (Muir et al., 1990), increasing with increasing Al content. The mechanism of leached layer formation is thought to involve three consecutive steps (Chou & Wollast, 1985; Muir et al., 1990):

1) rapid replacement of Ca^{2+} and Na^+ by H^+ or H_3O^+
2) hydrolysis reaction, resulting in the breaking of Si-O-Al bonds preferentially, and also Si-O-Si bonds, and the depolymerisation of the silicate structure, eventually resulting in a Al-depleted layer
3) slow dissolution of the residual layer at the solid-solution interface, together with diffusion of ions from the fresh feldspar surface, leading to steady state dissolution

The above model will result in the formation of a layer composed of Si, O and H, most likely a hydrated silica gel, overlying the fresh feldspar mineral (Chou & Wollast, 1985; Hellmann et al., 2003; Muir et al., 1990). In addition to this gel-layer, Hellmann et al. (2003) suggested an additional layer of clays and/or metal oxy-hydroxides of μm to mm thickness, overlying the silica gel.

2.2.5 Secondary mineral precipitation

As observed by Nugent et al. (1998) dissolution rates obtained in the laboratory are several orders of magnitude higher than those obtained from field data. Part of this discrepancy can be explained by the difference in hydrological conditions in soils and flow-through experiments, as well as the difference in solution saturation. However, the presence of surface coatings by the precipitation of secondary minerals may influence the dissolution rates (Hodson, 2003). Minerals in soils are often coated by clays (Berner & Holdren Jr., 1977; Nugent et al., 1998), organic material and oxyhydroxides of Al, Fe, and Mn. This coating can either be discontinuous (Berner & Holdren Jr., 1977; Nugent et al.,

1998), or continuous. Even if the coating is discontinuous, as a result of its porosity or patchy distribution, it may affect the dissolution of the mineral where this is in contact with the coating rather than with the solution (Hodson, 2003).

Investigation of natural mineral coatings on feldspars (Berner & Holdren Jr., 1977; Nugent et al., 1998) has shown that the weathering of feldspar minerals indeed results in the formation of a patchy hydrous coating consisting of aluminosilicates, e.g. kaolinite or other clay minerals. In spite of the presence of this clay-like coating the underlying feldspar showed the same textural features as laboratory weathered feldspar without a coating. Therefore, Berner and Holdren Jr. (1977) concluded that it is unlikely that the presence of this coating inhibited dissolution. However, they did not take into account the possibility that the observed dissolution textures, e.g. etch pits, could either have developed before the precipitation of the coating, or just developed more slowly below the coating (Hodson, 2003).

To investigate the effect of coatings on the dissolution rate of feldspar under conditions where effect of solution saturation state can be discounted Hodson (2003) studied the dissolution behaviour on anorthite in the presence of a, laboratory produced, Fe-rich coating. He concluded that the formed coating was porous, containing both meso- and micropores, and that this porous coating of secondary minerals did not inhibit the dissolution of the feldspar mineral, as the obtained dissolution rates were in the same order of magnitude as those for uncoated minerals. However, this also means that the presence of porous surface coatings on minerals does not explain the observed discrepancy between mineral dissolution rates obtained in the field and those in the laboratory.
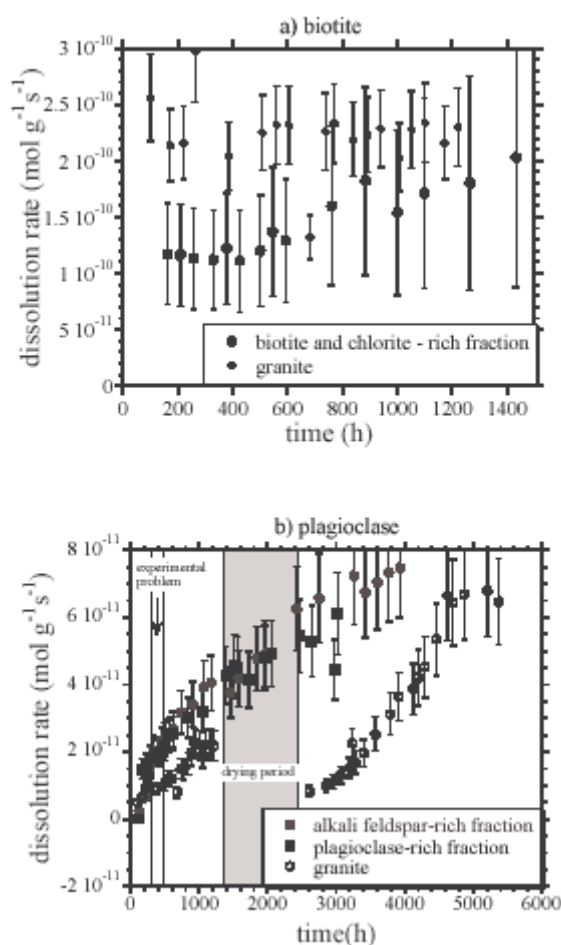

Fig. 9 Comparison of the calculated dissolution rates of a) biotite, b) plagioclase, and c) microcline during the dissolution of the bulk granite to those rates during the experiments of the mineral-rich fractions *(Ganor et al., 2005)*.

A similar study was performed on anorthite (Murakami et al., 1998), but with different secondary mineral precipitates; boehmite, "modified" boehmite, and kaolinite, which are reaction products derived from the dissolving feldspar. Though their obtained dissolution rates were in the same order of magnitude as those for uncoated minerals, they concluded, on the basis of calculated Gibbs free energies for anorthite dissolution, that the precipitation of secondary minerals promoted dissolution. They stated that, even though the dissolution rate decreased as a result of precipitation, the formation of the coating required elements present in solution, thereby reducing the saturation state of the fluid, and hence, promoting more dissolution of the feldspar.

2.2.6 Mineral vs. rock dissolution

At present almost all dissolution experiments have been performed on unconsolidated, single mineral samples, though it is to be expected that dissolution rates of minerals in consolidated, polymineralic rocks are different from those derived in the laboratory. In addition, most experiments

14

used very pure, cleaned samples, when, in nature, minerals are usually coated by secondary minerals, as was discussed earlier.

Ganor et al. (2004) acknowledged this gap in the available literature and therefore compared dissolution rates of minerals in bulk granite to those of the same minerals in mineral-rich fractions that were separated from the granite; plagioclase and biotite/chlorite. Any iron oxide coatings, present on the samples beforehand, were not removed as they were considered a feature of many rock samples. In addition, the samples were also subjected to repeating wetting and drying, simulating the natural wetting and drying cycles rocks are exposed to.

Comparison of the obtained dissolution rates for the various minerals in the bulk granite and mineral-fractions are shown in Fig. 9 (Ganor et al., 2005). Dissolution of the biotite/chlorite in the mineral fraction was significantly different from that in the biotite/chlorite bulk granite, as can be seen in Fig. 9a. The differences in dissolution rates are the result of differences in solution saturation, as the amount of biotite/chlorite in the mineral fraction is approximately 20 times higher than that in the bulk granite, i.e. the biotite/water ratio is higher. Therefore, the concentrations of the major elements in solution in the former experiment are higher, and hence, the dissolution rate is inhibited.

Plagioclase dissolution rates are depicted in Fig. 8b and show slower dissolution rates for the granite compared to the mineral fraction. Initially, an iron oxide coating on grain surfaces inhibited the dissolution of plagioclase. As the iron coating dissolved, and hence grew thinner, the plagioclase dissolution rate increased almost linearly. The iron concentration in solution in the bulk granite experiment was significantly higher than that in the mineral-rich experiments, due to the dissolution of the present biotite. Therefore, the removal of the Fe-rich coatings from grains in the granite sample was slower, and, as a result, the increase in dissolution rate of the plagioclase was slower. In contrast to the conclusion of Hodson (2003), the presence of a Fe-rich coating did seem to inhibit feldspar dissolution in this case.

Fig. 10 Comparison of the ratio of the release rates of Mg/(Mg + Na) during the dissolution of the bulk granite (closed circles) to the stoichiometric ratio in its constituent minerals (horizontal lines) *(Ganor et al., 2005).*

Wetting and drying of the samples also appeared to have significant influence on the dissolution rates of the various minerals in the bulk granite (Fig. 9b). As the release rates of Mg and Na are controlled by the dissolution rate of biotite and plagioclase, respectively, the relative release rate of the two can be used to examine the relative dissolution rate of both minerals during the dissolution of granite, as seen in Fig. 10. Dissolution with a molar $Mg/(Mg + Na)$ ratio close to 1 implies dissolution of biotite, while a molar ratio closer to 0 means more plagioclase dissolution. It is clear from Fig. 10 that the initial dissolution of the bulk granite is biotite/chlorite-dominated, but with time there is a transition to more plagioclase-dominated dissolution. Also evident is that the dissolution rate of biotite is significantly enhanced as a result of drying, when, in contrast, the dissolution rate of plagioclase clearly decreases as a result of drying.

In summary, from this study it is evident that the dissolution rates of plagioclase and biotite/chlorite in the granite are significantly different from those of the constituent minerals in the mineral-fractions, which were separated from the same granite. Both the presence of secondary mineral coatings and the near-equilibrium conditions significantly reduce the dissolution rates in the field, compared to the dissolution rates of clean pure minerals under far from equilibrium conditions. In addition, drying of the samples during the experiments significantly enhanced the dissolution rate of biotite, and decreased the dissolution rate of plagioclase.

2.3 The dissolution of clays

In addition to quartz and feldspar impure sandstones also contain various clays, e.g. montmorillonites, illites, and smectites. The compositions of these clays can vary strongly and it is mainly the Ca-, Mg-, or Fe –rich clays that we are interested in.
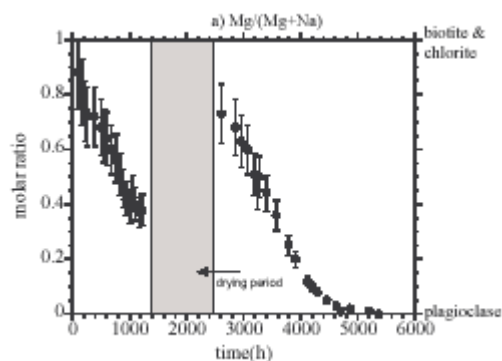
15

2.3.1 Dissolution reactions and equilibrium constants

The wide variation in clay compositions makes it difficult to describe the dissolution, or hydrolysis, of clay in a limited number of reactions and reaction constants, as is the case for quartz and feldspars. No simple dissolution or hydrolysis reaction, similar to the one for feldspar, can be stated for clay, though the products formed are usually aqueous ions, e.g. Ca^{2+}, Na^+, and Mg^{2+}, silicic acid, and various hydroxides, e.g. $Al(OH)_4^-$ and $Fe(OH)_4^-$. Köhler et al. (2003) also observed that the hydrolysis of illite was stoichiometric in the acid (pH < 4) and alkaline (pH > 11) pH range, and non-stoichiometric in the near-neutral (4 < pH < 11) pH range. Cama et al. (2000) observed a similar behaviour for the dissolution of smectite under alkaline conditions.

In addition, the very slow dissolution of clays, and hence the slow approach to a steady state, makes it difficult to determine the solubility and hydrolysis constants for these dissolution reactions, though attempts have been made (Cama et al., 2000). Other approaches to estimate the reaction constants for various compositions of clays are (1) calculating K_{eq} from the Gibbs free energies of formation (Köhler et al., 2003); or, (2) deriving the reaction constant from the ion activity product (IAP) obtained during solubility experiments (Kittrick, 1966; May et al., 1986; Misra & Upchurch, 1976). All data on dissolution and hydrolysis reactions for various types of clay obtained from the literature are summarized in Appendix 1c. As the reactions presented are for a wide composition range all equations are considered to be suitable to calculate the solubility of clay.
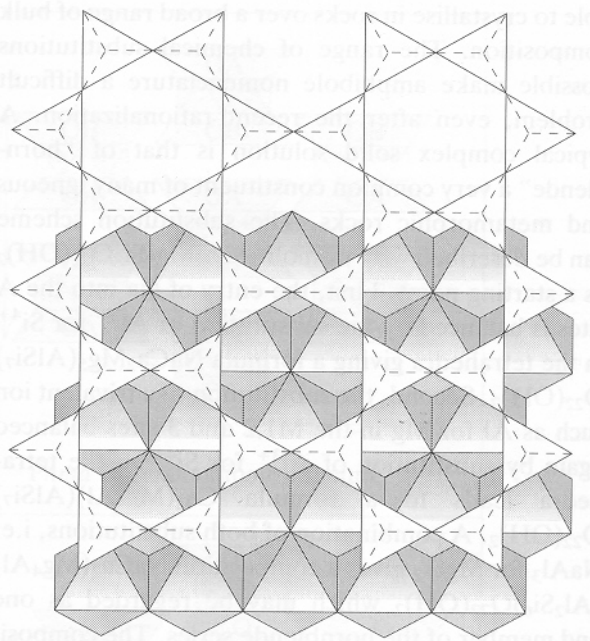

Fig. 11 The way in which a sheet of downward pointing tetrahedra links to an octahedral sheet below *(Putnis, 1993)*.

2.3.2 Dissolution rates

The same methods as those for quartz and feldspar dissolution were used for the determination of reaction rates of dissolving clays: (1) batch experiments (Bauer & Berger, 1998; Huertas et al., 2001; Köhler et al., 2003; Zysset & Schindler, 1996); (2) flow-through experiments (Ganor et al., 1995); or, (3) both batch and flow-through experiments (Cama et al., 2000). Concentration vs. time plots for various elements were used to derive reaction rates. All measured reaction rates for various pH and temperature conditions are plotted in a graph, shown in Appendix 4c. Reaction rate-pH graphs, either with (Huertas et al., 2001), or without (Bauer & Berger, 1998; Cama et al., 2000; Ganor et al., 1995; Köhler et al., 2003; Zysset & Schindler, 1996) data from other authors, were used to derive reaction rate equations as a function of pH (Appendix 3c).

The dissolution of clay minerals proceeds in a similar manner as the dissolution of feldspar minerals, though the rates are two orders of magnitude lower than those for feldspar dissolution. Even though the compositions of the various clay minerals may differ, the dissolution mechanism is most likely similar, as was also seen for feldspar minerals of different composition. Also, the same pH regions, that can be discerned for feldspar dissolution, can be distinguished for clay dissolution: 1) a dissolution rate minimum at near-neutral pH, together with incongruent dissolution, and 2) strong pH dependent congruent dissolution at more acid or alkaline pH. Similar to feldspars, clay dissolution rates become more pH dependent at higher temperatures. Though the dissolution rates for clay are slower than those for feldspar, less energy is required to activate the reactions, ~ 50 kJ/mol and ~ 80 kJ/mol at acid, or alkaline, conditions.

In contrast to feldspar research, only little attention has been paid to other factors affecting the dissolution rates of clays. Cama et al. (2000) suggested that the dissolution rate of smectite might decrease as a result of the degree of saturation or element inhibition, in both cases caused by Si.
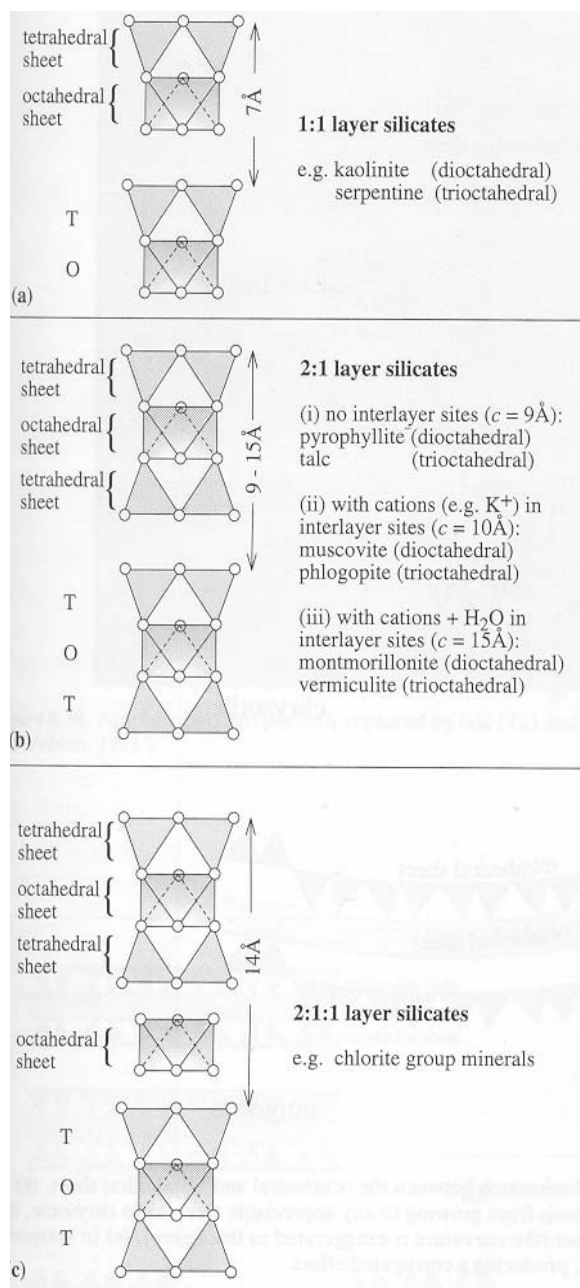
Fig. 12 Schematic representation of the way in which
(a) the 1:1 layer silicates, (b) the 2:1 layer silicates ,
and (c) the 2:1:1 layer silicates are built up from
tetrahedral and octahedral sheets *(Putnis, 1993)*.

Therefore they suggest a Si-inhibited reaction rate, which describes the dissolution rate of smectite as a function of the Si-concentration. Ganor et al. (1995) developed a theoretical model, which accounted for Al-inhibition of the reaction rate. If their model is correct, kaolinite dissolution becomes more pH dependent when Al inhibition occurs. Dissolution of kaolinite in Si and Al doped solutions (Bauer & Berger, 1998) showed that the addition of Al significantly decreased the dissolution rates, however, the addition of Si did not seem to have an effect. In contrast, smectite dissolution was not influenced by the presence of either aqueous Al or Si.

The dissolution rate equations stated in Appendix 3c are mainly incomplete; the best equation to use for our conditions of interest is equation 33, for illite dissolution.

2.3.3 Mechanism of dissolution

Layer silicates are built up from two basic sheets: (1) the SiO_4 tetrahedral sheets, and (2) the edge-sharing octahedral sheet, as shown in Fig. 11. There are three groups of layer silicates: (1) 1:1 layer silicates, e.g. kaolinite; (2) 2:1 layer silicates, e.g. smectite, illite and montmorillonite; and, (3) 2:1:1 layer silicates, e.g. chlorite. The octahedral sheet can be considered to be dioctahedral, when the octahedral sites are occupied by trivalent ions, such as Al^{3+} and Fe^{3+}, or trioctahedral, when the octahedral sites are occupied by divalent ions, such as Mg^{2+} and Fe^{2+}. The layer silicates are built up from different stacking combinations of the two basic sheets, as seen in Fig. 12 (Putnis, 1993).

The basic principle for clay dissolution is the same as that for quartz and feldspar: the formation of Al- and Si-surface complexes, resulting in preferential removal of Al in acid environments, and of Si in alkaline environments (Carroll & Walther, 1990). Most likely the breaking of, the weaker, Al-O-Si bonds also controls dissolution of clays, similar to the dissolution of feldspar. Structural differences among different layer silicates may explain the observed differences, several orders of magnitude, in dissolution rates. In contrast to kaolinite, the aluminous octahedral layer in smectite is bonded to two silica rich tetrahedral layers. The accessibility of water to the, weaker, Al-O or Al-OH bonds is limited to the edges of the particles until the tetrahedral layers are dissolved. Therefore, the dissolution of smectite can be considered to be a serial process, with the rate-limiting step being the dissolution of the tetrahedral layers. In contrast, the dissolution of kaolinite is a parallel process, with the dissolution of the octahedral layer being the rate-limiting step as the partial hydrolysis of Si, resulting from the dissolution of the octahedral layer, most likely promotes the dissolution of the tetrahedral layer, this step being non rate-limiting.

Ganor et al. (1995) suggested a reaction mechanism for kaolinite that consisted of a sequence of slow hydrogen ion mediated hydrolysis steps. In their model (Fig. 13) the release of Al and Si takes place after the sequential clipping of the covalent bonds anchoring them to the surface. An important

assumption made is that the rate-limiting step is the breakdown of the Al-O-Si bonds; therefore implying that breaking of these bonds is a slow process, which is in contradiction with the observation made by Hamilton et al. (2001). After the breaking of these bonds the breaking the other Al-O-Al and Si-O-Si bonds are much easier ruptured, leading to the release of Al^{3+} and H_4SiO_4 into solution. As this process of proton adsorption and rupture of Al-O-Si bonds is repeated numerous time on the kaolinite surface it will eventually lead to the "unzipping" of the octahedral and tetrahedral sheets.
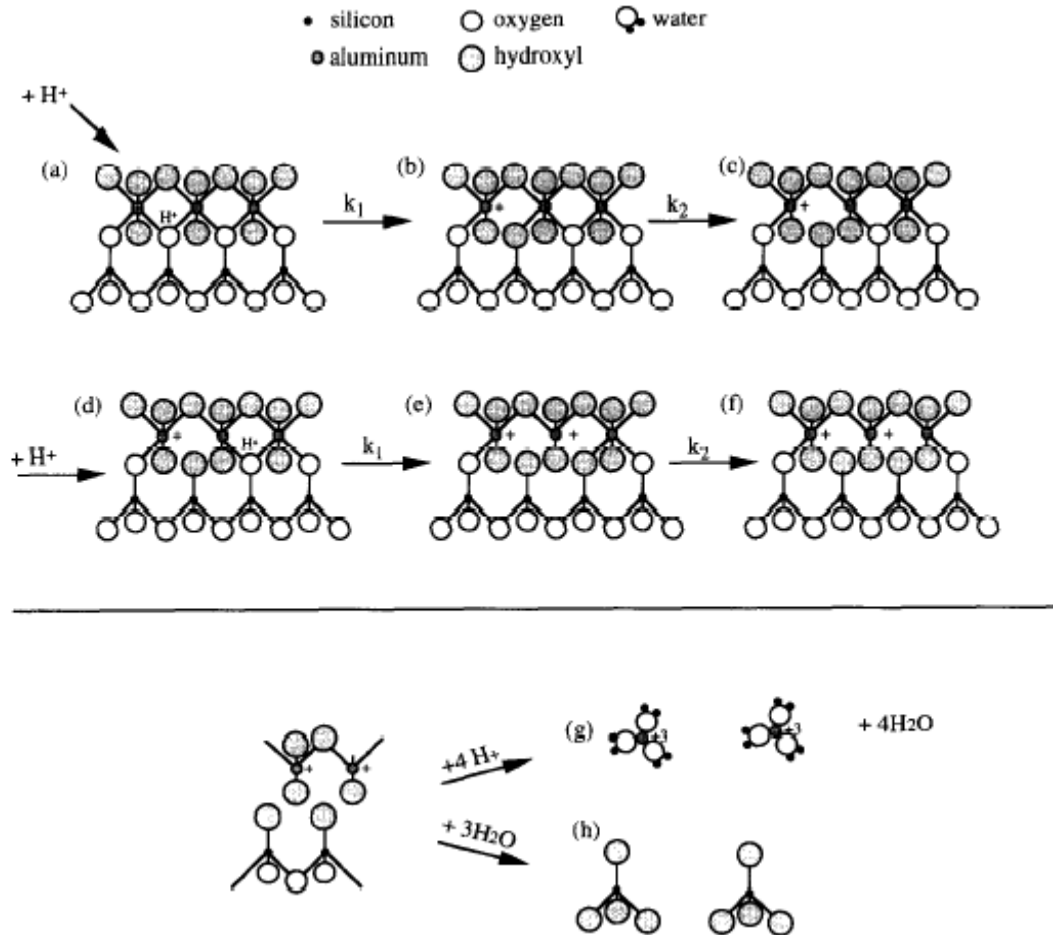
Fig. 13 Sequence of steps in the proposed model for the kaolinite dissolution reaction *(Ganor et al., 1995)*.

3 Thermodynamic data

In addition to the equilibrium constants and kinetic data presented above, an inventory has been made on the available thermodynamic data for the principal clastic rock-forming minerals, i.e. quartz, feldspars and clays, as well as the formed products, i.e. carbonates and kaolinite, CO_2, H_2O, and common aqueous ions (App. 5 and 6). From the available standard Gibbs free energy, enthalpy and entropy data it is possible to estimate equilibrium constants for reactions, which are not considered in the literature, or occur at temperatures deviating from room temperature.

Determination of thermodynamic properties of minerals can be approached in various ways. The most common one is calorimetric heat measurement (Arnórsson & Stefánsson, 1999); and references therein), which is used to determine the standard enthalpy of formation and heat capacity of a mineral. As heat is released during exothermic reactions, and heat is consumed in endothermic reactions, either by reaction, state transition or mixing of substances, this heat development can be measured using a calorimeter. The simplest heat measurement involves the temperature change in a fixed volume of fluid, with known heat capacity, during an exothermic or endothermic process. The accuracy of the

measurement depends on the assumption that all heat produced is transferred into, or out of, the fluid in which the temperature change is measured, no heat is lost to the environment or absorbed by the container. The amount of heat given of by the source can be very accurately measured in this way. After determining the standard free enthalpy of formation by calorimetry, and calculating the standard entropy of formation from the elements, the standard Gibbs free energy of formation can be calculated by using

$$\Delta G^0_{f,T_r,P_r,i} = \Delta H^0_{f,T_r,P_r,i} - T\Delta S^0_{f,T_r,P_r,i} \tag{14}$$

Another approach combines data from solubility experiments with already known thermodynamic properties of various substances (Kittrick, 1966; May et al., 1986; Misra & Upchurch, 1976). From the solubility data the solubility constant for dissolution was derived. As K_s is related to the Gibbs free energy of reaction

$$\Delta G^0_r = -RT \ln K_s \tag{15}$$

and, $\Delta G^0_r = -\Delta G^0_f(\text{reactants}) + \Delta G^0_f(\text{products})$ \hfill (16)

The standard Gibbs free energy of formation can be calculated, assuming that the dissolution reaction of the mineral in known. Accuracy depends on the accuracy of the performed dissolution experiments and the chosen data for the formed products.

A third option assumes that minerals are formed by the combination, or "polymerisation", of simple hydroxides or oxides (Mattigod & Sposito, 1978; Nriagu, 1975). A small correction is made for the change in free energy of the hydroxides and oxides as a result of this polymerisation. The accuracy of this method depends on the accuracy of the standard Gibbs free energies of formation of the (hydr)oxides, though it is shown that there is good agreement between the predicted and experimental values.

The last option considered structural analogue algorithms to provide the best estimates of the standard molal heat capacity, entropy, and volumes (Ransom & Helgeson, 1994). They found that any standard molal thermodynamic property could be expressed as

$$\Xi^\circ = \sum_{i}^{\bar{i}} \hat{n}_i \Xi^\circ_{i,T,P} \tag{17}$$

where, Ξ° represents the appropriate standard molal thermodynamic property of a target mineral at the temperature and pressure of interest, Ξ°_i designates the corresponding standard molal property of the ith species in the analogue reaction, and $\hat{n}_i$ denotes the stoichiometric coefficient of the ith species in the reaction which is positive for products and negative for reactants. Ransom and Helgeson (1994) used this equation to calculate the molal heat capacity, standard entropy, and molar volume of various clay minerals. In addition, they made corrections on the heat capacity and molar volume for the presence of interlayer water.

All data found on the standard Gibbs free energy of formation, standard enthalpy of formation, and standard entropy for quartz, plagioclase feldspars, various clay minerals, calcite, CO_2, and aqueous ions are given in Appendix 5. In addition, Appendix 6 contains all data found on the heat capacity and molar volume of the mentioned species. No recommendations are made on the use of these data, as they do not differ much among various authors.

4 Thermodynamic properties of CO₂ and H₂O

For completeness existing data is also given here on the thermodynamic properties of carbon dioxide and water. Of crucial importance to our experimental programme, as described below, is to accurately know the molar volume of the two substances at various temperatures and pressures (P-V-T relations or equations of state), as well as their phases. The latter can be derived from so–called phase diagrams, which are shown for both H_2O and CO_2 in Fig. 14. The PT conditions for the critical point of both substances are given in Table 2. Beyond the critical point carbon dioxide and water become supercritical, a phase which is neither liquid, nor gas.

It has proven to be difficult to find Equations of State (EOS) that accurately describe the molar volume of CO_2 and H_2O at the pressures and temperatures of interest. The Redlich-Kwong equation often used (Kerrick & Jacobs, 1981) does not apply well to the experimental range of PT conditions. Other equations that have been used to calculate the molar volume of carbon dioxide (Duan et al., 1992; Span & Wagner, 1996) and water (Duan et al., 1992) have proven to work well for CO_2, but not for H_2O. In the future more research will be done in order to obtain equations that are more accurate.

Table 2 The critical properties of CO_2, and H_2O

component	CO_2	H_2O
T_c (°C)	31.05	374.1
P_c (bar)	73.825	221.19

5 Recommendations on the use of the data

As seen in the appendices the amount of data available for some minerals is very limited, usually only one reaction or equation is given, which is not always complete, e.g. missing reaction rate constants or other variables. When nothing is known for a given mineral one should go for the "next-best-thing", e.g. no reaction rate is given for labradorite so one could use either a dissolution rate for albite, or the equations given by Casey et al., (1991). In the previous sections recommendations have been made on the choice of the available data. In the following a preliminary model will be derived to estimate the rate and extent of carbonate precipitation. We will restrict the discussion to anorthite-rich sandstone, as that is the mineral of interest in our first series of experiments.

5.1 Conditions allowing calcite precipitation

The precipitation of calcite, or other carbonates, is limited by various conditions: (1) the anorthite content; (2) the water content; and, (3) the carbon dioxide pressure. It is safe to assume that CO_2 will be added in sufficient amounts and therefore, the extent of CO_2 sequestration will depend on the availability of anorthite and water. When either one of the two runs out, the process will come to a halt and a new equilibrium will be established. However, excess carbon dioxide will strongly influence this equilibrium, or even already the precipitation of carbonate, as the dissolution of carbon dioxide results in acidification of the system. When the acidity is too high, calcite will dissolve again when the sequestration process comes to a halt, or, it may even not precipitate at all, if the driving force for precipitation cannot overcome that for dissolution. In the future a careful analysis of the chemical system will be made in order to identify the range of conditions in which calcite precipitation can take place.

5.2 Likely rate-limiting step in CO_2 sequestration

Predictions have been made, in the literature and by the author, on the expected order of magnitude of the reaction rate, which depends on the rate-limiting step in the system. The precipitation of carbonate relies on the availability of Ca^{2+} and CO_3^{2-}, or HCO_3^-, which in turn relies on the dissolution of feldspar, the calcium source, and the dissolution of CO_2, which provides the carbonate or bicarbonate ions, as schematically shown in Fig. 1a. All of the steps, shown in Fig. 1a, either for the dissolution of CO_2 or the dissolution of feldspar, can be rate-limiting, including the precipitation of carbonate. Previous experiments with CO_2 (Czernichowski-Lauriol et al., 1996) have shown that the dissolution of carbon dioxide at high pressure is a rather fast process, therefore, the formation of CO_3^{2-} and HCO_3^- is not considered to be rate limiting. However, it is possible that carbon dioxide dissolution is rate limiting, as the contact area of the carbon dioxide with the pore water is significantly different in nature compared with a laboratory set-up. In a laboratory set-up CO_2 can usually dissolves into the reacting fluid across a fairly large contact area, which makes it possible for dissolution to be fast. However, in a reservoir the dissolution of carbon dioxide can be rate-limiting in various ways, mainly as an effect of the contact area between the gas phase and the fluid phase: (1) pores are only partially filled with water, which makes it easy for the CO_2 to spread through the system, but only little CO_2 can dissolve at a time; (2) the pores are completely filled with water, which prevents the CO_2 from entering the pores and dissolve there, but instead it dissolves at the injection well and diffuses its way through the system; and, (3) CO_2 spreads through the system parallel to fractures, or layering, and diffusion controls further spreading. However, for now it is assumed that carbon dioxide dissolution is not the
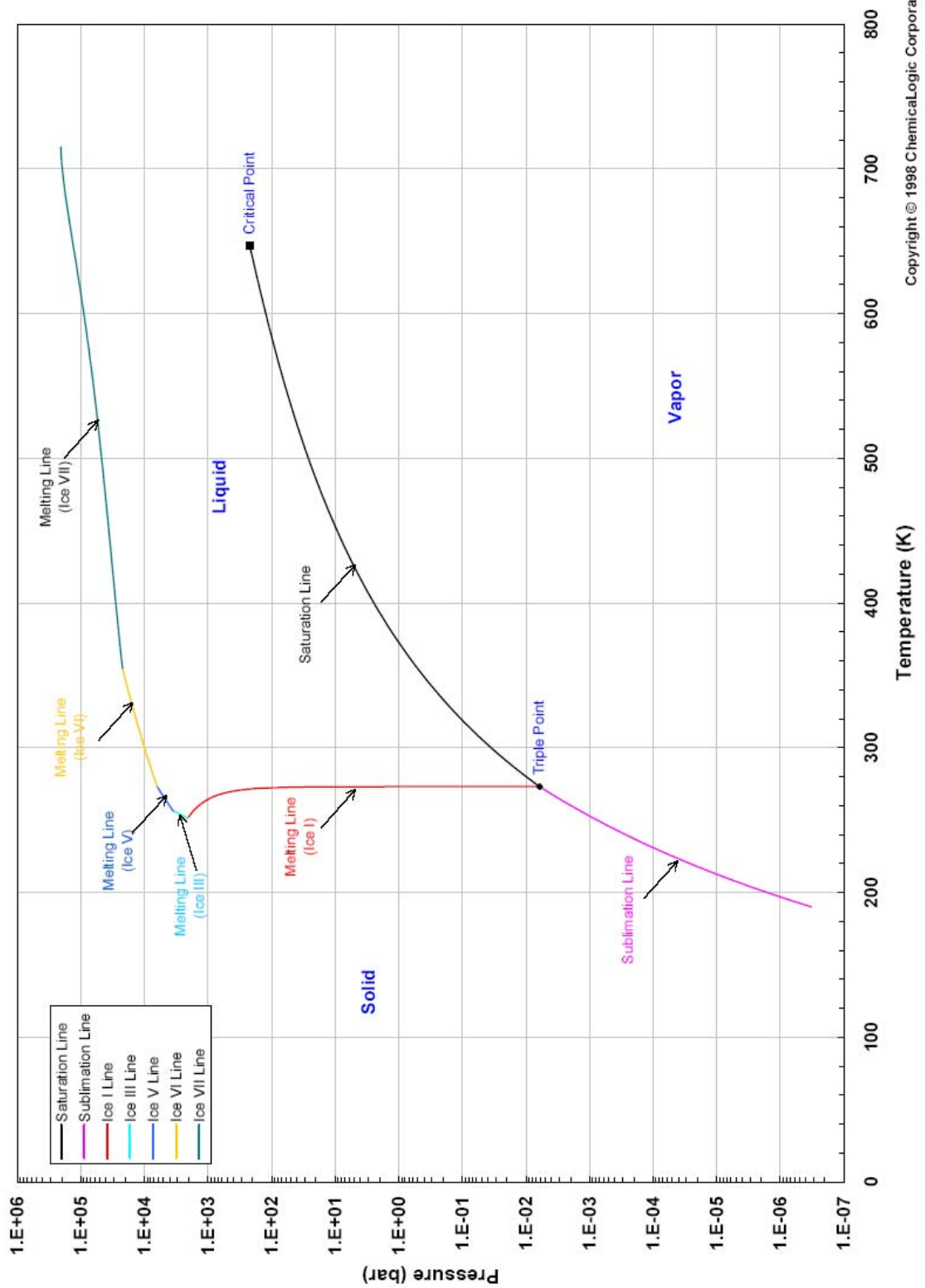
Fig. 14a Phase diagram for water showing the various phases of water at given pressures and temperatures *(ChemicaLogic Corporation, drawn with SteamTab).*

rate-limiting step in the process, which leaves us with the dissolution of feldspar or the precipitation of carbonate, or both, as the rate-limiting step(s).
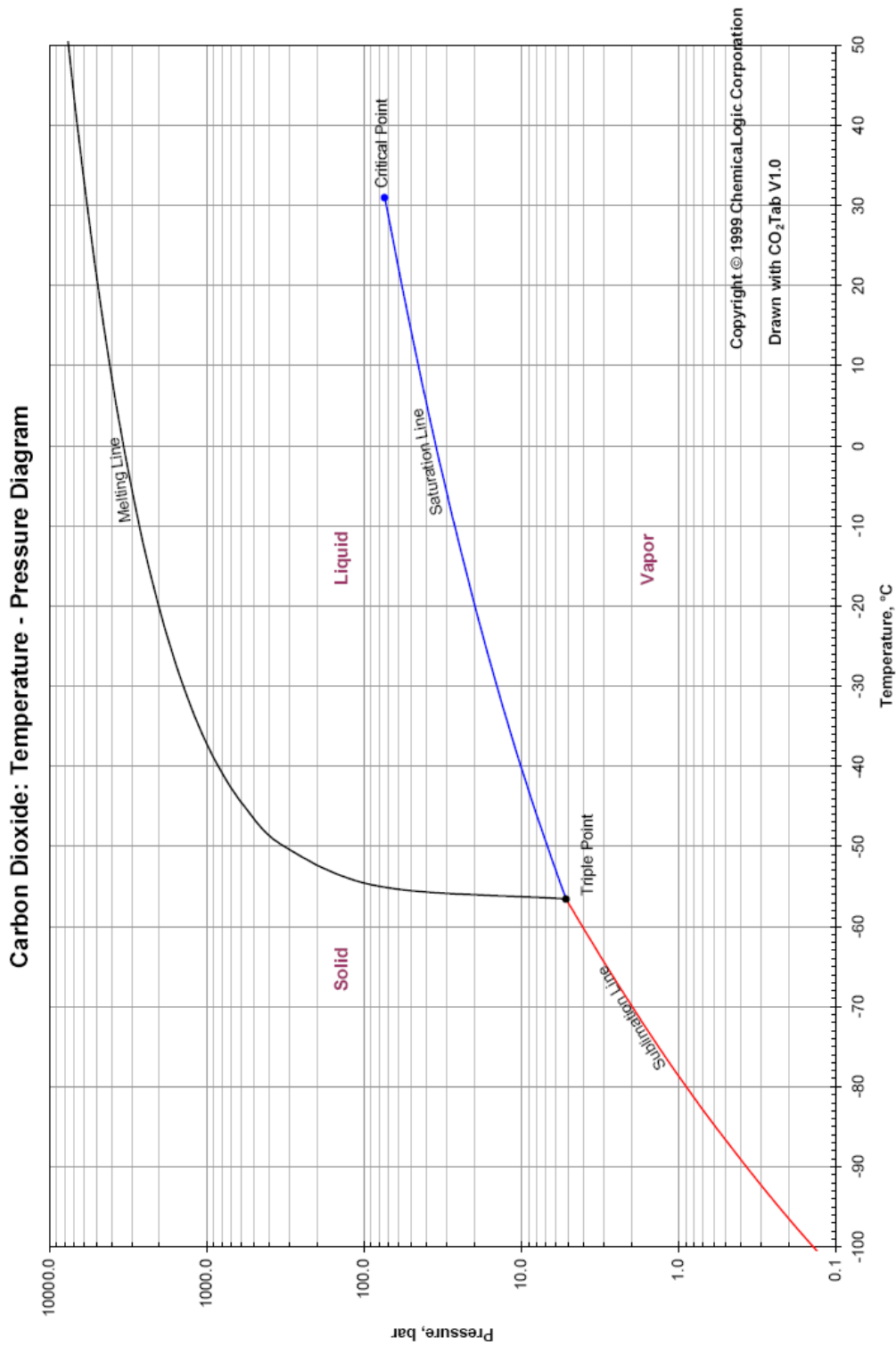
Fig. 14b Phase diagrams for carbon dioxide showing the various phases of CO_2 as a function of pressure and temperature *(ChemicaLogic Corporation, drawn with CO₂Tab)*.

At a CO_2 pressure of 15 MPa we calculated that the pH of the pore water would be ~ 3.1, and would not differ much over a considerable temperature range. Sorai et al. (2003) obtained similar values for solution pH, 3.1 to 3.2, at temperatures of 25° to 80°C, and at a $P(CO_2)$ of 10 MPa. Using the calculated value for the pH plus the reaction rate equations of Casey et al. (1991) and Hellmann (1994) (equations 18a and 29, App. 3b), the dissolution rates of albite and anorthite were calculated at various temperatures and compared to those obtained in other dissolution experiments at elevated CO_2 pressure (Sorai et al., 2003) (Fig. 15). In the temperature range 25° to 100°C the dissolution rate of feldspar, at pH 3, will be in the order of 10^{-9} to 10^{-8} mol/m^2 s.

A similar calculation was performed to determine the precipitation rate of calcite, assuming the system to be at equilibrium. In total two calculation were performed: (1) assuming an infinite anorthite source; and, (2) assuming a finite anorthite source, being a sandstone containing 20 vol.-% of anorthite and 50% porosity, completely water saturated. In order to calculate the calcium concentration at equilibrium for the first situation, the equilibrium constant for the dissolution of anorthite in acid was used (equation 22, App. 1b). In the second scenario, it was assumed that at equilibrium all feldspar present in the rock was dissolved into the pore water. From these values and the H^+, HCO_3^- and H_2CO_3 concentrations, obtained from the pH calculation, the precipitation rate of calcite was calculated using the stated rate equation by Plummer et al. (1978). In both cases calcite precipitation proved to be non-rate-limiting. So, in summary, it is predicted that the reaction rate of reaction (3) will be in the order of 10^{-8} to 10^{-9} mol/m^2 s, with feldspar dissolution most likely being the rate-limiting step.

Fig. 15 Comparison between the dissolution rates of albite and anorthite at various temperatures, at pH ~ 3 *(after Sorai et al., 2003).*

5.3 Preliminary model for CO_2 fixation in feldspathic sandstone

The data presented above can be used to derive equations that relate

- the anorthite dissolution rate to the rate of carbonate precipitation per cubic meter of feldspar-rich sandstone rock per second, and
- the total amount of carbonate formed to the available amount of anorthite, or water content.

In order to do so several assumptions have to be made: (1) all feldspar dissolves into the pore water; and, (2) the rate of CO_2 dissolution is not influenced by the contact area of carbon dioxide with the pore fluid.

5.3.1 Rate of carbonate precipitation

Consider a cubic meter of anorthite-rich sandstone rock with a given porosity φ, a constant grainsize d, and containing X volume-% of anorthite. Reaction of this rock with CO_2 can be described by the following reaction

$$CaAl_2Si_2O_{8\,(s)} + CO_{2\,(g)} + 2\,H_2O_{(l)} \leftrightarrow CaCO_{3\,(s)} + Al_2Si_2O_5(OH)_{4\,(s)} \qquad (3)$$

The reaction rate of this reaction is given as follows

$$R = k_+ a_{anorthite} a_{CO_2} a_{H_2O}^2 - k_- a_{calcite} a_{kaolinite} \quad [mol/m^2 s] \quad (18)$$

where, k_+ and k_- are the forward and backward reaction rate constants, respectively, and a_i is the activity of species i. The reaction rate predicts that the amount of carbonate formed depends on the total grain surface area of anorthite involved in reaction. The total grain surface area of anorthite, A_s, per m^3 of sandstone rock is given as

$$A_s = N_{grains} A_{grain} \quad [m^2/m^3] \quad (19)$$

where, N_{grains} is the number of anorthite grains present per unit volume of rock, and A_{grain} is the surface area of one grain [m^2]. The number of anorthite grains in one unit volume of rock can be calculated from the volume-% of anorthite present in the rock. Assuming that all grains are spherical and of equal size N_{grains} can be expressed as

$$N_{grains} = 6 \cdot 10^{15} \left(\frac{m_{anorthite}}{\pi \rho_{anorthite} d^3} \right) \quad [m^{-3}] \quad (20)$$

where, $m_{anorthite}$ is the total mass of anorthite present in a unit volume of sandstone rock [kg], $\rho_{anorthite}$ is the density of anorthite [g/cm^3], and d is the grain size [μm]. The mass of anorthite per unit volume is related to the vol.-%, or actually the volume fraction, of anorthite in the sandstone:

$$m_{anorthite} = 10 \, \rho_{anorthite} X \quad [kg/m^3] \quad (21)$$

The reaction rate predicts that per m^2 of anorthite surface area R moles of Ca^{2+} are released per second. In turn, each mole of Ca^{2+} converts to 1 mole of carbonate. Therefore, the amount of carbonate produced per unit volume of sandstone rock per second, $\dot{M}$, can be described as

$$\dot{M} = \frac{R \, A_s \, m_{calcite}}{1000} \quad [kg/m^3 s] \quad (22)$$

where, m_{CaCO3} is the molar mass of calcite [g/mol].

The only variable left is the total surface area of anorthite involved in reaction, which, in turn, is related to the reactive surface area of each anorthite grain. There are two end-member models to predict the surface area involved in reaction per grain. The maximum surface area model assumes that the whole surface of the grain, including the grain-to-grain contacts, is active during reaction

$$A_{grain, max} = 10^{-12} \pi d^2 \quad [m^2] \quad (23)$$

In contrast, the minimum surface area model assumes that the area at grain-to-grain contacts is excluded from reaction. By using a simple grain contact area equation the minimum surface area can be expressed as

$$A_{contact} = \frac{4\pi r^2}{N} (1 - 2\varphi) \quad [m^2] \quad (24)$$

where, N is the coordination number, and r is the radius of the grains.

$$A_{grain, min} = A_{grain, max} - A_{contact}$$
$$A_{grain, min} = 10^{-12} \pi d^2 \left(1 - \frac{1 - 2\varphi}{N} \right) \quad [m^2] \quad (25)$$

Now two equations can be derived to quantify the minimum and maximum amount of carbonate that can precipitate in one cubic meter of feldspar-rich sandstone rock per second

$$\dot{M}_{\text{max}} = 60\left(\frac{X\,\text{R}(P_{\text{CO}_2},T)\,m_{\text{calcite}}}{d}\right) \qquad [\text{kg/m}^3\text{s}]$$

$$\dot{M}_{\text{min}} = 60\left(\frac{X\,\text{R}(P_{\text{CO}_2},T)\,m_{\text{calcite}}}{d}\right)\left(1-\frac{1-2\varphi}{N}\right) \qquad [\text{kg/m}^3\text{s}] \qquad (26\text{a,b})$$

The dependence of the rate of reaction, R, on temperature and pressure, can be expressed as follows:

$$\text{R} = \text{k}_+ a_{\text{anorthite}} a_{\text{H}_2\text{O}}^2 \phi_{\text{CO}_2} P_{\text{CO}_2} - \text{k}_- a_{\text{calcite}} a_{\text{kaolinite}} \qquad [\text{mol/m}^2\text{s}] \qquad (27)$$

and k has a temperature dependence, according to Arrhenius relationship; $\text{k} = Ae^{-\text{E}_\text{a}/\text{R}T}$

where, ϕ_{CO_2} is the fugacity coefficient of CO_2, P_{CO_2} is the CO_2 pressure, A is a pre-exponential frequency factor, R is the universal gas constant, E_a is the activation energy for the forward/backward reaction, and T is the temperature. At a later stage equation 26 can be expressed as a function of feldspar composition, or anorthite content, and as a function of time, since the surface area of the grains will decrease with time, as a result of reaction.

5.3.2 Extent of calcite precipitation

If the total amount of carbonate, which is formed in one cubic meter of rock, is known the time needed to precipitate that amount can be predicted. The total amount of $CaCO_3$ that can be precipitated depends on the availability of anorthite and the water content of the system, the reaction will come to a halt when either one is depleted. Taking this into account an equation can be derived which can calculate the maximum amount of carbonate that can precipitate, as a function of either the anorthite or water content.

$$M_{\text{T,anorthite}} = \text{N}_{\text{anorthite}}^{\text{moles}} m_{\text{calcite}} = \frac{10\,\rho_{\text{anorthite}}\,m_{\text{calcite}}\,X}{m_{\text{anorthite}}} \qquad [\text{kg/m}^3]$$

$$M_{\text{T,H}_2\text{O}} = 0.5\,\text{N}_{\text{water}}^{\text{moles}} m_{\text{calcite}} = \frac{5\,\rho_{\text{H}_2\text{O}}\,m_{\text{calcite}}\,W}{m_{\text{H}_2\text{O}}} \qquad [\text{kg/m}^3] \qquad (28\text{a,b})$$

where, $M_{\text{T,i}}$ is the total amount of calcite formed per unit volume of sandstone rock, either as a function of anorthite or as a function of water content, N^{moles} is the number of moles of water, or anorthite, per unit volume of sandstone rock, ρ_i is the density of species i [g/cm^3], m_i is the molar mass of species i [g/mol], and X and W are the vol.-% of anorthite and water, respectively.

The choice of equation depends on the availability of anorthite and water; the one that runs out first controls the amount carbonate that precipitates. Reaction (3) requires one mole of anorthite and two moles of water to form one mole of calcite, hence the following holds:

if, $\dfrac{\text{N}_{\text{anorthite}}^{\text{moles}}}{\text{N}_{\text{water}}^{\text{moles}}} \geq 0.5$: the water content limits the amount of calcite formed

and if, $\dfrac{\text{N}_{\text{anorthite}}^{\text{moles}}}{\text{N}_{\text{water}}^{\text{moles}}} \leq 0.5$: the anorthite content limits the amount of calcite formed

When the ratio is equal to 0.5 both anorthite and water will run out at the same time, and hence, both will be the limiting factor.

This ratio can also be expressed as a function of the anorthite and water content of the sandstone rock:

$$\left(\frac{\rho_{\text{anorthite}}\,m_{\text{water}}}{\rho_{\text{water}}\,m_{\text{anorthite}}}\right)\frac{X}{W} = 0.5 \qquad (29)$$

a

Instron loading frame

load cell

pressure transducer

compression of CO2 from
65 to 150 bar

Monel vessel

CO2
P = ~ 65 bar

N2
P = 150 bar

b

pore fluid in/outlet

top piston

compaction vessel

Teflon jacket

porous plates

sand sample
(diameter ~ 20 mm)

top segment
bottom piston

lower segment
bottom piston

pore fluid in/outlet
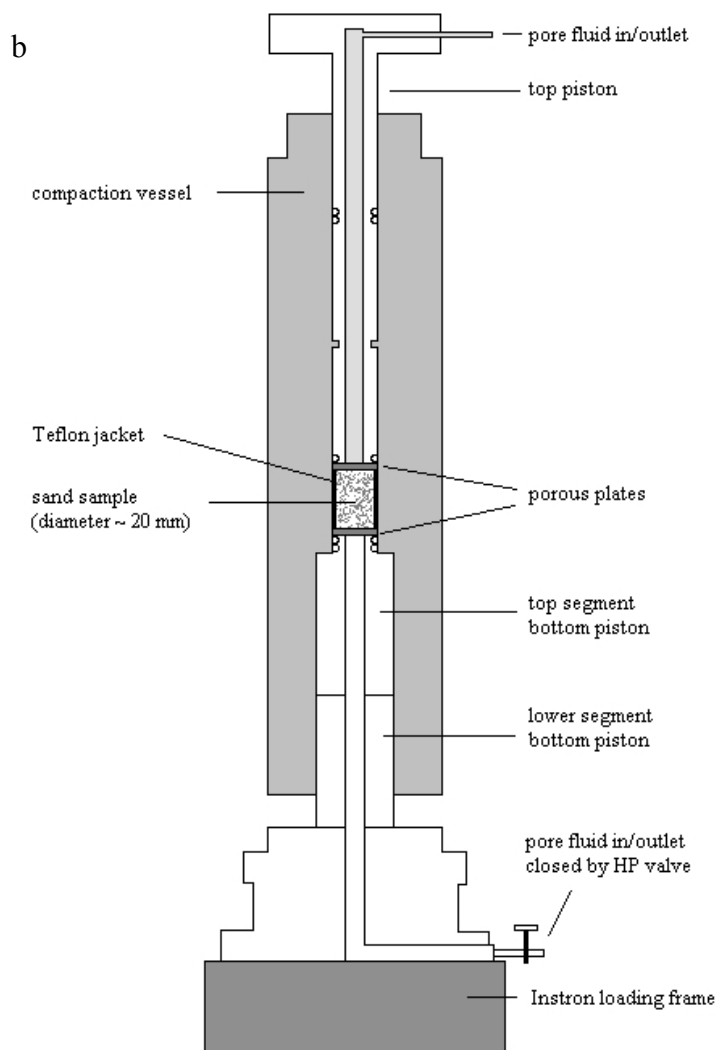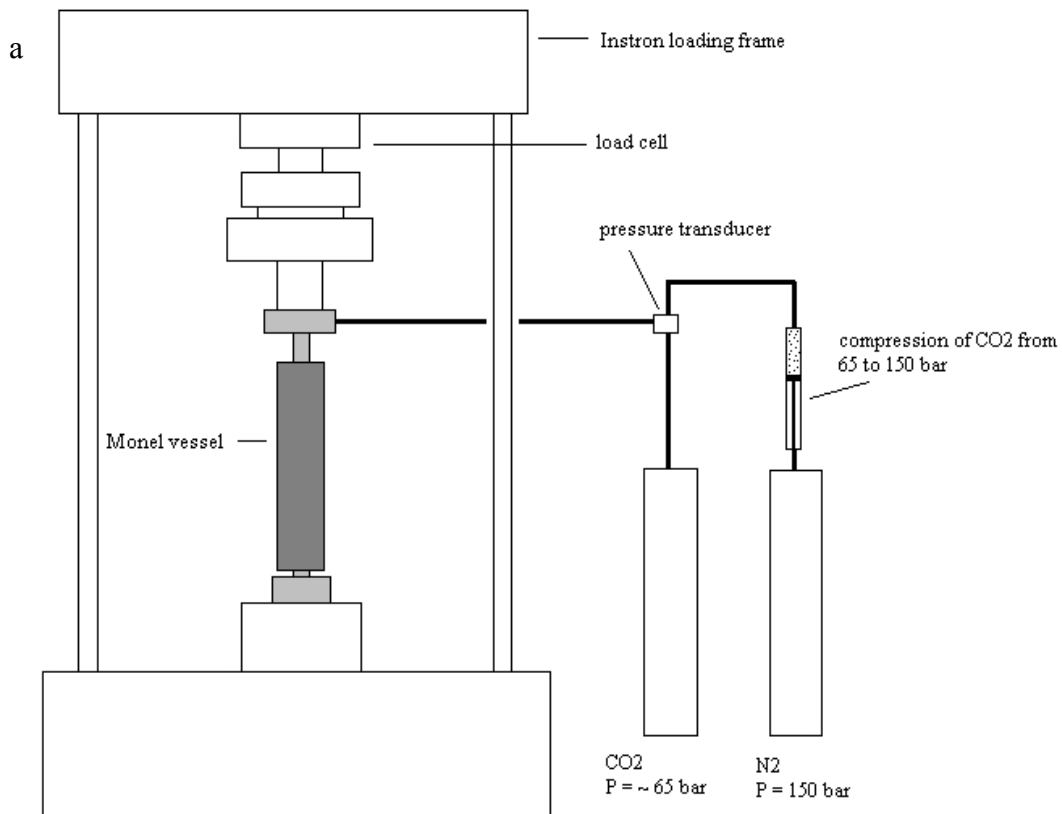closed by HP valve

Instron loading frame

Fig. 16 a) Overview of the experimental set-up showing the location of the Monel reaction vessel in the Instron loading frame and the carbon dioxide pressure control. b) Schematic diagram showing the reaction vessel used in the reaction rate experiments.

26

The density of water varies with pressure and temperature, as can be seen in pressure-temperature-density graphs given in the literature (Fisher, 1976). However, under the conditions considered for CO_2 sequestration (P < 500 bar, T < 100°C) this variation is less than 0.05%. Therefore, the density of water is considered to be constant at a value of 0.98 g/cm³. The density of anorthite is taken to be 2.75 g/cm³, the molar masses of water and anorthite are 18.02 g/mol and 277.41 g/mol, respectively. Taking these values into account, the ratio between the anorthite and water content predicts the following:

$$\text{if, } \frac{X}{W} \geq 2.74 : \text{the water content is the limiting factor} \rightarrow \text{use equation 28b}$$

$$\text{or if, } \frac{X}{W} \leq 2.74 : \text{the anorthite content is the limiting factor} \rightarrow \text{use equation 28a}$$

By using equations 26 and 28 it is possible to make an estimate of the reaction time of reaction (3), or, in other words, the time it will take for the maximum amount of calcite to be precipitated, and the maximum amount of CO_2 is sequestered as carbonate.

6 Planned experiments: design

The equations available in the literature are not sufficient to make adequate calculations in the experimental range we are interested in. Therefore, a new experimental set-up has been designed in order to determine reaction rates at elevated temperature and carbon dioxide pressure.

During the first series of experiments that will be performed the reaction rate of the following reaction will be determined

$$CaAl_2Si_2O_{8\,(s)} + CO_{2\,(g)} + 2H_2O_{(l)} \leftrightarrow CaCO_{3\,(s)} + Al_2Si_2O_5(OH)_{4\,(s)} \qquad (3)$$
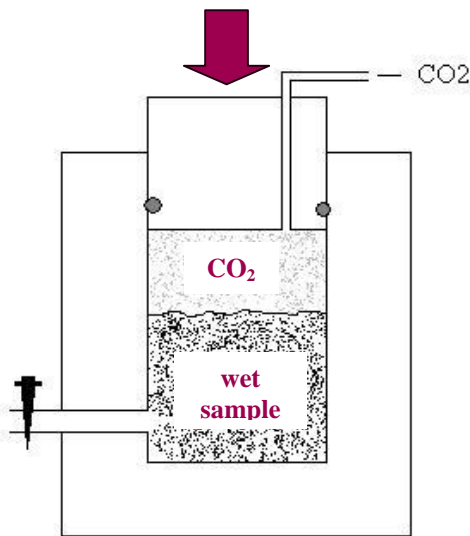

Fig. 17 Schematic blow-up of the reaction vessel, as set-up for reaction rate experiments.

The method used will not be the one that is commonly adopted: solubility experiments, either in a batch or flow-through reactors, with occasional fluid sampling. Instead, a servo-controlled loading machine, or Instron, will be used. A schematic representation of this machine, and its reaction vessel, are shown in Fig. 16. The reaction vessel consists of a free-moving top piston and a fixed bottom piston, both encapsulated by the compaction vessel, with the sample in between. In "load-control" the loading frame will exert a constant load on the sample. When a load is applied to the sample the top piston will start to move when the sample is being compacted under this load. This movement of the top piston can be carefully logged and tracked through time. Usually the Instron is used for compaction creep experiments, however, for the reaction rate experiments it will be used for a quite different purpose.

A schematic blow-up of the set-up of the reaction vessel, for the reaction rate experiments, is shown in Fig. 16. As can be seen the top piston will not exerts any force on the sample, as is usually the case, it will merely be used to keep the CO_2 pressure in the system constant. This will be done as follows: when reaction occurs in the system carbon dioxide, and water, will be consumed, resulting in a reduction of CO_2 pressure, since the loading frame is set to keep the pressure constant, the top piston will be moved into the vessel to correct the pressure drop. The resulting piston displacement, or volume change, will be monitored carefully and is directly related to the reaction rate of anorthite, or consumption rate of CO_2 and H_2O. For now this relationship can be described as

$$R = \frac{\dot{V}}{(A_s C)} \qquad\qquad\qquad (30)$$

where, R is the reaction rate [mol/m^2 s], $\dot{V}$ is the measured volume change with time [m^3/s], A_s is the total surface area of the system [m^2], and C is a constant, as a function of pressure and temperature, which contains the molar volumes of the dissolving and precipitating solids, as well as those of carbon dioxide and water, which are a function of P and T. In a later stage this equation will be expanded to also include the *reactive* surface area of the system, instead of the total surface area, and the change of grain size over time.

7 Conclusions

An extensive review has been made on the data available in the literature on kinetic data, e.g. dissolution reactions, solubility, and reaction rates, and thermodynamic data, e.g. standard Gibbs free energy, enthalpies and entropies, as well as heat capacities and molar volumes. This was done in view of CATO WP 4.1 Subsurface mineralisation, and, therefore, research was focused on the principle clastic rock-forming minerals, i.e. quartz, feldspar and clays, but for completeness also data on the formed products, i.e. kaolinite and carbonates, as well as CO_2, H_2O, and common aqueous species was added. All data is tabled and depicted in the appendices, and recommended reactions and equations are shown in bold. The main findings of this literature research are:

- Regarding quartz dissolution, it was established from the literature that this occurs by a surface-controlled mechanism at solution pH of more than 7.5, at lower pH the dissolution of quartz appears to be pH-independent. The negative surface charge of quartz, at near neutral to basic pH, leads to the formation of siloxane groups, which weaken the structure. Breaking of these Si-O-Si bonds leads to the dissolution of quartz, which is also significantly improved by the addition of cations to the solution. A summary of the dissolution reactions, solubility equations, and dissolution rate equations for quartz were summarised in Appendix 1a, 2, 3a, and 4b respectively. In general, at room temperature and at a pH of 7, the solubility constant for quartz is $10^{-3.96}$, quartz solubility is $\sim$ 11.0 ppm, and dissolution proceeds at a rate of $\sim 10^{-12}$ mol/m^{2}s.

- The dissolution of feldspar appears to be strongly pH-dependent at acid and alkaline pH, and pH-independent at near neutral pH. Also, dissolution rates increase from albite to anorthite, and with increasing temperature. The dissolution mechanism of feldspar is controlled by a surface-controlled mechanism, related to the formation of Al and Si surface groups and the breaking of Al-O-Si and Si-O-Si bonds. In acid environments, leached, or altered layers may be formed, and coatings may be formed on the mineral surface, which also may influence the dissolution rate. All the data on feldspar dissolution reactions and dissolution rates is summarised in Appendix 1b, 3b, and 4b. For anorthite, our feldspar of interest, at room temperature and acid pH, the solubility constant is $10^{14.4}$, and the dissolution rate is $\sim 10^{-12}$ mol/m^{2}s, so one order of magnitude slower than quartz.

- Dissolution behaviour of clay minerals is similar to that of feldspar, so pH-dependent dissolution at acid and alkaline pH, and pH-independent dissolution at near-neutral pH. Though there is a large variation in the composition of clays, dissolution most likely occurs by a similar mechanism, which is related to the tetrahedral and octahedral sheets that form the building blocks of clays. Dissolution of clays is slower than of feldspars by approximately two orders of magnitude. Available reactions and rates are summarised in Appendix 1c, 3c, and 4c. At room temperature and acid pH, the solubility constant of clay may vary between $\sim 10^{-9}$ and 10^{-16}, depending on composition, and the dissolution rate is $\sim 10^{-14}$ mol/m^{2}s.

Though the data available in the literature is not always complete and does not cover our in-situ conditions, preliminary equations have been derived that can be used for estimating the extent and rate of CO_2 sequestration. The maximum, and minimum, amount of carbonate that can precipitate in one cubic meter of anorthite-rich sandstone rock per second is given by:

$$\dot{M}_{\text{max}} = 60 \left(\frac{X \, \text{R}(P_{\text{CO}_2}, T) \, m_{\text{calcite}}}{d} \right) \qquad [\text{kg/m}^3\text{s}]$$

$$\dot{M}_{\text{min}} = 60 \left(\frac{X \, \text{R}(P_{\text{CO}_2}, T) \, m_{\text{calcite}}}{d} \right) \left(1 - \frac{1 - 2\varphi}{N} \right) \qquad [\text{kg/m}^3\text{s}]$$

And, the maximum amount of carbonate that can precipitate, as a function of either the anorthite or water content is given by:

$$M_{\text{T,anorthite}} = \text{N}_{\text{anorthite}}^{\text{moles}} m_{\text{calcite}} = \frac{10 \, \rho_{\text{anorthite}} \, m_{\text{calcite}} \, X}{m_{\text{anorthite}}} \qquad [\text{kg/m}^3]$$

$$M_{\text{T,H}_2\text{O}} = 0.5 \, \text{N}_{\text{water}}^{\text{moles}} m_{\text{calcite}} = \frac{5 \, \rho_{\text{H}_2\text{O}} \, m_{\text{calcite}} \, W}{m_{\text{H}_2\text{O}}} \qquad [\text{kg/m}^3]$$

At a later stage these equations will be expanded to include the feldspar composition, and a time dependence of the grain size.

As the literature does not provide adequate data for estimating the reaction rate of CO_2 sequestration in impure sandstone, a new experimental set-up has been designed in order to determine these reaction rates at elevated temperature and carbon dioxide pressure. Work will begin with determining the reaction rate of a simple system of pure anorthite and carbon dioxide.

References

Amrhein, C. and D. L. Suarez, 1992, Some factors affecting the dissolution kinetics of anorthite at 25°C, *Geochim. Cosmochim. Acta, 56, #*, 1815-1826.

Arnórsson, S. and A. Stefánsson, 1999, Assessment of feldspar solubility constants in water in the range 0° to 350°C at vapor saturation pressures, *Am. J. Sci., 299, #*, 173-209.

Bachu, S., W. D. Gunter and E. H. Perkins, 1996, Chapter 3: Carbon dioxide disposal, *Aquifer disposal of carbon dioxide: hydrodynamic and mineral trapping - proof of concept,*

Bauer, A. and G. Berger, 1998, Kaolinite and smectite dissolution rate in high molar KOH solutions at 35° and 80°C, *Appl. Geochem., 13, # 7*, 905-916.

Berg, A. and S. A. Banwart, 2000, Carbon dioxide mediated dissolution of Ca-feldspar: implications for silicate weathering, *Chem. Geol., 163, #*, 25-42.

Berner, R. A. and G. R. Holdren Jr., 1977, Mechanism of feldspar weathering: some observational evidence, *Geology, 5, #*, 369-372.

Blake, R. E. and L. M. Walter, 1999, Kinetics of feldspar and quartz dissolution at 70-80 C and near-neutral pH: effects of organic acids and NaCL, *Geochim. Cosmochim. Acta, 63, # 13-14*, 2043-2059.

Blum, A. and A. Lasaga, 1988, Role of surface speciation in the low-temperature dissolution of minerals, *Nature, 331, #*, 431-433.

Brady, P. V. and J. V. Walther, 1989, Controls on silicate dissolution rates in neutral and basic pH solutions at 25°C, *Geochim. Cosmochim. Acta, 53, #*, 2823-2830.

Brady, P. V. and J. V. Walther, 1990, Kinetics of quartz dissolution at low temperatures, *Chem. Geol., 82, #*, 253-264.

Cama, J., J. Ganor, C. Ayora and C. A. Lasaga, 2000, Smectite dissolution kinetics at 80°C and pH 8.8, *Geochim. Cosmochim. Acta, 64, # 15*, 2701-2717.

Carroll, S. A. and J. V. Walther, 1990, Kaolinite dissolution at 25°, 60°, and 80°C, *Am. J. Sci., 290, #*, 797-810.

Casey, W. H., H. R. Westrich and G. W. Arnold, 1988, Surface chemistry of labradorite feldspar reacted with aqueous solutions at pH = 2, 3, and 12, *Geochim. Cosmochim. Acta, 52, #*, 2795-2807.

Casey, W. H., H. R. Westrich and G. R. Holdren, 1991, Dissolution rates of plagioclase at pH = 2 and 3, *Am. Mineral., 76, #*, 211-217.

Chou, L. and R. Wollast, 1985, Steady-state kinetics and dissolution mechanisms of albite, *Am. J. Sci., 285, #*, 963-993.

Czernichowski-Lauriol, I., B. Sanjuan, C. Rochelle, K. Bateman, J. Pearce and P. Blackwell, 1996, Chapter 7: Inorganic geochemistry, *The underground disposal of carbon dioxide, JOU2 CT92-0031,* 183-276.

Dove, P., 1994, The dissolution of quartz in sodium chloride solutions at 25° to 300°C, *Am. J. Sci., 294, #,* 665-712.

Dove, P. M. and D. A. Crerar, 1990, Kinetics of quartz dissolution in electrolyte solutions using a hydrothermal mixed flow reactor, *Geochim. Cosmochim. Acta, 54, #,* 955-969.

Dove, P. M. and S. F. Elston, 1992, Dissolution kinetics of quartz in sodium chloride solutions: analysis of existing data and a rate model for 25°C, *Geochim. Cosmochim. Acta, 56, #,* 4147-4156.

Dove, P. M. and C. J. Nix, 1997, The influence of the alkaline earth cations, magnesium, calcium, and barium on the dissolution kinetics of quartz, *Geochim. Cosmochim. Acta, 61, # 16,* 3329-3340.

Duan, Z., N. Moller and J. H. Weare, 1992, An equation of state for the CH_4-CO_2-H_2O system: pure systems from 0 to 1000°C and 0 to 8000 bar, *Geochim. Cosmochim. Acta, 56, #,* 2605-2617.

Fisher, J. R., 1976, The volumetric properties of H_2O - a graphical portrayal, *J. Res. USGS, 4, # 2,* 189-193.

Fleming, B. A. and D. A. Crerar, 1982, Silicic acid ionization and calculation of silica solubility at elevated temperature and pH: application to geothermal fluid processing and reinjection, *Geothermics, 11, # 1,* 15-29.

Fournier, R. O. and R. W. Potter, 1982, An equation correlating the solubility of quartz in water from 25°C to 900°C at pressures up to 10,000 bars, *Geochim. Cosmochim. Acta, 46, #,* 1969-1973.

Ganor, J., J. L. Mogollón and A. C. Lasaga, 1995, The effect of pH on kaolinite dissolution rates and activation energy, *Geochim. Cosmochim. Acta, 59, # 6,* 1037-1052.

Ganor, J., E. Roueff, Y. Erel and J. Blum, 2005, The dissolution kinetics of a granite and its minerals - implications for comparison between laboratory and field dissolution rates, *Geochim. Cosmochim. Acta, 69, # 3,* 607-621.

Gíslason, S. R., P. J. Heaney, E. H. Oelkers and J. Schott, 1997, Kinetic and thermodynamic properties of moganite, a novel silica polymorph, *Geochim. Cosmochim. Acta, 61, # 6,* 1193-1204.

Gunnarsson, I. and S. Arnórsson, 2000, Amorphous silica solubilty and the thermodynamic properties of $H_4SiO_4°$ in the range of 0° to 350°C at P_{sat}, *Geochim. Cosmochim. Acta, 64, # 13,* 2295-2307.

Hamilton, J. P., S. L. Brantley, C. G. Pantano, L. J. Criscenti and J. D. Kubicki, 2001, Dissolution of nepheline, jadeite and albite glasses: toward better models for aluminosilicate dissolution, *Geochim. Cosmochim. Acta, 65, # 21,* 3683-3702.

Hellmann, R., 1994, The albite-water system: part I The kinetics of dissolution as a function of pH at 100, 200, and 300°C, *Geochim. Cosmochim. Acta, 58, # 2,* 595-611.

Hellmann, R., 1999, The dissoluton behaviour of albite feldspar at elevated temperatures and pressures: the role of surface charge and speciation, *Mitt. Osterr. Miner. Ges., 144, #,* 69-100.

Hellmann, R., J.-M. Penisson, R. L. Hervig, J.-H. Thomassin and M.-F. Abrioux, 2003, An EFTEM/HRTEM high-resolution study of the near surface of labradorite feldspar altered at acid pH: evidence for interfacial dissolution-reprecipitation, *Phys. Chem. Minerals, 30, #,* 192-197.

Hodson, M. E., 2003, The influence of Fe-rich coatings on the dissolution of anorthite at pH 2.6, *Geochim. Cosmochim. Acta, 67, # 18,* 3355-3363.

Holdren Jr., G. R. and P. M. Speyer, 1985, Reaction rate-surface area relationships during the early stages of weathering I: initial observations, *Geochim. Cosmochim. Acta, 49, #,* 675-681.

Holdren Jr., G. R. and P. M. Speyer, 1987, Reaction rate-surface area relationships during the early stages of weathering II: data on eight additional feldspars, *Geochim. Cosmochim. Acta, 51, #,* 2311-2318.

Holloway, S., 1996, Chapter 2: Background, *The underground disposal of carbon dioxide, JOU2 CT92-0031,*

Huertas, F. J., E. Caballero, C. Jiménez de Cisneros, F. Huertas and J. Linares, 2001, Kinetics of montmorillonite dissolution in granitic solutions, *Appl. Geochem., 16, #,* 397-407.

Inskeep, W. P., E. A. Nater, P. R. Bloom, D. S. Vandervoort and M. S. Erich, 1991, Characterization of laboratory weathered labradorite surfaces using X-ray photoelecton spectroscopy and transmission electron microscopy, *Geochim. Cosmochim. Acta, 55, #,* 787-800.

Kerrick, D. M. and G. K. Jacobs, 1981, A modified Redlich-Kwong equation for H_2O, CO_2, and H_2O-CO_2 mixtures at elevated pressures and temperatures, *Am. J. Sci., 281, #,* 735-767.

Kittrick, J. A., 1966, Free energy of formation of kaolinite from solubility measurements, *Am. Mineral., 51, #,* 1457-1466.

Knauss, K. G. and T. J. Wolery, 1986, Dependence of albite dissolution kinetics on pH and time at 25°C and 70°C, *Geochim. Cosmochim. Acta, 50, #*, 2481-2497.

Knauss, K. G. and T. J. Wolery, 1988, The dissolution kinetics of quartz as a function of pH and time at 70°C, *Geochim. Cosmochim. Acta, 52, #*, 43-53.

Köhler, S. J., F. Dufaud and E. H. Oelkers, 2003, An experimental study of illite dissolution kinetics as a function of pH from 1.4 to 12.4 and temperature from 5° to 50°C, *Geochim. Cosmochim. Acta, 67, # 19*, 3583-3594.

Mattigod, S. V. and G. Sposito, 1978, Improved method for estimating the standard free energies of formation ($\Delta G^0_{f,298.15}$) of smectites, *Geochim. Cosmochim. Acta, 42, #*, 1753-1762.

May, H. M., D. G. Kinniburgh, P. A. Helmke and M. L. Jackson, 1986, Aqueous dissolution, solubilities and thermodynamic stabilities of common aluminosilicate clay minerals: kaolinite and smectites, *Geochim. Cosmochim. Acta, 50, #*, 1667-1677.

Misra, U. K. and W. J. Upchurch, 1976, Free energy of formation of beidellite from apparent solubility measurement, *Clays Clay Min., 24, #*, 327-331.

Muir, I. J., G. M. Bancroft, W. Shotyk and H. W. Nesbitt, 1990, A SIMS and XPS study of dissolving plagioclase, *Geochim. Cosmochim. Acta, 54, # 2247-2256*.

Muir, I. J. and H. W. Nesbitt, 1991, Effects of aqueous cations on the dissolution of labradorite dissolution, *Geochim. Cosmochim. Acta, 55, #*, 3181-3189.

Murakami, T., T. Kogure, H. Kadohara and T. Ohnuki, 1998, Formation of secondary minerals and its effect on anorthite dissolution, *Am. Mineral., 83, #*, 1209-1219.

Nesbitt, H. W. and I. J. Muir, 1988, SIMS depth profiles of weathered plagioclase and processes affecting dissolved Al and Si in some acidic soil solutions, *Nature, 334, #*, 336-338.

Nriagu, J. O., 1975, Thermochemical approximations for clay minerals, *Am. Mineral., 60, #*, 834-839.

Nugent, M. A., S. L. Brantley, C. G. Pantano and P. A. Maurice, 1998, The influence of natural mineral coatings on feldspar weathering, *Nature, 395, #*, 588-590.

Oxburgh, R., J. I. Drever and Y.-T. Sun, 1994, Mechanism of plagioclase dissolution in acid solution at 25°C, *Geochim. Cosmochim. Acta, 58, # 2*, 661-669.

Putnis, A., 1993, Introduction to mineral sciences, *Press Syndicate of the University of Cambridge*, 457.

Ransom, B. and H. C. Helgeson, 1994, Estimation of the standard molal heat capacities, entropies, and volumes of 2:1 clay minerals, *Geochim. Cosmochim. Acta, 58, # 21*, 4537-4547.

Rimstidt, J. D., 1997, Quartz solubility at low temperatures, *Geochim. Cosmochim. Acta, 61, # 13*, 2553-2558.

Rimstidt, J. D. and H. L. Barnes, 1980, The kinetics of silica-water reactions, *Geochim. Cosmochim. Acta, 44, #*, 1683-1699.

Sorai, M., T. Ohsumi and M. Ishikawa, 2003, Measurements of feldspar dissolution rates under supercritical CO_2-water-mineral system based on nanoscale surface observation, *Greenhouse Gas Control Technologies 6*.

Span, R. and W. Wagner, 1996, A new equation of state for carbon dioxide covering the fluid region from the triple-point temperature to 1100K at pressures up to 800 MPa, *J. Phys. Chem. Ref. Data, 25, # 6*, 1509-1596.

Stefánsson, A., 2001, Dissolution of primary minerals of basalt in natural waters I. Calculation of mineral solubilities from 0°C to 350°C, *Chem. Geol., 172, #*, 225-250.

Stumm, W. and J. J. Morgan, 1981, Aquatic chemistry, *J. Wiley and sons Inc.*, 780.

Tester, J. W., W. G. Worley, B. A. Robinson, C. O. Grigsby and J. L. Feerer, 1994, Correlating quartz dissolution kinetics in pure water from 25 to 625°C, *Geochim. Cosmochim. Acta, 58, # 11*, 2407-2420.

van Lier, J. A., P. L. de Bryun and J. T. G. Overbeek, 1960, The solubility of quartz, *J. Phys. Chem., 64, # 11*, 1675-1682.

Volosov, A. G., I. L. Khodakovskiy and B. N. Ryzhenko, 1972, Equilibria in the system SiO_2-H_2O at elevated temperatures along the lower three-phase curve, *Geochem. Int., 9, #*, 362-377.

Wawersik, W. R., J. W. Rudnicki, P. Dove, J. Harris, J. M. Logan, L. Pyrak-Nolte, F. M. Orr Jr., P. J. Ortoleva, F. Richter, N. R. Warpinski, J. L. Wilson and T.-F. Wong, 2001, Terrestrial sequestration of CO_2: an assessment of research needs, *Advances in Geophysics, 43, #*, 97-177.

Zysset, M. and P. W. Schindler, 1996, The proton promoted dissolution kinetics of K-montmorillonite, *Geochim. Cosmochim. Acta, 60, # 6*, 921-931.

Appendices

1. Reactions and equilibrium constants: a) quartz and silica species; b) feldspars; c) clays; d) carbonate and carbonate species; e) water
2. Quartz solubility: a) solubility equations; b) graph of silica concentration as a function of temperature
3. Reaction rates, reaction constants, and activation energies: a) quartz; b) feldspars; c) clays; d) carbonates
4. Dissolution rates as a function of pH and temperature: a) quartz; b) feldspar; c) clays
5. Gibbs free energy, enthalpy, and entropy: a) quartz; b) feldspars; c) clays; d) carbonates and CO_2; e) ions in solution
6. Heat capacity and molar volume: a) quartz; b) feldspars; c) carbonates; d) clays

Appendix 1. Reactions and equilibrium constants

A. Quartz and silica species dissolution reactions

Eq nr	Reaction	Log K (at 25°C, 1atm)	Log K, at other conditions	ref
	Quartz			
1	$SiO_{2\ (s)\ (quartz)} + 2H_2O_{(l)} \leftrightarrow H_4SiO_{4\ (aq)}$	-3.96	$\log K_s = 1.881 - 2.028 \cdot 10^{-3}\ T - 1560/T$ [†]	1
2		-3.75	$\log K_s = -34.188 + 197.47/T - 5.851 \cdot 10^{-6}\ T^2 + 12.245 \log T$ [‡]	2
3		-4.24	$\log K_s = -1.468 + 252.9/T - 3.217 \cdot 10^5/T^2$ [◊]	3
	α-Cristobalite			
4	$SiO_{2\ (s)\ (α\text{-}cristobalite)} + 2H_2O_{(l)} \leftrightarrow H_4SiO_{4\ (aq)}$	-3.35	$\log K_s = -0.0321 - 988.2/T$ [†]	1
5		-3.35	$\log K_s = -35.575 + 391.75/T - 6.119 \cdot 10^{-6}\ T^2 + 12.712 \log T$ [‡]	2
	β-Cristobalite			
6	$SiO_{2\ (s)\ (β\text{-}cristobalite)} + 2H_2O_{(l)} \leftrightarrow H_4SiO_{4\ (aq)}$	-2.92	$\log K_s = -0.2560 - 793.6/T$ [†]	1
	Amorphous silica			
7	$SiO_{2\ (s)\ (amorphous\ silica)} + 2H_2O_{(l)} \leftrightarrow H_4SiO_{4\ (aq)}$	-2.72	$\log K_s = 0.3380 - 7.889 \cdot 10^{-4}\ T - 8.40.1/T$ [†]	1
8		-2.71	$\log K_s = -8.476 - 485.24/T - 2.268 \cdot 10^{-6}\ T^2 + 3.068 \log T$ [‡]	2
9		-2.71	$\log K_s = 0.338 - 840.1/T - 7.899 \cdot 10^{-4}T$ [◊]	3
	Silicic acid dissociation			
10	$H_4SiO_{4\ (aq)} \leftrightarrow H_3SiO_4^-{}_{(aq)} + H^+{}_{(aq)}$	-9.77	$\log K_1 = 8.0355 - 0.021748\ T - 3375.5/T$ [□]	4
11	$H_3SiO_4^-{}_{(aq)} \leftrightarrow H_2SiO_4^{2-}{}_{(aq)} + H^+{}_{(aq)}$	-13.17	$\log K_2 = 8.354 - 0.021962\ T - 4465.2/T$ [□]	4
12	$4H_3SiO_4^-{}_{(aq)} + 2H^+{}_{(aq)} \leftrightarrow H_2Si_4O_{10}^{2-}{}_{(aq)} + 6H_2O_{(l)}$	25.7	$\log K_s = -35.939 + 0.073294\ T + 11865.4/T$ [□]	4

[†] 0° to 300°C at pH 7, in pure water

[‡] 0° to 350°C, at 1 bar below 100°C and at vapor saturation pressures (P_{sat}) at higher temperatures, in water

[◊] 0° to 300°C at pH 12, in vapour saturated liquid water

[□] 25° to 350°C, in water

B. Feldspar dissolution reactions

Eq nr	Reaction	Log K (at 25°C, 1atm)	Log K, at other conditions	ref
	Albite			
13	$NaAlSi_3O_{8(s)} + 8H_2O_{(l)} \leftrightarrow Na^+_{(aq)} + Al(OH)_4^-{}_{(aq)} + 3H_4SiO_4^0{}_{(aq)}$	-18.77	$\log K_s = -39.819 + 9.5309 \cdot 10^{-2}\, T - 8.3903 \cdot 10^{-5}\, T^{2\,\dagger}$	5
14	low-albite $+ 8H_2O_{(l)} \leftrightarrow Na^+_{(aq)} + Al(OH)_4^-{}_{(aq)} + 3H_4SiO_4^0{}_{(aq)}$	-20.18	$\log K_s = -96.267 + 305{,}542/T^2 - 3985.50/T - 28.588 \cdot 10^{-6}\, T^2 + 35.790 \log T^{\,\ddagger}$	6
15	high-albite $+ 8H_2O_{(l)} \leftrightarrow Na^+_{(aq)} + Al(OH)_4^-{}_{(aq)} + 3H_4SiO_4^0{}_{(aq)}$	-18.78	$\log K_s = -97.275 + 306{,}065/T^2 - 3313.51/T - 28.622 \cdot 10^{-6}\, T^2 + 35.851 \log T^{\,\ddagger}$	6
16	$NaAlSi_3O_{8(s)} + H^+_{(aq)} + 4.5H_2O_{(l)} \leftrightarrow Na^+_{(aq)} + 2H_4SiO_{4(aq)} + 0.5Al_2Si_2O_5(OH)_{4(s)}$	-1.9		7
17	$NaAlSi_3O_{8(s)} + CO_{2(g)} + 5.5H_2O_{(l)} \leftrightarrow Na^+_{(aq)} + HCO_3^-{}_{(aq)} + 2H_4SiO_{4(aq)} + 0.5Al_2Si_2O_5(OH)_{4(s)}$	-9.7		7
	Oligoclase/andesine			
18	$Ca_{0.29}Na_{0.71}Al_{1.29}Si_{2.71}O_8 + 8H_2O_{(l)} \leftrightarrow 0.29Ca^{2+} + 0.71Na^+_{(aq)} + 1.29Al(OH)_4^-{}_{(aq)} + 2.71H_4SiO_4^0{}_{(aq)}$	-18.80	$\log K_s = -37.229 + 8.5681 \cdot 10^{-2}\, T - 8.1055 \cdot 10^{-5}\, T^{2\,\dagger}$	5
	Labradorite/bytownite			
19	$Ca_{0.7}Na_{0.3}Al_{1.7}Si_{2.3}O_8 + 8H_2O_{(l)} \leftrightarrow 0.7Ca^{2+} + 0.3Na^+_{(aq)} + 1.7Al(OH)_4^-{}_{(aq)} + 2.3H_4SiO_4^0{}_{(aq)}$	-18.82	$\log K_s = -31.365 + 6.6318 \cdot 10^{-2}\, T - 7.4330 \cdot 10^{-5}\, T^{2\,\dagger}$	5
	Anorthite			
20	$CaAl_2Si_2O_{8(s)} + 8H_2O_{(l)} \leftrightarrow Ca^{2+}_{(aq)} + 2Al(OH)_4^-{}_{(aq)} +$	-20.46	$\log K_s = -36.064 + 7.7532 \cdot 10^{-2}\, T - 8.5617 \cdot 10^{-5}\, T^{2\,\dagger}$	5
21	$2H_4SiO_4^0{}_{(aq)}$	- 20.48	$\log K_s = -88.591 + 326{,}546/T^2 - 2720.61/T - 40.100 \cdot 10^{-6}\, T^2 + 31.168 \log T^{\,\ddagger}$	6
22	$CaAl_2Si_2O_{8(s)} + 2H^+_{(aq)} + H_2O_{(l)} \leftrightarrow Al_2Si_2O_5(OH)_{4(s)} + Ca^{2+}_{(aq)}$	14.4		7

[†] 0° to 350°C at saturated water vapour pressure; equation derived by the author by fitting a polynomial function through the given data
[‡] 0° to 350°C, at 1 bar below 100°C and at vapor saturation pressures (P_{sat}) at higher temperatures, in water

34

C. Clay dissolution reactions

Eq nr	Reaction	Log K (at 25°C, 1atm)	Log K, at other conditions	ref
	Montmorillonite			
23	3Na-montmorillonite + $H^+_{(aq)}$ + 11.5$H_2O_{(l)}$ ↔ 3.5$Al_2Si_2O_5(OH)_{4\,(s)}$ + 4$H_4SiO_{4\,(aq)}$ + $Na^+_{(aq)}$	-9.1		7
24	3Ca-montmorillonite + 2$H^+_{(aq)}$ + 23$H_2O_{(l)}$ ↔ 7$Al_2Si_2O_5(OH)_{4\,(s)}$ + 8$H_4SiO_{4\,(aq)}$ + $Ca^{2+}_{(aq)}$	-15.4		7
25	Mg-beidellite + 4.40 $H_2O_{(l)}$ + 15.60$H^+_{(aq)}$ ↔ 0.68$Mg^{2+}_{(aq)}$ + 0.02$Ca^{2+}_{(aq)}$ + 0.14$Na^+_{(aq)}$ + 0.19$K^+_{(aq)}$ + 0.83$Fe^{2+}_{(aq)}$ + 0.11$Fe^{3+}_{(aq)}$ + 3.72$Al^{3+}_{(aq)}$ + 7.10$Si(OH)_{4\,(aq)}$	-15.67	log K = -16.42 [†]	8
26	K-beidellite + 4.40 $H_2O_{(l)}$ + 15.60$H^+_{(aq)}$ ↔ 0.73$K^+_{(aq)}$ + 0.02$Ca^{2+}_{(aq)}$ + 0.14$Na^+_{(aq)}$ + 0.83$Fe^{2+}_{(aq)}$ + 0.41$Mg^{2+}_{(aq)}$ + 0.11$Fe^{3+}_{(aq)}$ + 3.72$Al^{3+}_{(aq)}$ + 7.10$Si(OH)_{4\,(aq)}$	-15.83	log K = -16.57 [†]	8
	Illite			
27	Illite + 7.8$H^+_{(aq)}$ ↔ 3.55$SiO_{2\,(aq)}$ + 1.72$Al^{3+}_{(aq)}$ + 0.36$Fe^{3+}_{(aq)}$ + 0.44$Mg^{2+}_{(aq)}$ + 0.01$Ca^{2+}_{(aq)}$ + 0.13$Na^+_{(aq)}$ + 0.53$K^+_{(aq)}$ + 4.9$H_2O_{(l)}$	6.58		9
28				
	Smectite			
29	Smectite + 20$H_2O_{(l)}$ ↔ 0.51 $Na^+_{(aq)}$ + 0.29$K^+_{(aq)}$ + 0.195$Ca^{2+}_{(aq)}$ + 1.1$Mg^{2+}_{(aq)}$ + 0.42$Fe(OH)_4^-{}_{(aq)}$ + 2.79$Al(OH)_4^-{}_{(aq)}$ + 7.77$H_4SiO_{4\,(aq)}$ + 0.08$OH^-_{(aq)}$		log K_s = -33.2 to –50.2 [‡]	10
	Kaolinite			
30	$Al_2Si_2O_5(OH)_{4\,(s)}$ + 5$H_2O_{(l)}$ ↔ $Al_2O_3 \cdot 3H_2O_{(s)}$ + 2$H_4SiO_{4\,(aq)}$	-9.4		7
31	0.5$Al_2Si_2O_5(OH)_{4\,(aq)}$ + 2.5$H_2O_{(l)}$ ↔ $Al^{3+}_{(aq)}$ + $H_4SiO_{4\,(aq)}$ + 3$OH^-_{(aq)}$	-38.7		7
32	0.5$Al_2Si_2O_5(OH)_{4\,(aq)}$ + 2.5$H_2O_{(l)}$ + $OH^-_{(aq)}$ ↔ $Al(OH)_4^-{}_{(aq)}$ + $H_4SiO_{4\,(aq)}$	-5.7		7
33	$Al_2Si_2O_5(OH)_{4\,(s)}$ + 6$H^+_{(aq)}$ ↔ 2$Al^{3+}_{(aq)}$ + 2$Si(OH)_4°_{(aq)}$ + $H_2O_{(l)}$	7.43		11
34		7.38		12

[†] 25°C and 1 atm, in dilute acid
[‡] over the experimental range at 80°C and pH 8.6-8.96

D. Carbonates and carbonate species dissolution reactions

Eq nr	Reaction	Log K (at 25°C, 1atm)	Log K, at other conditions	ref
	Calcite			
35	$CaCO_{3\,(s)} \leftrightarrow Ca^{2+}_{(aq)} + CO_3^{2-}_{(aq)}$	-8.3		7
36		-8.480	$\log K_C = -171.9065 - 0.077993\,T + 2839.319/T + 71.595 \log T$ [†]	13
37		-8.48	$\log K = -9.17$ [‡]	14
	Aragonite			
38	$CaCO_{3\,(s)} \leftrightarrow Ca^{2+}_{(aq)} + CO_3^{2-}_{(aq)}$	-8.336	$\log K_A = -171.9773 - 0.077993\,T + 2903.293/T + 71.595 \log T$ [†]	13
	Vaterite			
39	$CaCO_{3\,(s)} \leftrightarrow Ca^{2+}_{(aq)} + CO_3^{2-}_{(aq)}$	-7.913	$\log K_v = -172.1295 - 0.077993\,T + 3074.688/T + 71.595 \log T$ [†]	13
	Carbonate ion pairs			
40	$Ca^{2+}_{(aq)} + HCO_3^{-}_{(aq)} \leftrightarrow CaHCO_3^{+}_{(aq)}$	1.11	$\log K_{CaHCO3+} = 1209.120 + 0.31294\,T - 34765.05/T - 478.782 \log T$ [†]	13
41		1.11	$\log K_{CaHCO3+} = 1.00$ [‡]	14
42	$Ca^{2+}_{(aq)} + CO_3^{2-}_{(aq)} \leftrightarrow CaCO_3^{0}_{(aq)}$	3.22	$\log K_{CaCO3\,0} = -1228.732 - 0.299444\,T + 35512.75/T + 485.818 \log T$ [◊]	13
43		3.22	$\log K_{CaCO3\,0} = 4.17$ [‡]	14
	CO$_2$			
44	$CO_{2\,(g)} + H_2O_{(l)} \leftrightarrow H_2CO_{3\,(aq)}$	-1.5		7
45		-1.47	$\log K_H = 108.3865 + 0.01985076\,T - 6919.53/T - 40.45154 \log T + 669365/T^2$ [□]	13
46		-1.47	$\log K_H = -1.91$ [‡]	14
47	$CO_{2\,(g)} + H_2O_{(l)} \leftrightarrow H^{+}_{(aq)} + HCO_3^{-}_{(aq)}$	-7.8		7
48	$H_2CO_{3\,(aq)} \leftrightarrow H^{+}_{(aq)} + HCO_3^{2-}_{(aq)}$	-6.35	$\log K_1 = -356.3094 - 0.06091964\,T + 21834.37/T + 126.8339 \log T - 1684915/T^2$ [□]	13
49		-6.35	$\log K_1 = -6.38$ [‡]	14
50	$HCO_3^{-}_{(aq)} \leftrightarrow H^{+}_{(aq)} + CO_3^{2-}_{(aq)}$	-10.3		7
51		-10.33	$\log K_2 = -107.8871 - 0.03252849\,T + 5151.79/T + 38.92561 \log T - 563713.9/T^2$ [□]	13
52		-10.33	$\log K_2 = -10.11$ [‡]	14

[†] 0° to 90°C, in CO$_2$-H$_2$O solutions   [◊] 5° to 80°C, in CO$_2$-H$_2$O solutions   [□] up to 250°C, at 1 bar below 100°C and at water
[‡] 100°C and 100 bar   vapor saturation pressures (P$_{sat}$) at higher temperatures

E. Water dissociation

Eq nr	Reaction	Log K (at 25°C, 1atm)	Log K, at other conditions	ref
53	$H_2O_{(l)} \leftrightarrow H^+_{(aq)} + OH^-_{(aq)}$	-13.99	$\log K_W = -12.22$ [†]	14
54		-13.995	$\log K_W^* = -4.098 - 3245.2/T + 2.2362 \cdot 10^5/T^2 - 3.984 \cdot 10^7/T^3 + (13.957 - 1262.3/T + 8.5641 \cdot 10^5/T^2) \log \rho_w$ [*] [‡]	15

[†] 100°C and 100 bar
[‡] up to 250°C at saturated water vapour pressures

References

1. Rimstidt, J.D., and H.L. Barnes, 1980, The kinetics of silica-water reactions, *Geochim. Cosmochim. Acta, 44*, 1683-1699.
2. Gunnarsson, I., and S. Arnórsson, 2000, Amorphous silica solubility and the thermodynamic properties of $H_4SiO_4^0$ in the range of 0°C to 350°C at P_{sat}, *Geochim. Cosmochim. Acta, 64 #13*, 2295-2307.
3. Fleming, B.A., and D.A. Crerar, 1982, Silicic acid ionization and calculation of silica solubility at elevated temperature and pH, *Geothermics, 11 #1*, 15-29.
4. Volosov, A.G., I.L., Khodakovskiy, and B.N. Ryzhenko, 1972, Equilibria in the system SiO_2-H_2O at elevated temperatures along the lower three-phase curve, *Geochem. Int., 9*, 362-377.
5. Stefánsson, A., 2001, Dissolution of primary minerals of basalt in natural waters I. Calculation of mineral solubilities from 0°C to 350°C, *Chem. Geol., 172*, 225-250.
6. Arnórsson, S., and A. Stefánsson, 1999, Assessment of feldspar solubility constants in water in the range 0° to 350°C at vapor saturation pressures, *Am. J. Sci., 299*, 173-209.
7. Stumm, W., and J.J. Morgan, 1981, *Aquatic chemistry*, J.Wiley & sons Inc., 780 p.
8. Misra, U.K., and W.J. Upchurch, 1976, Free energy of formation of beidellite from apparent solubility measurements, *Clays Clay Minerals, 24*, 327-331.
9. Köhler, S.J., F. Dufaud, and E.H. Oelkers, 2003, An experimental study of illite dissolution kinetics as a function of pH from 1.4 to 12.4 and temperature from 5 to 50°C, *Geochim. Cosmochim. Acta, 67 #19*, 3583-3594.
10. Cama, J., J. Ganor, C. Ayora, and C.A. Lasaga, 2000, Smectite dissolution kinetics at 80°C and pH 8.8, *Geochim. Cosmochim. Acta, 64 #15*, 2701-2717.
11. May, H.M., D.G. Kinniburgh, P.A. Helmke, and M.L. Jackson, 1986, Aqueous dissolution, solubilities and thermodynamic stabilities of common aluminosilicate clay minerals: kaolinite and smectites, *Geochim. Cosmochim. Acta, 50*, 1667-1677.
12. Kittrick, J.A., 1966, Free energy of formation of kaolinite from solubility measurements, *Am. Min., 51*, 1457-1466.
13. Plummer, L.N., and E. Busenberg, 1982, The solubilities of calcite, aragonite, and vaterite in CO_2-H_2O solutions between 0 and 90°C, and an evaluation of the aqueous model for the system $CaCO_3$-CO_2-H_2O, *Geochim. Cosmochim. Acta, 46*, 1011-1040.
14. Shiraki, R., and S.L. Brantley, Kinetics of near-equilibrium calcite precipitation at 100°C: an evaluation of elementary reaction-based and affinity-based rate laws, *Geochim. Cosmochim. Acta, 59 #8*, 1457-1471.
15. Release on the ion product of water substance, 1980, *International Association for the Properties of Steam*, 9 p.

Appendix 2. Quartz solubility

A. Quartz solubility equations

Eq nr	mineral	solubility equation [units]	conditions (T, P, fluid)	[SiO$_2$] ppm at 25°C	ref
1	**Quartz**	$\log c_{H4SiO4} = 0.151 - 1162/T$ [mol SiO$_2$/kg H$_2$O]	25°-473°C, water	10.8	1
2	**α-quartz**	$\log m_{H4SiO4} = -0.094 - 1069.6/T \ (\pm 0.05)$ [mol SiO$_2$/kg H$_2$O]	25°-300°C, water	12.5	2
3	**Quartz**	$\log m = A + B \log V + C \ (\log V)^2$, [mol SiO$_2$/l] with $A = -4.66206 + 0.0034063T + 2179.7/T - 1.1292 \cdot 10^6/T^2 + 1.3543 \cdot 10^8/T^3$ $B = -0.0014180T - 806.97/T$ $C = 3.9465 \cdot 10^{-4}T$	25°-900°C, < 10000 bar, pure water	6	3
4	**Quartz**	$\log m = -1107.12 \ (\pm 10.77)/T - 0.0254 \ (\pm 0.0247)$ [mol SiO$_2$/l]	0°-300°C, P$_{sat}$, pure water	11.0	4
5	**Amorphous silica**	$\log m_{H4SiO4} = -0.599 - 588/T \ (\pm 0.10)$ [mol SiO$_2$/kg H$_2$O]	25°-300°C, water	161	2

References

1. Van Lier, J.A., P.L. de Bryun, and J.Th.G. Overbeek, 1960, The solubility of quartz, *J. Phys. Chem., 64 #11*, 1675-1682.
2. Volosov, A.G., I.L. Khodakovskiy, and B.N. Ryzhenko, 1972, Equilibria in the system SiO$_2$-H$_2$O at elevated temperatures along the lower three-phase curve, *Geochem. Int., 9*, 362-377.
3. Fournier, R.O, and R.W. Potter, 1982, An equation correlating the solubility of quartz in water from 25° to 900°C at pressures up to 10,000 bars, *Geochim. Cosmochim. Acta, 46*, 1969-1973.
4. Rimstidt, J.D., 1997, Quartz solubility at low temperatures, *Geochim. Cosmochim. Acta, 61 #13*, 2553-2558.

quartz concentration as a function of temperature
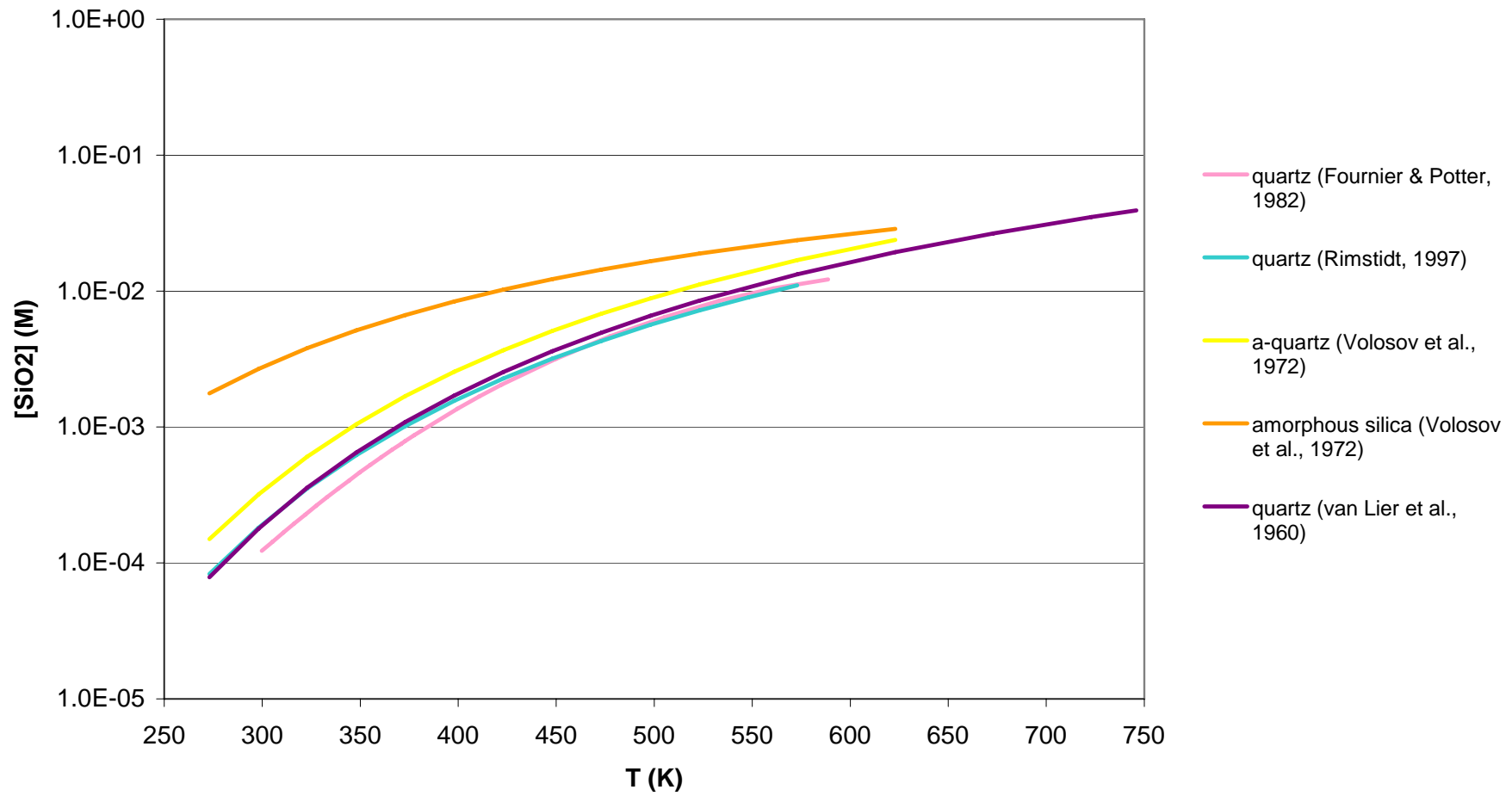
Appendix 3. Reaction rates, reaction constants, and activation energies

A. Quartz

Eq nr	Reaction rate, R [units]	Conditions ($T\ °C$, pH)	Reaction constants, k [units]	Activation energy (kJ/mol)	ref
	Quartz dissolution				
1a	$R = sk$ [mol/cm^2 s]	70°C, 1 < pH < 6	log k' = -20.3 [mol/cm^2 s]	91.2	1
1b	$R = sk'a_{H^+}{}^{0.5}$ [mol/cm^2 s]	70°C, 6 < pH < 12	log k' = -17.8 [mol/cm^2 s]	108.4	
2	$R = 10^{-13.0}\ (\theta_{\equiv SiOH})* + 10^{-10.8}\ (\theta_{\equiv SiOsum}) + 10^{-9.2}$ $(\theta_{\equiv SiOsum})^2$ [mol/m^{2}s]	25°C, pH 2-13			2
3	$R = $ constant [mol/cm^2 s] $R = k_b\ [\equiv Si\text{-}O^-]$ [mol/cm^2 s]	25°C and 70°C, pH < 7 25°C and 70°C, pH > 7.5		~146.0 ~96.2	3
4	$R = k_f\ A_s/M_w\ (1 - m_{H4SiO4}\ /\ m^{sat}_{H4SiO4})$ [mol/m^2 s]	25°C to 625°C, pH 7	$k_{f,\ geom} = (276 \pm 193)\exp(-E_a/RT)$ [mol/m^2 s] $k_{f,\ BET} = (24 \pm 34)\exp(-E_a/RT)$ [mol/m^2 s]	90.1 ± 2.5 87.7 ± 4.7	4
5	-	25°C to 200°C, pH 3.5	log k$_+$ = -0.0463 – 80480/RT [mol/m^2 s]	80.5 ± 1.9	5
6	$R = (A/M)(\gamma_{H4SiO4})\ (k_+a_{SiO2}a_{H2O}{}^2 - k_-a_{H4SiO4})$ [mol/s]	0°C to 300°C, pH 7	log k$_+$ = 1.174 – 2.028·10^{-3} T – 4158/T [s^{-1}] log k$_-$ = -0.707 –2598/T [s^{-1}]	forward: 67.4-76.6 reverse: 49.8	6
7	$R = k_+\ (a_{SiO2})(a_{H2O})^2\ (1 - Q/K)$	100°C to 300°C, pH 7	at 200°C: k$_+$ = 2.14·10^{-8} mol/m^2 s	71.3 ± 8.7	7
	α-Cristobalite dissolution				
8	$R = (A/M)(\gamma_{H4SiO4})\ (k_+a_{SiO2}a_{H2O}{}^2 - k_-a_{H4SiO4})$ [mol/s]	0°C to 300°C, pH 7	log k$_+$ = -0.739 – 3586/T [s^{-1}] log k$_-$ = -0.707 –2598/T [s^{-1}]	forward: 68.7 reverse: 49.8	6
	β-Cristobalite dissolution				
9	$R = (A/M)(\gamma_{H4SiO4})\ (k_+a_{SiO2}a_{H2O}{}^2 - k_-a_{H4SiO4})$ [mol/s]	0°C to 300°C, pH 7	log k$_+$ = -0.963 - 3392/T [s^{-1}] log k$_-$ = -0.707 –2598/T [s^{-1}]	forward: 65.0 reverse: 49.8	6
	Amorphous silica dissolution				
10	$R = (A/M)(\gamma_{H4SiO4})\ (k_+a_{SiO2}a_{H2O}{}^2 - k_-a_{H4SiO4})$ [mol/s]	0°C to 300°C, pH 7	log k$_+$ = - 0.369 – 7.890·10^{-4} T – 3438/T [s^{-1}] log k$_-$ = -0.707 –2598/T [s^{-1}]	forward: 60.9-64.9 reverse: 49.8	6

Eq nr	Reaction rate, R [units]	Conditions (T °C, pH)	Reaction constants, k [units]	Activation energy (kJ/mol)	ref
	Cation promoted quartz dissolution				
11	$R = [k_+ + k_{ad} (k_{me+} m_{me+}/ (1 + K_{me+} m_{me+}))]$ $(a_{SiO2})(a_{H2O})^2 (1 - Q/K)$	100°C to 300°C, pH 7	at 200°C: $k_+ = 2.14 \cdot 10^{-8}$ mol/m² s *NaCl*: $k_{ad} = 6.35 \cdot 10^{-7} \pm 4.4 \cdot 10^{-8}$ [mol/m² s]; $K_{me+} = 58.3 \pm 10.6$ [mol^{-1}] *KCl*: $k_{ad} = 5.60 \cdot 10^{-7}$ [mol/m² s]; $K_{me+} = 46.6$ [mol^{-1}]	*0.05 M NaCl:* 71.2 ± 5.5 *0.05 M KCl:* 71.5 ± 9.2	7
12	$R = e^{-10.7} T \exp(-66000/RT) (\theta_{>SiOH})^1 +$ $e^{4.7} T \exp (-82700/RT) (\theta_{>SiO\text{-} tot})^{1.1}$ [mol/m² s]	25°C to 300°C, pH 2 – 12, 0 –0.3 M Na$^+$			8
13	$\log R = -7.61 + 0.152 \log k_{ex}$	200°C, pH 7, I = 0.15	$k_{ex}(Mg^{2+}) = 10^{5.2}$ s^{-1}; $k_{ex}(Ca^{2+}) = 10^{8.5}$ s^{-1}; $k_{ex}(Ba^{2+}) = 10^{9.3}$ s^{-1}; $k_{ex}(Li^+) = 10^{8.8}$ s^{-1}; $k_{ex}(Na^+) = 10^{9.0}$ s^{-1}; $k_{ex}(K^+) = 10^{9.2}$ s^{-1};		9

B. Feldspars

Eq nr	Reaction rate, R [units]	Conditions (T °C, pH)	Reaction constants, k [units]	Activation energy (kJ/mol)	ref
	Albite dissolution				
14	$R = k_{H+} (a_{H+})^{-0.19 \pm 0.04} + k_{OH-} (a_{OH-})^{0.42 \pm 0.14}$ [mol glass/cm^2 s]	25°C, pH 1-12	k_{H+} is the rate constant in acid (pH 1-4), k_{OH-} is the rate constant in base (pH 6.4-12)		10
15a	$R = ka_{H+}^{-0.49}$ [mol/m^2 s]	low T, $2 \leq pH \leq 6$			11
15b	$R = $ constant [mol/m^2 s]	low T, $6 \leq pH \leq 8$			
15c	$R = ka_{H+}^{0.30}$ [mol/m^2 s]	low T, $8 \leq pH \leq 12$			
16a	$R = k_a c_{S-OH2(+)}$ [mol/m^2 s]	low T, pH < 6	$k_a = 10^{-6.5}$ [s^{-1}]		11
16b	$R = k_b c_{S-OH2(+)}$ [mol/m^2 s]	low T, pH > 7	$k_b = 10^{-6.1}$ [s^{-1}]		
17a	$R = fsk_j a_{H+}^{-1}$ [mol feldspar/cm^2 s]	25-70°C, low pH	at 25°C: $k_j = 10^{-15.0}$; at 70°C: $k_j = 10^{-12.2}$ [mol/cm^2 s]	119.1	12
17b	$R = fsk_j$ [mol feldspar/cm^2 s]	25-70°C, neutral pH	at 25°C: $k_j = 10^{-16.4}$; at 70°C: $k_j = 10^{-15.1}$ [mol/cm^2 s]	53.9	
17c	$R = fsk_i a_{H+}^{0.5}$ [mol feldspar/cm^2 s]	25-70°C, acid pH	at 25°C: $k_i = 10^{-20.3}$; at 70°C: $k_i = 10^{-19.5}$ [mol/cm^2 s]	32.1	
18a	$R = k_+ (a_{H+})^{-0.2 \pm 0.1}$ [mol/m^2 s]	100°C, pH $\leq$ 5	log $k_+ = -8.5 \pm 0.5$ [mol/m^2 s]	88.9 ± 14.6	13
18b	$R = k_+$ [mol/m^2 s]	100°C, 5 < pH < 8.6	log $k_+ = -9.5 \pm 0.3$ [mol/m^2 s]	68.8 ± 4.5	
18c	$R = k_+ (a_{OH-})^{0.3}$ [mol/m^2 s]	100°C, pH $\geq$ 8.6	log $k_+ = -8.3$ [mol/m^2 s]	85.2	
19a	$R = k_+ (a_{H+})^{-0.4 \pm 0.1}$ [mol/m^2 s]	200°C, pH $\leq$ 5	log $k_+ = -5.9 \pm 0.3$ [mol/m^2 s]	88.9 ± 14.6	13
19b	$R = k_+$ [mol/m^2 s]	200°C, 5 < pH < 8.6	log $k_+ = -7.7 \pm 0.2$ [mol/m^2 s]	68.8 ± 4.5	
19c	$R = k_+ (a_{OH-})^{0.4 \pm 0.2}$ [mol/m^2 s]	200°C, pH $\geq$ 8.6	log $k_+ = -6.3 \pm 0.7$ [mol/m^2 s]	85.2	
20a	$R = k_+ (a_{H+})^{-0.6 \pm 0.2}$ [mol/m^2 s]	300°C, pH $\leq$ 5	log $k_+ = -4.1 \pm 0.5$ [mol/m^2 s]	88.9 ± 14.6	13
20b	$R = k_+$ [mol/m^2 s]	300°C, 5 < pH < 8.6	log $k_+ = -6.2 \pm 0.1$ [mol/m^2 s]	68.8 ± 4.5	
20c	$R = k_+ (a_{OH-})^{0.6 \pm 0.3}$ [mol/m^2 s]	300°C, pH $\geq$ 8.6	log $k_+ = -4.5 \pm 0.6$ [mol/m^2 s]	85.2	
	Oligoclase dissolution				
21a	$R = x_a A \exp(E_a/kT) (C_H^s)^{0.46}$ [mol feldspar/m^2 s]	22°C, pH 3-5			14
21b	$R = x_a A \exp(E_a/kT)$ [mol feldspar/m^2 s]	22°C, pH 5-7			
	Labradorite dissolution				
22a	$R = x_a A \exp(E_a/kT) (C_H^s)^{1.2}$ [mol feldspar/m^2 s]	22°C, pH 3-5			14
22b	$R = x_a A \exp(E_a/kT)$ [mol feldspar/m^2 s]	22°C, pH 5-7			

Eq nr	Reaction rate, R [units]	Conditions (T °C, pH)	Reaction constants, k [units]	Activation energy (kJ/mol)	ref
	Bytownite dissolution				
23	$R = x_a\, A \exp(E_a/kT)\, (C^s_H)^{2.0}$ [mol feldspar/m^2 s] $R = x_a\, A \exp(E_a/kT)$ [mol feldspar/m^2 s]	22°C, pH 3-5 22°C, pH 5-7			14
	Anorthite dissolution				
24	$R_{CO2} = k\,(P_{CO2}\,[H_2O]\,K_{a2}/[H^+]^2)^{0.24}$ [mol/m^2 h], with $P_{CO2} = 0.0097$ atm	25°C, 5.5 < pH < 8.5	$k = 1.1\,(\pm 1) \cdot 10^{-7}$ mol$^{0.76}$ m$^{-1.52}$ [h^{-1}]		15
	Nepheline dissolution				
25	$R = k_{H+}\,(a_{H+})^{-0.96 \pm 0.09} + k_{OH-}\,(a_{OH-})^{0.43 \pm 0.01}$ [mol glass/cm^2 s]	25°C, pH 1-12	k_{H+} is the rate constant in acid (pH 1-4), k_{OH-} is the rate constant in base (pH 6.4-12)		10
26	$R = k_+ a_{H+}^{1.0}$ [mol/m^2 s] $R = 4.9 \cdot 10^{-9}$ [mol/m^2 s] $R = k_+'\, a_{H+}^{-0.2}$ [mol/m^2 s]	25°C, pH 2-5 25°C, pH 5-7 25°C, pH 7-11		53-77 (pH independent)	16
	Jadeite dissolution				
27	$R = k_{H+}\,(a_{H+})^{-0.62 \pm 0.05} + k_{OH-}\,(a_{OH-})^{0.36 \pm 0.08}$ [mol glass/cm^2 s]	25°C, pH 1-12	k_{H+} is the rate constant in acid (pH 1-4), k_{OH-} is the rate constant in base (pH 6.4-12)		10
	All plagioclase feldspars				
28	$\log R\,(X) = -14.7484 - 0.0135083X + 0.000505238X^2$, with X being the mol% An [mol feldspar/cm^2 s]	25°C, pH 2			17
29	$\log R\,(X) = -15.023 - 0.001131X + 0.0003176X^2$, with X being the mol% An [mol feldspar/cm^2 s]	25°C, pH 3			17
	Ligand promoted dissolution				
30	*labradorite:* $R = 10^{-13.45}$ [Ox, Cit]$^{0.6}$ [mol/cm^2 s] *albite:* $R = 10^{-14.65}$ [Ox, Cit]$^{0.8}$ [mol/cm^2 s]	80°C, pH 6			18

C. Clays

Eq nr	Reaction rate, R [units]	Conditions (T °C, pH)	Reaction constants, k [units]	Activation energy (kJ/mol)	ref
	Montmorillonite dissolution				
31	$R = 10^{-11.39} a_{H+}^{0.34}$ [mol/m^2 s] $R = 10^{-12.31} a_{OH-}^{0.34}$ [mol/m^2 s]	20°C, pH < 8 20°C, pH > 8.5		30.5 ± 1.3 (at pH 8)	19
32	$R = k\{H^+\}$ [mol/g h], where $\{H^+\}$ is the adsorbed H^+ concentration	25°C, pH 1-5	$k = 6.02 \cdot 10^{-4} \pm 2.4 \cdot 10^{-5}$ [h^{-1}] ([K$^+$] = 0.03 M) $k = 9.98 \cdot 10^{-4} \pm 7.1 \cdot 10^{-5}$ [h^{-1}] ([K$^+$] = 0.10 M) $k = 2.61 \cdot 10^{-3} \pm 3.9 \cdot 10^{-4}$ [h^{-1}] ([K$^+$] = 1.0 M)		20
	Illite dissolution				
33	$R = k_{H+} a_{H+}^{0.6} + k_{H2O} + k_{OH-} a_{OH-}^{0.6}$ [mol/m^2 s]	5-50°C, pH 1.4-12.4	$k_{H+} = 2.2 \cdot 10^{-4} \exp(-E_{AH+}/RT)$ [mol/m^2 s] $k_{H2O} = 2.5 \cdot 10^{-13} \exp(-E_{AH2O}/RT)$ [mol/m^2 s] $k_{OH-} = 0.27 \exp(-E_{AOH}/RT)$ [mol/m^2 s]	$E_{AH+} = 46$; $E_{AH2O} = 14$; $E_{AOH-} = 67$	21
	Smectite dissolution				
34	$R = k (1 - \exp(-6 \cdot 10^{-10} (\Delta G/RT)^6))$ [mol/m^2 s], with ΔG = -14 to –129 kJ/mol over the experimental range	80°C, pH 8.60 – 8.96	$k = -8.1 \cdot 10^{-12}$ [mol/m^2 s]		22
35	$R = k_+ a_{OH-}^{0.15 \pm 0.06}$ [mol/m^2 s]	35°C and 80°C, pH 13-14.6		52 ± 4 (pH independent)	23
	Kaolinite dissolution				
36	$R = k_+ a_{OH-}^{0.56 \pm 0.12}$ [mol/m^2 s] $R = k_+ a_{OH-}^{0.81 \pm 0.12}$ [mol/m^2 s]	35°C, pH 13-14.6 80°C, pH 13-14.6		33 ± 8 at pH 13, 51 ± 8 at pH 13.7	23
37	R = constant $R = k a_{H+}^{0.4 \pm 0.2}$ [mol/m^2 s] $R = k a_{H+}^{0.4 \pm 0.14}$ [mol/m^2 s]	25° and 50°C, pH 2-3 80°C, pH 2-3 25° and 50°C, pH 3-4		29.3 ± 4.6 (pH independent)	20
	Cation dissolution inhibition				
38	*Si inhibition:* $R = 3.7 \cdot 10^{-17}/C_{Si}$ [mol/m^2 s]				22
39	*Al inhibition:* $R = k\, a_{Al3+}^{-1}\, a_{H+}^{1.3 \pm 0.1}$ [mol/m^{2}s] $R = k\, a_{Al3+}^{-1}\, a_{H+}^{1.0 \pm 0.2}$ [mol/m^{2}s]	25°C, pH 2 – 4.2 50°C, pH 2 – 4.2			24

D. Carbonates

| Eq nr	Reaction rat, R [units]	Conditions (T °C, pH)	Reaction constants, k [units]	Activation energy (kJ/mol)	ref
	Calcite dissolution				
40	$R = k_1\, a_{H+} + k_2\, a_{H2CO3*} + k_3\, a_{H2O} - k_4\, a_{Ca2+}\, a_{HCO3-}$ [mol/cm^2 s]	5°-60°C, P_{CO2} = 0.0 –1.0 atm	$\log k_1 = 0.198 - 444.0/T$ [mol/cm^2 s] $\log k_2 = 2.84 - 2177.0/T$ [mol/cm^2 s] $\log k_3 = -5.86 - 317.0/T$ [mol/cm^2 s] $\log k_4 = -1.10 - 1737.0/T$ [mol/cm^2 s]		25

References

1. Knauss, K.G., and T.J. Wolery, 1988, The dissolution kinetics of quartz as a function of pH and time at 70°C, *Geochim. Cosmochim. Acta, 52*, 43-53.
2. Dove, P.M., and S.F. Elston, 1992, Dissolution kinetics of quartz in sodium chloride solutions: analysis of existing data and a rate model for 25°C, *Geochim. Cosmochim. Acta, 56*, 4147-4156.
3. Brady, P.V., and J.V. Walther, 1990, Kinetics of quartz dissolution at low temperatures, *Geochim. Cosmochim. Acta, 82*, 253-264.
4. Tester, J.W., W.G. Worley, B.A. Robinson, C.O. Grigsby, and J.L. Feerer, 1994, Correlating quartz dissolution kinetics in pure water from 25 to 625°C, *Geochim. Cosmochim. Acta, 58 #11*, 2407-2420.
5. Gíslason, S.R., P.J. Heaney, E.H. Oelkers, and J. Schott, 1997, Kinetic and thermodynamic properties of moganite, a novel silica polymorph, *Geochim. Cosmochim. Acta, 61 #6*, 1193-1204.
6. Rimstidt, J.D., and H.L. Barnes, 1980, The kinetics of silica-water interactions, *Geochim. Cosmochim. Acta, 44*, 1683-1699.
7. Dove, P.M., and D.A. Crerar, 1990, Kinetics of quartz dissolution in electrolyte solutions using a hydrothermal mixed flow reactor, *Geochim. Cosmochim. Acta, 54*, 955-969.
8. Dove, P.M., 1994, The dissolution of quartz in sodium chloride solutions at 25° to 300°C, *Am. J. Sci., 294*, 665-712.
9. Dove, P.M., and C.J. Nix, 1997, The influence of the alkaline earth cations, magnesium, calcium, and barium on the dissolution kinetics of quartz, *Geochim. Cosmochim. Acta, 61 #16*, 3329-3340.
10. Hamilton, J.P., S.L. Brantley, C.G. Pantano, L.J. Criscenti, and J.D. Kubicki, 2001, Dissolution of nepheline, jadeite, and albite glasses: toward better models for aluminosilicate dissolution, *Geochim. Cosmochim. Acta, 65 #21*, 3683-3702.
11. Blum, A., and A. Lasaga, 1988, Role of surface speciation in the low-temperature dissolution of minerals, *Nature, 331*, 431-433.
12. Knauss, K.G., and T.J. Wolery, 1986, Dependence of albite dissolution kinetics on pH and time at 25°C and 70°C, *Geochim. Cosmochim. Acta, 50*, 2481-2497.
13. Hellmann, R., 1994, The albite-water system: Part I. The kinetics of dissolution as a function of pH at 100, 200, and 300°C, *Geochim. Cosmochim. Acta, 58 #2*, 595-611.

14. Oxburgh, R., J.I. Drever, and Y-T. Sun, 1994, Mechanism of plagioclase dissolution in acid solution at 25°C, *Geochim. Cosmochim. Acta, 58 #2*, 661-669.
15. Berg, A., and S.A. Banwart, 2000, Carbon dioxide mediated dissolution of Ca-feldspar: implications for silicate weathering, *Chem. Geol., 163*, 25-42.
16. Tole, M.P., A.C. Lasaga, C. Pantano, and W.B. White, 1986, The kinetics of dissolution of nepheline ($NaAlSiO_4$), *Geochim. Cosmochim. Acta, 50*, 379-392.
17. Casey, W.H., H.R. Westrich, and G.R. Holdren, 1991, Dissolution rates of plagioclase at pH = 2 and 3, *Am. Min., 76*, 211-217.
18. Blake, R.E., and L.M. Walter, 1999, Kinetics of feldspar and quartz dissolution at 70-80°C and near-neutral pH: effects of organic acids and NaCl, *Geochim. Cosmochim. Acta, 63 #13/14*, 2043-2059.
19. Huertas, F.J., E. Caballero, C. Jiménez de Cisneros, F. Huertas, and J. Linares, 2001, Kinetics of montmorillonite dissolution in granitic solutions, *Appl. Geochem., 16*, 397-407.
20. Zysset, M. ,and P.W. Schindler, 1996, The proton promoted dissolution kinetics of K-montmorillonite, *Geochim. Cosmochim. Acta, 60 #6*, 921-931.
21. Köhler, S.J., F. Dufaud, and E.H. Oelkers, 2003, An experimental study of illite dissolution kinetics as a function of pH from 1.4 to 12.4 and temperature from 5 to 50°C, *Geochim. Cosmochim. Acta, 67 #19*, 3583-3594.
22. Cama, J., J. Ganor, C. Ayora, and C.A. Lasaga, 2000, Smectite dissolution kinetics at 80°C and pH 8.8, *Geochim. Cosmochim. Acta, 64 #15*, 2701-2717.
23. Bauer, A., and G. Berger, 1998, Kaolinite and smectite dissolution rate in high molar KOH solutions at 35° and 80°C, *Geochim. Cosmochim. Acta, 13 #7*, 905-916.
24. Ganor, J., J.L. Mogollón, and A.C. Lasaga, 1995, The effect of pH on kaolinite dissolution rates and on activation energy, *Geochim. Cosmochim. Acta, 59 #6*, 1037-1052.
25. Plummer, L.N., T.M.L. Wigley, and D.L. Parkhurst, 1978, The kinetics of calcite dissolution in CO_2-water systems at 5° to 60°C and 0.0 to 1.0 atm CO_2, Am. J. Sci., 278, 179-216.

Appendix 4. Dissolution rates of silicate minerals

A1. Dissolution rates for quartz as a function of pH and temperature
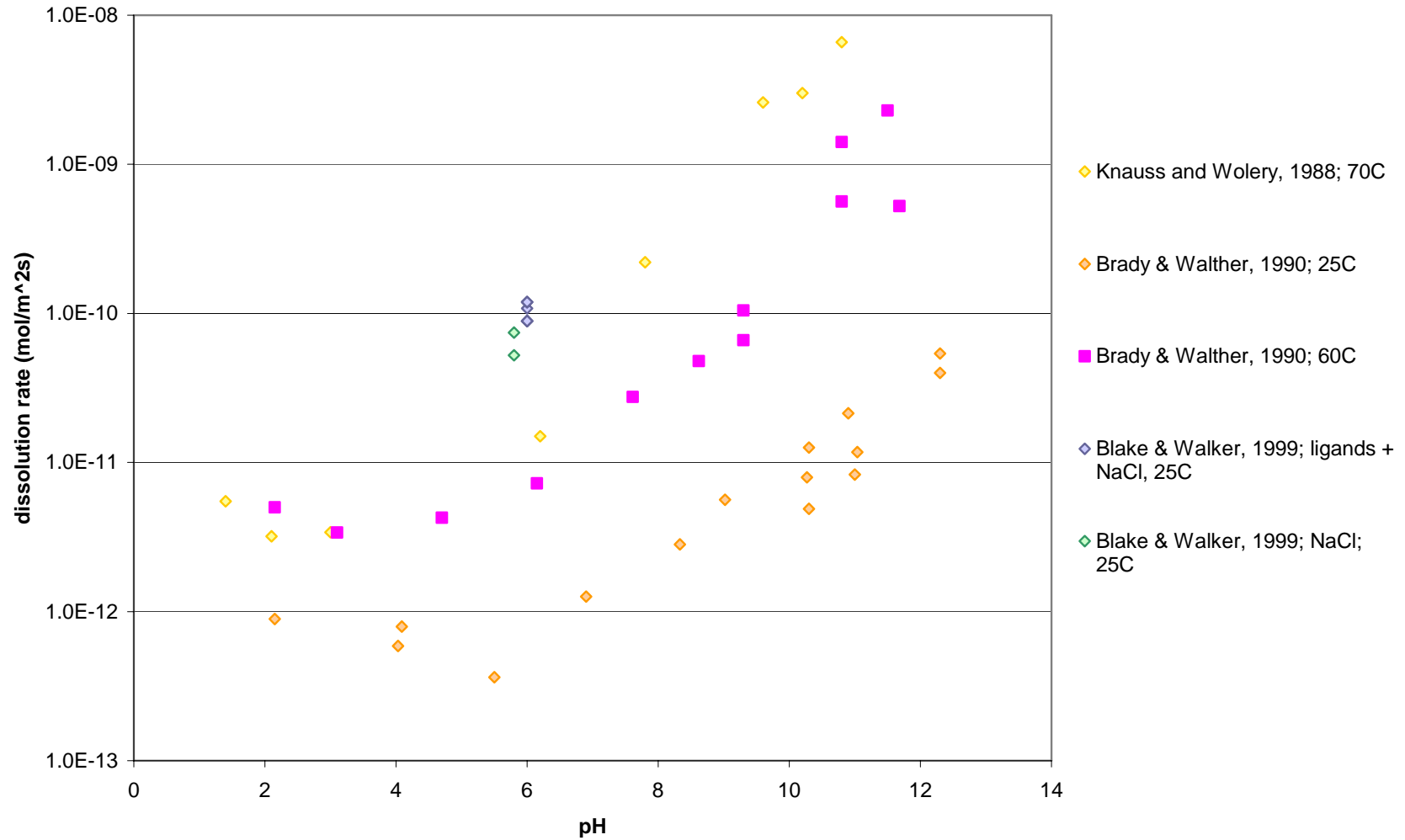
A2. Forward rate constants for quartz as a function of temperature
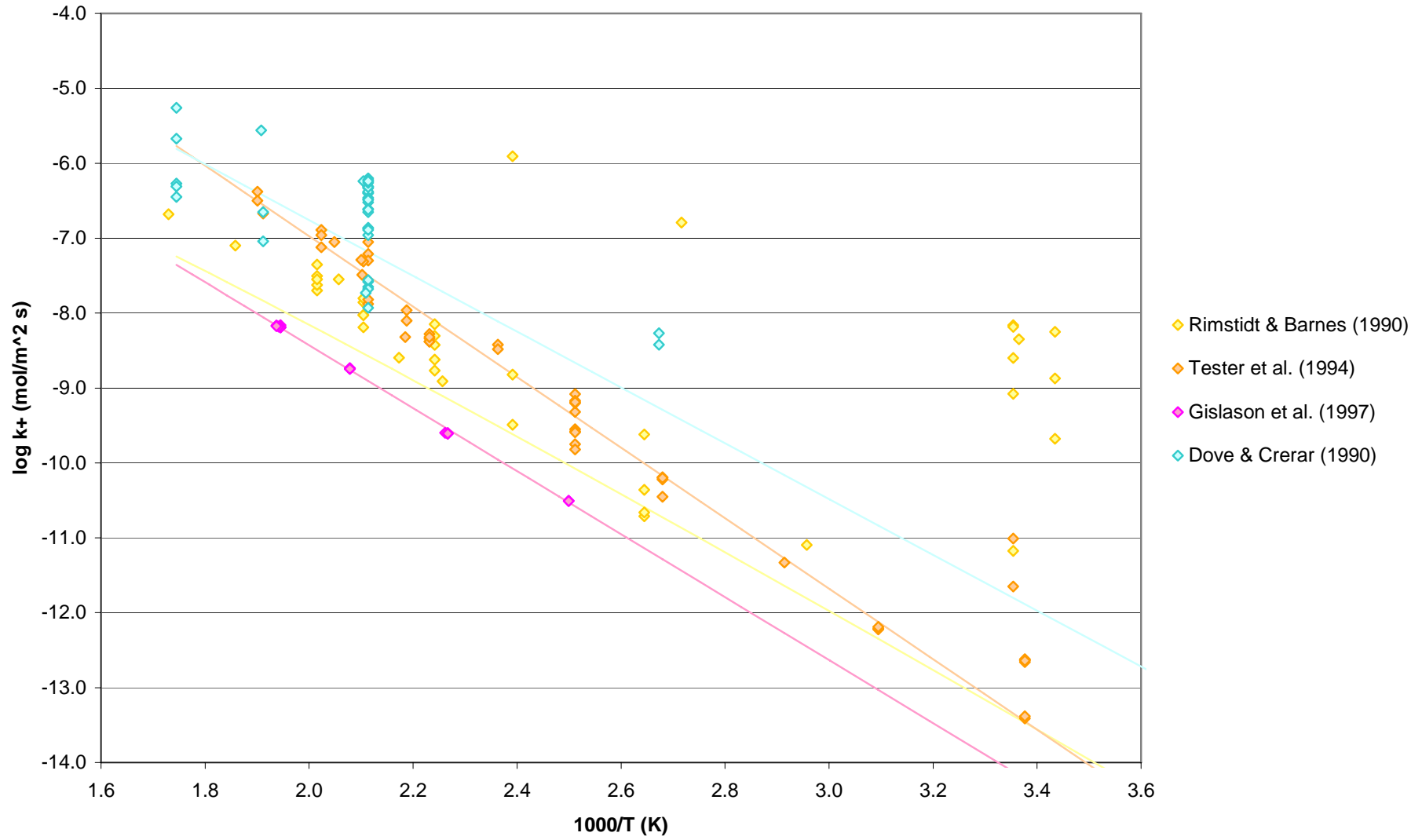
B. Dissolution rates for feldspar minerals as a function of pH and temperature
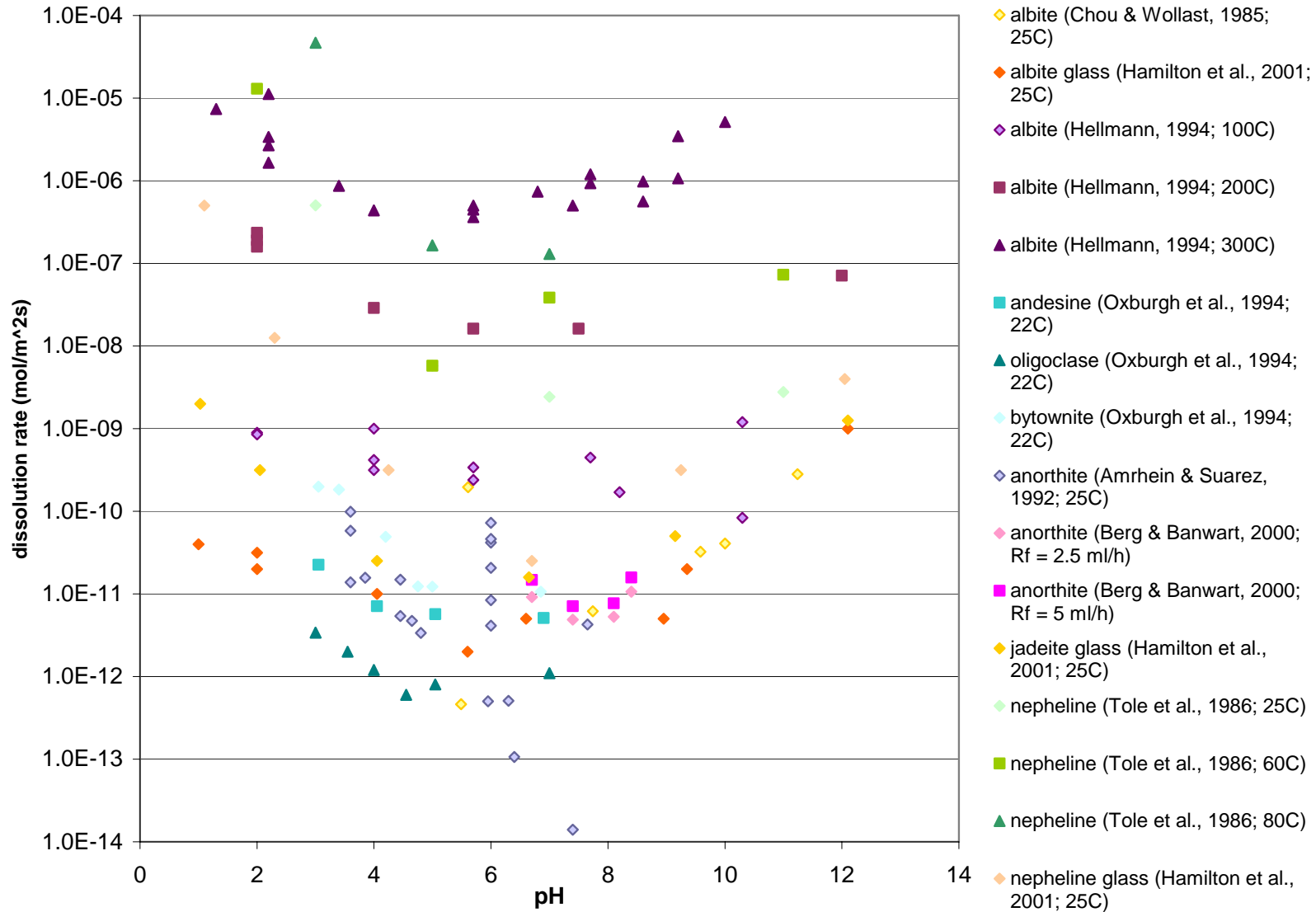
C. Dissolution rates for clay minerals as a function of pH and temperature

Legend:
- montmorillonite (Zysset & Schindler, 1996; 25C, 0.03 M KCl)
- montmorillonite (Zysset & Schindler, 1996; 25C, 0.1 M KCl)
- montmorillonite (Zysset & Schindler, 1996; 25C, 1.0 M KCl)
- montmorillonite (Bauer & Berger, 1998; 35C)
- montmorillonite (Bauer & Berger, 1998; 80C)
- montmorillonite (Huertas et al., 2001; 20C)
- montmorillonite (Huertas et al., 2001; 40C)
- montmorillonite (Huertas et al., 2001; 60C)
- illite (Kohler et al., 2003; 5C)
- illite (Kohler et al., 2003; 20C)
- illite (Kohler et al., 2003; 25C)
- illite (Kohler et al., 2003; 50C)
- smectite (Bauer & Berger, 1998; 35C)
- smectite (Bauer & Berger, 1998; 80C)
- smectite (Cama et al., 2000; 80C)
- kaolinite (Carroll & Walther, 1990; 25C)
- kaolinite (Carroll & Walther, 1990; 60C)
- kaolinite (Carroll & Walther, 1990; 80C)
- kaolinite (Ganor et al., 1995; 25C)
- kaolinite (Ganor et al., 1995; 50C)
- kaolinite (Ganor et al., 1995; 80C)
- kaolinite (Bauer & Berger, 1998; 35C)
- kaolinite (Bauer & Berger, 1998; 80C)

50

References

Amrhein, C. and D. L. Suarez, 1992, Some factors affecting the dissolution kinetics of anorthite at 25°C, _Geochim. Cosmochim. Acta, 56, #_, 1815-1826.

Bauer, A. and G. Berger, 1998, Kaolinite and smectite dissolution rate in high molar KOH solutions at 35° and 80°C, _Appl. Geochem., 13, # 7_, 905-916.

Berg, A. and S. A. Banwart, 2000, Carbon dioxide mediated dissolution of Ca-feldspar: implications for silicate weathering, _Chem. Geol., 163, #_, 25-42.

Blake, R. E. and L. M. Walter, 1999, Kinetics of feldspar and quartz dissolution at 70-80 C and near-neutral pH: effects of organic acids and NaCL, _Geochim. Cosmochim. Acta, 63, # 13-14_, 2043-2059.

Brady, P. V. and J. V. Walther, 1990, Kinetics of quartz dissolution at low temperatures, _Chem. Geol., 82, #_, 253-264.

Cama, J., J. Ganor, C. Ayora and C. A. Lasaga, 2000, Smectite dissolution kinetics at 80°C and pH 8.8, _Geochim. Cosmochim. Acta, 64, # 15_, 2701-2717.

Carroll, S. A. and J. V. Walther, 1990, Kaolinite dissolution at 25°, 60°, and 80°C, _Am. J. Sci., 290, #_, 797-810.

Chou, L. and R. Wollast, 1985, Steady-state kinetics and dissolution mechanisms of albite, _Am. J. Sci., 285, #_, 963-993.

Dove, P. M. and D. A. Crerar, 1990, Kinetics of quartz dissolution in electrolyte solutions using a hydrothermal mixed flow reactor, _Geochim. Cosmochim. Acta, 54, #_, 955-969.

Ganor, J., J. L. Mogollón and A. C. Lasaga, 1995, The effect of pH on kaolinite dissolution rates and activation energy, _Geochim. Cosmochim. Acta, 59, # 6_, 1037-1052.

Gíslason, S. R., P. J. Heaney, E. H. Oelkers and J. Schott, 1997, Kinetic and thermodynamic properties of moganite, a novel silica polymorph, _Geochim. Cosmochim. Acta, 61, # 6_, 1193-1204.

Hamilton, J. P., S. L. Brantley, C. G. Pantano, L. J. Criscenti and J. D. Kubicki, 2001, Dissolution of nepheline, jadeite and albite glasses: toward better models for aluminosilicate dissolution, _Geochim. Cosmochim. Acta, 65, # 21_, 3683-3702.

Hellmann, R., 1994, The albite-water system: part I The kinetics of dissolution as a function of pH at 100, 200, and 300°C, _Geochim. Cosmochim. Acta, 58, # 2_, 595-611.

Huertas, F. J., E. Caballero, C. Jiménez de Cisneros, F. Huertas and J. Linares, 2001, Kinetics of montmorillonite dissolution in granitic solutions, _Appl. Geochem., 16, #_, 397-407.

Knauss, K. G. and T. J. Wolery, 1988, The dissolution kinetics of quartz as a function of pH and time at 70°C, _Geochim. Cosmochim. Acta, 52, #_, 43-53.

Köhler, S. J., F. Dufaud and E. H. Oelkers, 2003, An experimental study of illite dissolution kinetics as a function of pH from 1.4 to 12.4 and temperature from 5° to 50°C, _Geochim. Cosmochim. Acta, 67, # 19_, 3583-3594.

Oxburgh, R., J. I. Drever and Y.-T. Sun, 1994, Mechanism of plagioclase dissolution in acid solution at 25°C, _Geochim. Cosmochim. Acta, 58, # 2_, 661-669.

Rimstidt, J. D. and H. L. Barnes, 1980, The kinetics of silica-water reactions, _Geochim. Cosmochim. Acta, 44, #_, 1683-1699.

Tester, J. W., W. G. Worley, B. A. Robinson, C. O. Grigsby and J. L. Feerer, 1994, Correlating quartz dissolution kinetics in pure water from 25 to 625°C, _Geochim. Cosmochim. Acta, 58, # 11_, 2407-2420.

Tole, M. P., C. A. Lasaga, C. G. Pantano and W. B. White, 1986, The kinetics of dissolution of nepheline ($NaAlSiO_4$), _Geochim. Cosmochim. Acta, 50, #_, 379-392.

Zysset, M. and P. W. Schindler, 1996, The proton promoted dissolution kinetics of K-montmorillonite, _Geochim. Cosmochim. Acta, 60, # 6_, 921-931.

Appendix 5 Gibbs free energy, enthalpy, and entropy

A. Quartz

species	reference	conditions	$\Delta G°_f$ [kJ/mol]	$\Delta H°_f$ [kJ/mol]	$S°_{Tr}$ [J/mol K]
quartz	Stumm & Morgan, 1981	25°C, 1atm	-856.67	-910.94	41.8
	Helgeson et al., 1978	25°C, 1atm	-856.24	-910.65	41.3
	Volosov et al., 1972	25°C	-856.51	-910.94	41.3
		50°C	-851.95		
		100°C	-842.78		
		150°C	-833.62		
		200°C	-824.50		
		250°C	-815.38		
		300°C	-806.30		
	Gíslason et al., 1997	0°C, 1bar	-855.252		
		10°C, 1bar	-855.636		
		20°C, 1bar	-856.034		
		25°C, 1bar	-856.239		
		30°C, 1bar	-856.447		
		40°C, 1bar	-856.876		
		50°C, 1bar	-857.319		
		60°C, 1bar	-857.776		
		70°C, 1bar	-858.248		
		80°C, 1bar	-858.735		
		90°C, 1bar	-859.235		
		100°C, 1bar	-859.750		

species	reference	conditions	$\Delta G°_f$ [kJ/mol]	$\Delta H°_f$ [kJ/mol]	$S°_{Tr}$ [J/mol K]
cristobalite	*Stumm & Morgan, 1981*	25°C, 1atm	-855.88	-909.48	42.7
	Helgeson et al., 1978	25°C, 1atm	-853.1	-906.9	43.4
	Volosov et al., 1972	25°C	-854.25	-908.26	42.7
		50°C	-849.69		
		100°C	-840.61		
		150°C	-831.53		
		200°C	-822.41		
		250°C	-813.37		
		300°C	-804.46		
tridymite	*Stumm & Morgan, 1981*	25°C, 1atm	-855.29	-909.06	43.5
amorphous silica	*Stumm & Morgan, 1981*	25°C, 1atm	-850.73	-903.49	46.9
	Helgeson et al., 1978	25°C, 1atm	-848.9	-897.75	60
	Volosov et al., 1972	25°C	-850.19	-901.74	51.0
		50°C	-845.88		
		100°C	-837.09		
		150°C	-828.43		
		200°C	-819.77		
		250°C	-811.15		
		300°C	-802.57		
H_4SiO_4	*Stumm & Morgan, 1981*	25°C, 1atm	-1316.7	-1468.6	180
	Stefánsson, 2001	25°C, 1atm	-1309.257	-1458.861	188.70
	Volosov et al., 1972	25°C	-1309.88	-1462.14	179.5
		50°C	-1297.21		
		100°C	-1272.06		
		150°C	-1247.42		
		200°C	-1223.15		
		250°C	-1199.22		
		300°C	-1175.49		
	Rimstidt, 1997	25°C, 1atm	-1309.231	-1460.913	180.87
	Gunnarsson & Arnórsson, 2000	25°C, 1atm	-1309.181		178.85

species	reference	conditions	$\Delta G°_f$ [kJ/mol]	$\Delta H°_f$ [kJ/mol]	$S°_{Tr}$ [J/mol K]
$H_3SiO_4^-$	*Volosov et al., 1972*	25°C	-1254.11	-1434.53	84.9
		50°C	-1238.80		
		100°C	-1206.83		
		150°C	-1173.36		
		200°C	-1138.09		
		250°C	-1101.15		
		300°C	-1062.23		
$H_2SiO_4^{2-}$	*Volosov et al., 1972*	25°C	-1178.93	-1386.41	-5.9
		50°C	-1161.10		
		100°C	-1122.44		
		150°C	-1080.27		
		200°C	-1034.20		
		250°C	-984.24		
		300°C	-930.35		
$HSi_4O_{10}^{2-}$	*Volosov et al., 1972*	25°C	-3740.12	-4125.42	69.5
		50°C	-3707.65		
		100°C	-3641.92		
		150°C	-3575.90		
		200°C	-3508.66		
		250°C	-3440.92		
		300°C	-3372.01		

B. Feldspars

mineral	reference	conditions	$\Delta G°_f$ [kJ/mol]	$\Delta H°_f$ [kJ/mol]	$S°_{Tr}$ [J/mol K]
albite, $NaAlSi_3O_8$	Stumm & Morgan, 1981	25°C, 1atm	-3711.7	-3935.1	
	Helgeson et al., 1978	25°C, 1atm	-3708.3	-3931.6	207.1
low albite	Helgeson et al., 1978	25°C, 1atm	-3708.3	-3931.6	207.1
	Arnórsson and Stefánsson, 1999	25°C, 1atm	-3713.038	-3936.185	208.20
high albite	Helgeson et al., 1978	25°C, 1atm	-3700.8	-3920.6	218.8
	Arnórsson and Stefánsson, 1999	25°C, 1atm	-3705.1	-3923.4	224.4
oligoclase/andesine, An30	Stefánsson, 2001	25°C, 1atm	-3788.5	-3988.3	225.2
labradorite/bytownite, An70	Stefánsson, 2001	25°C, 1atm	-3906.5	-4108.2	217.9
anorthite, $CaAl_2SiO_8$	Stumm & Morgan, 1981	25°C, 1atm	-4017.3	-4243.0	199
	Helgeson et al., 1978	25°C, 1atm	-3992.8	-4216.5	205.4
	Arnórsson and Stefánsson, 1999	25°C, 1atm	-4002.1	-4227.8	199.3

C. Clays

mineral	reference	conditions	$\Delta G°_f$ [kJ/mol]	$\Delta H°_f$ [kJ/mol]	$S°_{Tr}$ [J/mol K]
kaolinite, $Al_2Si_2O_5(OH)_4$	*Stumm & Morgan, 1981*	25°C, 1atm	-3799	-4120	203
	Helgeson et al., 1978	25°C, 1atm	-3789.1	-4109.6	203
	May, et al., 1986	25°C, 1atm	-3789.51		
	Kittrick, 1966	25°C, 1atm	-3778.6		
	Nriagu, 1975	25°C, 1atm	-3784.5		
smectite					
$Mg_{0.2075}(Al_{0.18}Si_{3.82})(Al_{1.29}Fe^{3+}_{0.335}Mg_{0.445})O_{10}(OH)_2$	*Mattigod & Sposito, 1978*	25°C, 1atm	-5218.6		
$Al_{0.1383}(Al_{0.18}Si_{3.82})(Al_{1.29}Fe^{3+}_{0.335}Mg_{0.445})O_{10}(OH)_2$		25°C, 1atm	-5182.8		
$Mg_{0.1325}(Al_{0.065}Si_{3.935})(Al_{1.515}Fe^{3+}_{0.225}Mg_{0.29})O_{10}(OH)_2$		25°C, 1atm	-5209.4		
$Al_{0.0883}(Al_{0.065}Si_{3.935})(Al_{1.515}Fe^{3+}_{0.225}Mg_{0.29})O_{10}(OH)_2$		25°C, 1atm	-5188.5		
$Mg_{0.225}(Al_{0.30}Si_{3.70})(Al_{1.345}Fe^{3+}_{0.405}Mg_{0.27})O_{10}(OH)_2$		25°C, 1atm	-5208.5		
$Mg_{0.135}Ca_{0.01}Na_{0.07}K_{0.095}(Al_{0.45}Si_{3.55})(Al_{1.41}Fe^{3+}_{0.415}Fe^{2+}_{0.055}Mg_{0.205})O_{10}(OH)_2$	*Mattigod & Sposito, 1978*	25°C, 1atm	-5185.0		
	Misra & Upchurch, 1976	25°C, 1atm	-5196.5		
$K_{0.37}Ca_{0.01}Na_{0.07}(Al_{0.45}Si_{3.55})(Al_{1.41}Fe^{3+}_{0.415}Fe^{2+}_{0.055}Mg_{0.205})O_{10}(OH)_2$	*Mattigod & Sposito, 1978*	25°C, 1atm	-5205.7		
	Misra & Upchurch, 1976	25°C, 1atm	-5211.8		
$Mg_{0.195}(Al_{0.19}Si_{3.81})(Al_{1.52}Fe^{3+}_{0.22}Mg_{0.29})O_{10}(OH)_2$	*Mattigod & Sposito, 1978*	25°C, 1atm	-5253.3		
	Nriagu, 1975	25°C, 1atm	-5249.7		
$Mg_{0.185}(Al_{0.19}Si_{3.80})(Al_{1.58}Fe^{3+}_{0.19}Mg_{0.26})O_{10}(OH)_2$		25°C, 1atm	-5253.1		
$Mg_{0.21}(Al_{0.19}Si_{3.81})(Al_{1.52}Fe^{3+}_{0.21}Mg_{0.29})O_{10}(OH)_2$		25°C, 1atm	-5261.9		
$Mg_{0.21}(Al_{0.32}Si_{3.68})(Al_{1.52}Fe^{3+}_{0.14}Mg_{0.46})O_{10}(OH)_2$		25°C, 1atm	-5333.0		
$Mg_{0.17}(Al_{0.07}Si_{3.93})(Al_{1.55}Fe^{3+}_{0.20}Mg_{0.24})O_{10}(OH)_2$		25°C, 1atm	-5226.8		
$Na_{0.27}Ca_{0.1}K_{0.02}(Al_{0.06}Si_{3.94})(Al_{1.52}Fe^{3+}_{0.19}Mg_{0.22})O_{10}(OH)_2$	*Mattigod & Sposito, 1978*	25°C, 1atm	-5242.1		
	Nriagu, 1975	25°C, 1atm	-5240.9		
$Ca_{0.185}Na_{0.02}K_{0.02}(Al_{0.07}Si_{3.93})(Al_{1.52}Fe^{3+}_{0.14}Mg_{0.33})O_{10}(OH)_2$	*Mattigod & Sposito, 1978*	25°C, 1atm	-5262.7		
	Nriagu, 1975	25°C, 1atm	-5243.0		

D. Carbonates

carbonate	reference	conditions	$\Delta G°_f$ [kJ/mol]	$\Delta H°_f$ [kJ/mol]	$S°_{Tr}$ [J/mol K]
calcite, CaCO₃	Stumm & Morgan, 1981	25°C, 1atm	-1128.8	-1207.4	91.7
	Helgeson et al., 1978	25°C, 1atm	-1130.1	-1208.2	92.7
aragonite, CaCO₃	Stumm & Morgan, 1981	25°C, 1atm	-1127.8	-1207.4	88.0
	Helgeson et al., 1978	25°C, 1atm	-1129.2	-1208.0	90.2
dolomite, (Ca,Mg)CO₃	Stumm & Morgan, 1981	25°C, 1atm	-2161.7	-2324.5	155.2
	Helgeson et al., 1978	25°C, 1atm	-2167.2	-2329.9	155.2
siderite, FeCO₃	Stumm & Morgan, 1981	25°C, 1atm	-666.7	-737.0	105
magnesite, MgCO₃	Helgeson et al., 1978	25°C, 1atm	-1027.8	-1111.4	65.7

CO₂

species	reference	conditions	$\Delta G°_f$ [kJ/mol]	$\Delta H°_f$ [kJ/mol]	$S°_{Tr}$ [J/mol K]
CO₂	Stumm & Morgan, 1981	25°C, 1atm	-394.37	-393.5	213.6
H₂CO₃*	Stumm & Morgan, 1981	25°C, 1atm	-623.2	-699.7	187.0
H₂CO₃ (true)	Stumm & Morgan, 1981	25°C, 1atm	-607.1		
HCO₃⁻	Stumm & Morgan, 1981	25°C, 1atm	-586.8	-692.0	91.2
CO₃²⁻	Stumm & Morgan, 1981	25°C, 1atm	-527.9	-677.1	-56.9

E. Ions in solution

ion	reference	conditions	$\Delta G°_f$ [kJ/mol]	$\Delta H°_f$ [kJ/mol]	$S°_{Tr}$ [J/mol K]
Al^{3+}	Stumm & Morgan, 1981	25°C, 1atm	-489.4	-531.0	-308
$AlOH^{2+}$	Stumm & Morgan, 1981	25°C, 1atm	-698		
$Al(OH)^{2+}$	Stumm & Morgan, 1981	25°C, 1atm	-911		
$Al(OH)_3$	Stumm & Morgan, 1981	25°C, 1atm	-1115		
$Al(OH)_4^-$	Stumm & Morgan, 1981	25°C, 1atm	-1325		
	Arnórsson and Stefánsson, 1999	25°C, 1atm	-1305.575	-1500.690	111.12
Ca^{2+}	Stumm & Morgan, 1981	25°C, 1atm	-553.54	-542.83	-53
	Arnórsson and Stefánsson, 1999	25°C, 1atm	-552.790	-543.083	-56.5
Cl^-	Stumm & Morgan, 1981	25°C, 1atm	-131.3	-167.2	56.5
Fe^{2+}	Stumm & Morgan, 1981	25°C, 1atm	-78.87	-89.10	-138
	Stefánsson, 2001	25°C, 1atm	-91.504	-92.257	-105.9
Fe^{3+}	Stumm & Morgan, 1981	25°C, 1atm	-4.60	-48.5	-316
H^+	Stumm & Morgan, 1981	25°C, 1atm	0	0	0
$H2O_{(l)}$	Stumm & Morgan, 1981	25°C, 1atm	-237.18	-285.83	69.91
	Volosov et al., 1972	25°C	-237.18	-285.83	69.91
		50°C	-233.16		
		100°C	-225.24		
		150°C	-217.54		
		200°C	-210.03		
		250°C	-202.66		
		300°C	-195.35		

ion	reference	conditions	$\Delta G°_f$ [kJ/mol]	$\Delta H°_f$ [kJ/mol]	$S°_{Tr}$ [J/mol K]
$H2O_{(l)}$	Arnórsson and Stefánsson, 1999	25°C, 1atm	-237.140	-285.830	69.95
K^+	Arnórsson and Stefánsson, 1999	25°C, 1atm	-282.462	-252.170	101.0
Na^+	Arnórsson and Stefánsson, 1999	25°C, 1atm	-261.881	-240.300	58.4
Mg^{2+}	Stumm & Morgan, 1981	25°C, 1atm	-454.8	-466.8	-138
	Stefánsson, 2001	25°C, 1atm	-453.985	-465.960	-138.1
OH^-	Stumm & Morgan, 1981	25°C, 1atm	-157.3	-230.0	-10.75
	Stefánsson, 2001	25°C, 1atm	-157.297	-230.024	-10.7
	Volosov et al., 1972	25°C, 1atm	-157.29	-229.99	-10.8
		50°C, 1atm	-151.13		
		100°C, 1atm	-137.74		
		150°C, 1atm	-123.01		
		200°C, 1atm	-107.03		
		250°C, 1atm	-89.45		
		300°C, 1atm	-70.37		

59

References

Arnórsson, S., and A. Stefánsson, 1999, Assessment of feldspar solubility constants in water in the range 0° to 350°C at vapour saturation pressures, *Am. J. Sci., 299*, 173-209.

Gíslason, S.R., P.J. Heaney, E.H. Oelkers, and J.Schott, 1997, Kinetic and thermodynamic properties of moganite, a novel silica polymorph, *Geochim. Cosmochim. Acta, 61 #6*, 1193-1204.

Gunnarsson, I., and S. Arnórsson, 2000, Amorphous silica solubility and the thermodynamic properties of H_4SiO_4 in the range of 0° to 350°C at Psat, *Geochim. Cosmochim. Acta, 64 # 13*, 2295-2307.

Helgeson, H.C., J.M. Delaney, H.W. Nesbitt, and D.K. Bird, 1978, Summary and critique of the thermodynamic properties of rock-forming minerals, *Am. J. Sci. 278A*, 220p.

Kittrick, J.A., 1966, Free energy of formation of kaolinite from solubility experiments, *Am. Min., 51*, 1457-1466.

Mattigod, S.V., and G. Sposito, 1978, Improved method for estimating the standard free energies of formation ($\Delta G°_{f, 298.15}$) of smectites, *Geochim. Cosmochim. Acta, 42*, 1753-1762.

May, H.M., D.G. Kinniburgh, P.A. Helmke, and M.L. Jackson, 1986, Aqueous dissolution, solubilities and thermodynamic stabilities of common aluminosilicate clay minerals: kaolinite and smectite, *Geochim. Cosmochim. Acta, 50*, 1667-1677.

Nriagu, J.O., Thermochemical approximations for clay minerals, *Am. Min., 60*, 834-839.

Rimstidt, J.D., 1997, Quartz solubility at low temperatures, *Geochim. Cosmochim. Acta, 61 #13*, 2553-2558.

Stefánsson, A., 2001, Dissolution of primary minerals of basalt in natural waters I. Calculation of mineral solubilities from 0°C to 350°C., *Chem. Geol., 172*, 225-250.

Stumm, W., and J.J. Morgan, 1981, *Aquatic chemistry*, J. Wiley & sons Inc., 780 p.

Volosov, A.G., I.L. Khodakovshiy, and B.N. Ryzhenko, 1972, Equilibria in the system SiO_2-H_2O at elevated temperatures along the lower three-phase curve, *Geochem. Int., 9*, 362-377.

Appendix 6. Heat capacity and molar volume of minerals

A. Quartz

mineral	heat capacity, $C°_P$ (T) [J/mol K]	$C°_P$ [J/mol K] at 25°C	molar volume, $V°$ [cm³/mol]	ref
Quartz	$C°_P = 11.22 + 8.20·10^{-3} T + 2.70·10^5/T^2$ [cal/mol K]	59.65	22.688	1
Cristobalite	$C°_P = 13.98 + 3.34·10^{-3} T + 3.81·10^5/T^2$ [cal/mol K]	80.59	25.74	1
Amorphous silica	$C°_P = 5.93 + 47.20·10^{-3} T + 22.78·10^5/T^2$ [cal/mol K]	190.91	29.0	1

B. Feldspar

mineral	heat capacity, $C°_P$ (T) [J/mol K]	$C°_P$ [J/mol K] at 25°C	molar volume, $V°$ [cm³/mol]	ref
Albite	$C°_P = 61.70 + 13.90·10^{-3} T + 15.01·10^5/T^2$ [cal/mol K]	346.14	100.25	1
	$C°_P = 6.714·10^2 – 14.67·10^{-2} T + 3.174·10^6/T^2 + 3.659·10^{-5} T^2 – 7.974·10^3/T^{0.5}$ * [J/mol K]	204.8	100.83	2
Oligoclase/andesine	$C°_P = 6.266·10^2 – 13.098·10^{-2} T + 1.845·10^6/T^2 + 3.812·10^{-5} T^2 – 6.992·10^3/T^{0.5}$ [J/mol K]	206.6	100.8	2
Labradorite/bytownite	$C°_P = 5.632·10^2 – 10.875·10^{-2} T – 0.033·10^6/T^2 + 4.029·10^{-5} T^2 – 5.605·10^3/T^{0.5}$ [J/mol K]	209.4	100.8	2
Anorthite	$C°_P = 63.311 + 14.794·10^{-3} T + 15.44·10^5/T^2$ [cal/mol K]	356.02	100.79	1
	$C°_P = 5.168·10^2 – 9.249·10^{-2} T – 1.408·10^6/T^2 + 4.188·10^{-5} T^2 – 4.589·10^3/T^{0.5}$ * [J/mol K]	211.34	100.79	2

C. Carbonates

mineral	heat capacity, $C°_P$ (T) [J/mol K]	$C°_P$ [J/mol K] at 25°C	molar volume, $V°$ [cm³/mol]	ref
Calcite	$C°_P = 24.98 + 5.24·10^{-3} T + 6.20·10^5/T^2$ [cal/mol K]	140.23	36.934	1
Aragonite	$C°_P = 20.13 + 10.24·10^{-3} T + 3.34·10^5/T^2$ [cal/mol K]	112.72	34.15	1
Dolomite	$C°_P = 41.557 + 23.952·10^{-3} T + 9.884·10^5/T^2$ [cal/mol K]	250.26	64.365	1
Magnesite	$C°_P = 19.731 + 12.539·10^{-3} T + 4.748·10^5/T^2$ [cal/mol K]	120.54	28.018	1

* best equations to calculate the heat capacity of albite and anorthite, as a function of temperature

D. Clays

clay structural formula	heat capacity, $C^{\bullet}_P(T)$ [units]	$C^{\bullet}_P$ [J/mol K] at 25°C	molar volume, $V^{\bullet}$ (cm^3/mol)	ref
Kaolinite	$C^{\circ}_P = 72.77 + 29.20 \cdot 10^{-3}\,T + 21.52 \cdot 10^5/T^2$ [cal/mol K]	442.18	99.52	1
Illite				
$(K_{0.69}Na_{0.03}Ca_{0.05})(Al_{1.55}Mg_{0.36}Fe^{2+}_{0.07}Fe^{3+}_{0.04})Al_{0.43}Si_{3.57}O_{10}(OH)_2$	$C^{\circ}_P = 186.13 - 18.17 \cdot 10^2/T^{0.5} + 0.538 \cdot 10^5/T^2 + 1.062 \cdot 10^7/T^3$ [cal/mol K]	325.64	145.06	3
$(K_{0.61}Na_{0.02}Ca_{0.01})(Al_{1.33}Mg_{0.18}Fe^{2+}_{0.19}Fe^{3+}_{0.42})Al_{0.64}Si_{3.36}O_{10}(OH)_2$	$C^{\circ}_P = 187.18 - 19.07 \cdot 10^2/T^{0.5} + 2.529 \cdot 10^5/T^2 - 2.105 \cdot 10^7/T^3$ [cal/mol K]	329.57	145.33	3
$(K_{0.58}Na_{0.03}Ca_{0.03})(Al_{1.65}Mg_{0.20}Fe^{2+}_{0.08}Fe^{3+}_{0.07})Al_{0.41}Si_{3.59}O_{10}(OH)_2$	$C^{\circ}_P = 184.92 - 18.88 \cdot 10^2/T^{0.5} + 0.506 \cdot 10^5/T^2 + 1.401 \cdot 10^7/T^3$ [cal/mol K]	320.87	145.31	3
$(K_{0.57}Na_{0.05}Ca_{0.07})(Al_{1.25}Mg_{0.17}Fe^{2+}_{0.22}Fe^{3+}_{0.45})Al_{0.65}Si_{3.35}O_{10}(OH)_2$	$C^{\circ}_P = 187.39 - 19.07 \cdot 10^2/T^{0.5} + 2.832 \cdot 10^5/T^2 - 2.647 \cdot 10^7/T^3$ [cal/mol K]	331.12	144.91	3
$(K_{0.73}Na_{0.01}Ca_{0.02})(Al_{1.67}Mg_{0.28}Fe^{2+}_{0.01}Fe^{3+}_{0.04})Al_{0.47}Si_{3.53}O_{10}(OH)_2$	$C^{\circ}_P = 185.88 - 18.88 \cdot 10^2/T^{0.5} + 0.274 \cdot 10^5/T^2 + 1.583 \cdot 10^7/T^3$ [cal/mol K]	323.97	144.58	3
$(K_{0.56}Na_{0.01}Ca_{0.05})(Al_{1.56}Mg_{0.40}Fe^{2+}_{0.02}Fe^{3+}_{0.05})Al_{0.33}Si_{3.67}O_{10}(OH)_2$	$C^{\circ}_P = 184.53 - 18.77 \cdot 10^2/T^{0.5} + 0.426 \cdot 10^5/T^2 + 1.124 \cdot 10^7/T^3$ [cal/mol K]	321.08	146.18	3
$(K_{0.71}Na_{0.01}Ca_{0.03})(Al_{0.97}Mg_{0.29}Fe^{2+}_{0.08}Fe^{3+}_{0.70})Al_{0.53}Si_{3.47}O_{10}(OH)_2$	$C^{\circ}_P = 187.33 - 19.02 \cdot 10^2/T^{0.5} + 4.191 \cdot 10^5/T^2 - 5.185 \cdot 10^7/T^3$ [cal/mol K]	334.39	145.97	3
$(K_{0.67}Na_{0.02}Ca_{0.02})(Al_{1.74}Mg_{0.23}Fe^{2+}_{0.02}Fe^{3+}_{0.03})Al_{0.55}Si_{3.45}O_{10}(OH)_2$	$C^{\circ}_P = 185.64 - 18.88 \cdot 10^2/T^{0.5} + 0.023 \cdot 10^5/T^2 + 2.022 \cdot 10^7/T^3$ [cal/mol K]	322.46	144.09	3
$(K_{0.64}Na_{0.02})(Al_{1.57}Mg_{0.26}Fe^{2+}_{0.05}Fe^{3+}_{0.15})Al_{0.43}Si_{3.57}O_{10}(OH)_2$	$C^{\circ}_P = 185.49 - 18.89 \cdot 10^2/T^{0.5} + 0.823 \cdot 10^5/T^2 + 0.728 \cdot 10^7/T^3$ [cal/mol K]	323.30	145.61	3
$(K_{0.62}Na_{0.01})(Al_{1.46}Mg_{0.35}Fe^{2+}_{0.07}Fe^{3+}_{0.15})Al_{0.30}Si_{3.70}O_{10}(OH)_2$	$C^{\circ}_P = 185.01 - 18.85 \cdot 10^2/T^{0.5} + 1.142 \cdot 10^5/T^2 + 0.168 \cdot 10^7/T^3$ [cal/mol K]	322.92	146.75	3
$(K_{0.58}Na_{0.01})(Al_{1.55}Mg_{0.30}Fe^{2+}_{0.03}Fe^{3+}_{0.14})Al_{0.31}Si_{3.69}O_{10}(OH)_2$	$C^{\circ}_P = 185.52 - 18.83 \cdot 10^2/T^{0.5} + 0.809 \cdot 10^5/T^2 + 0.726 \cdot 10^7/T^3$ [cal/mol K]	320.79	146.61	3
$(K_{0.76}Na_{0.03}Ca_{0.01})(Al_{1.65}Mg_{0.31}Fe^{2+}_{0.04}Fe^{3+}_{0.03})Al_{0.55}Si_{3.45}O_{10}(OH)_2$	$C^{\circ}_P = 186.55 - 18.91 \cdot 10^2/T^{0.5} + 0.198 \cdot 10^5/T^2 + 1.673 \cdot 10^7/T^3$ [cal/mol K]	325.98	144.08	3
$(K_{0.69}Na_{0.01})(Al_{1.35}Mg_{0.31}Fe^{2+}_{0.08}Fe^{3+}_{0.27})Al_{0.36}Si_{3.64}O_{10}(OH)_2$	$C^{\circ}_P = 185.74 - 18.92 \cdot 10^2/T^{0.5} + 1.919 \cdot 10^5/T^2 - 1.091 \cdot 10^7/T^3$ [cal/mol K]	326.10	146.23	3
$(K_{0.65}Ca_{0.07})(Al_{1.58}Mg_{0.38}Fe^{2+}_{0.03}Fe^{3+}_{0.03})Al_{0.41}Si_{3.59}O_{10}(OH)_2$	$C^{\circ}_P = 185.52 - 18.83 \cdot 10^2/T^{0.5} + 0.477 \cdot 10^5/T^2 + 1.038 \cdot 10^7/T^3$ [cal/mol K]	323.80	145.23	3
$(K_{0.70}Ca_{0.08})(Al_{1.67}Mg_{0.24}Fe^{2+}_{0.01}Fe^{3+}_{0.05})Al_{0.53}Si_{3.47}O_{10}(OH)_2$	$C^{\circ}_P = 185.76 - 18.88 \cdot 10^2/T^{0.5} + 0.495 \cdot 10^5/T^2 + 1.158 \cdot 10^7/T^3$ [cal/mol K]	323.84	143.68	3
$(K_{0.78}Ca_{0.05})(Al_{1.71}Mg_{0.16}Fe^{2+}_{0.05}Fe^{3+}_{0.07})Al_{0.64}Si_{3.36}O_{10}(OH)_2$	$C^{\circ}_P = 186.83 - 18.99 \cdot 10^2/T^{0.5} + 0.588 \cdot 10^5/T^2 + 1.165 \cdot 10^7/T^3$ [cal/mol K]	326.18	142.99	3
Smectite				
$Na_{0.54}(Al_{1.51}Mg_{0.41}Fe^{3+}_{0.07})Al_{0.10}Si_{3.90}O_{10}(OH)_2 \cdot 4.5H_2O$	$C^{\circ}_P = 324.26 - 35.43 \cdot 10^2/T^{0.5} - 2.660 \cdot 10^5/T^2 + 30.287 \cdot 10^7/T^3$ [cal/mol K]	533.54	217.79	3
$Na_{0.76}(Al_{1.51}Mg_{0.19}Fe^{3+}_{0.23})Al_{0.34}Si_{3.66}O_{10}(OH)_2 \cdot 4.5H_2O$	$C^{\circ}_P = 326.43 - 35.48 \cdot 10^2/T^{0.5} - 3.159 \cdot 10^5/T^2 + 31.305 \cdot 10^7/T^3$ [cal/mol K]	540.11	215.36	3
$Na_{0.39}(Al_{1.26}Mg_{0.39}Fe^{2+}_{0.01}Fe^{3+}_{0.37})Al_{0.07}Si_{3.93}O_{10}(OH)_2 \cdot 4.5H_2O$	$C^{\circ}_P = 323.92 - 35.53 \cdot 10^2/T^{0.5} - 0.290 \cdot 10^5/T^2 + 26.239 \cdot 10^7/T^3$ [cal/mol K]	534.30	219.33	3
$Na_{0.36}(Al_{1.57}Mg_{0.25}Fe^{2+}_{0.01}Fe^{3+}_{0.19})Al_{0.15}Si_{3.85}O_{10}(OH)_2 \cdot 4.5H_2O$	$C^{\circ}_P = 323.57 - 35.57 \cdot 10^2/T^{0.5} - 1.340 \cdot 10^5/T^2 + 28.223 \cdot 10^7/T^3$ [cal/mol K]	530.15	218.20	3
$Na_{0.49}(Al_{1.69}Mg_{0.30}Fe^{2+}_{0.01})Al_{0.20}Si_{3.80}O_{10}(OH)_2 \cdot 4.5H_2O$	$C^{\circ}_P = 324.05 - 35.48 \cdot 10^2/T^{0.5} - 2.951 \cdot 10^5/T^2 + 30.890 \cdot 10^7/T^3$ [cal/mol K]	530.99	216.96	3
$Na_{0.38}(Al_{1.43}Mg_{0.46}Fe^{2+}_{0.01}Fe^{3+}_{0.14})Al_{0.03}Si_{3.97}O_{10}(OH)_2 \cdot 4.5H_2O$	$C^{\circ}_P = 323.41 - 35.47 \cdot 10^2/T^{0.5} - 1.434 \cdot 10^5/T^2 + 28.146 \cdot 10^7/T^3$ [cal/mol K]	531.28	219.20	3
$Na_{0.36}(Al_{1.57}Mg_{0.25}Fe^{2+}_{0.01}Fe^{3+}_{0.19})Al_{0.15}Si_{3.85}O_{10}(OH)_2 \cdot 4.5H_2O$	$C^{\circ}_P = 323.57 - 35.57 \cdot 10^2/T^{0.5} - 1.340 \cdot 10^5/T^2 + 28.223 \cdot 10^7/T^3$ [cal/mol K]	530.15	218.20	3
$Na_{0.46}(Al_{1.43}Mg_{0.53}Fe^{2+}_{0.02}Fe^{3+}_{0.08})Al_{0.07}Si_{3.93}O_{10}(OH)_2 \cdot 4.5H_2O$	$C^{\circ}_P = 324.17 - 35.44 \cdot 10^2/T^{0.5} - 2.140 \cdot 10^5/T^2 + 29.215 \cdot 10^7/T^3$ [cal/mol K]	533.71	218.81	3
$Na_{0.22}(Al_{1.58}Mg_{0.32}Fe^{2+}_{0.01}Fe^{3+}_{0.15})Al_{0.06}Si_{3.94}O_{10}(OH)_2 \cdot 4.5H_2O$	$C^{\circ}_P = 322.55 - 35.58 \cdot 10^2/T^{0.5} - 0.816 \cdot 10^5/T^2 + 27.270 \cdot 10^7/T^3$ [cal/mol K]	526.68	219.40	3

$Na_{0.27}(Al_{1.47}Mg_{0.38}Fe^{2+}_{0.02}Fe^{3+}_{0.15})Al_{0.09}Si_{3.91}O_{10}(OH)_2 \cdot 4.5H_2O$	$C^\circ_P = 323.33 - 35.59 \cdot 10^2/T^{0.5} - 0.853 \cdot 10^5/T^2 + 27.256 \cdot 10^7/T^3$ [cal/mol K]	529.40	218.78	3
$Na_{0.43}(Al_{1.47}Mg_{0.38}Fe^{2+}_{0.02}Fe^{3+}_{0.15})Al_{0.09}Si_{3.91}O_{10}(OH)_2 \cdot 4.5H_2O$	$C^\circ_P = 323.85 - 35.50 \cdot 10^2/T^{0.5} - 1.669 \cdot 10^5/T^2 + 28.652 \cdot 10^7/T^3$ [cal/mol K]	532.20	218.49	3

References

1. Helgeson, H.C., J.M. Delaney, H.W. Nesbitt, and D.K. Bird, 1978, Summary and critique of the thermodynamic properties of rock-forming minerals, *Am. J. Sci. 278A*, 220p.
2. Stefánsson, A., 2001, Dissolution of primary minerals of basalt in natural waters I. Calculation of mineral solubilities from 0°C to 350°C., *Chem. Geol., 172*, 225-250.
3. Ransom, B, and H.C. Helgeson, 1994, Estimation of the standard molal heat capacities, entropies, and volume of 2:1 clay volumes, *Geochim. Cosmochim. Acta, 58 #21*, 4537-4547.